ENVIRONMENTAL EFFECTS ON SUBSURFACE DEFECT DETECTION IN CONCRETE STRUCTURES USING INFRARED THERMOGRAPHY

A Thesis presented to the Faculty of the Graduate School of the

University of Missouri - Columbia

In Partial Fulfillment of the Requirements for the Degree

Master of Science

By

NAVEEN KUMAR BOLLENI

Dr. Glenn Washer, Graduate Advisor

DECEMBER 2009

The undersigned, appointed by the Dean of the Graduate School, have examined the thesis entitled

ENVIRONMENTAL EFFECTS ON SUBSURFACE DEFECT DETECTION IN CONCRETE STRUCTURES USING INFRARED THERMOGRAPHY

Presented by **Naveen Kumar Bolleni**,

A candidate for the degree of **Master of Science**,

And hereby certify that, in their opinion, it is worth of acceptance.

Professor Glenn Washer

Professor Hani Salim

Professor Gregory Triplett

ACKNOWLEDGEMENTS

I would like to thank my advisor, Dr. Glenn Washer, Assistant Professor of the Department of Civil and Environmental Engineering at the University of Missouri. Dr. Washer's knowledge and oversight was critical in all of the progress made on this project.

I would like to thank Rich Oberto for his skill and shared wisdom in electronics. Thanks to Seth Nelson, Richard Fenwick, Frank Blum, and Scott Morris for their assistance in many facets of the project.

CONTENTS

LIST OF FIGURES

LIST OF TABLES

ABSTRACT

Deterioration of concrete due to corrosion of embedded steel reinforcing bars and prestressing strands represent a significant challenge for inspection and maintenance engineers. Cracking, delaminations and spalling that can occur as a result of corrosion of embedded reinforcing steel accelerate bridge deterioration and lead to pot holes and even punch-through of concrete bridge decks. The typical method for detecting delaminations is hammer sounding, which requires hands-on access to the material under inspection. Specialized equipment and lane closures are frequently necessary to achieve the required access. The application of infrared thermography to detect subsurface damage in concrete has the potential to image delaminations from a distance, such that direct access to the surface of the concrete is not required. Thermographic imaging relies on certain environmental conditions to create thermal gradients in the concrete such that subsurface features can be detected. This thesis presents the results of an investigation to determine necessary environmental conditions for the detection of subsurface damage in concrete. To evaluate environmental effects, a large concrete test block has been constructed. Embedded targets in the test block were used to model delaminations in concrete. Environmental factors including wind speed, relative humidity, solar loading and variations in the ambient temperature have been measured by a weather station located on-site with the block. The effects of these environmental factors have been examined to determine their impact on the

detectability of the subsurface targets. Characteristics of optimum inspection conditions for utilizing infrared thermography in the field are discussed.

1

INTRODUCTION

1.1 Goal

Subsurface deterioration in concrete structures presents a significant challenge for inspection and maintenance engineers. Cracking, delaminations and spalling that can occur as a result of corrosion of embedded reinforcing steel can lead to pot holes and even punch-through of concrete bridge decks. Concrete in overpass bridges can separate from the structure and fall into traffic below, presenting a safety hazard for motorists. To prevent these hazards and maintain bridge safety, periodic inspections are performed. These inspections typically consist of visual assessments of bridge condition. Delaminations created by corrosion of reinforcing steel are not visually observable until deterioration has become advanced such that spalling of concrete occurs and repair needs may be urgent. To detect this deterioration during its early stages, when cost-effective repair and mitigation activities can be initiated, improved inspection technologies are needed. Infrared (IR) Thermography is an inspection

technology that measures the infrared radiation from the surface of the concrete. Defects are detected by evaluating the thermal variations across the surface of the concrete. When the temperature of the material is increasing, such as during the daytime when the sun and ambient environment (air temperature) are heating the concrete, the surface area above a delamination warms at a faster rate than surface areas where the concrete is intact. During the nighttime, when air temperatures are falling and the material is cooling, the surface area above the delaminations cools at a faster rate than the intact concrete. Therefore, during the daytime, delaminations can be detected as “hot spots” on the surface of the material, relative to intact concrete. During the nighttime, those areas appear as “cold spots” relative to the intact concrete. Real-time results are acquired using hand held cameras which are easy to use and provide an image of the concrete surface. The overall goal of the research reported here was to provide maintenance and inspection personnel with an effective tool for detecting and monitoring deterioration of concrete bridge without disrupting the traffic flow. The objectives of the research are to

- Determine environmental conditions that enable detection of subsurface defects in concrete
- Develop written guidelines for applying IR in the field

To evaluate the environmental effects, a large concrete test block was constructed with embedded targets to model the effects of delaminations in concrete. Environmental factors including average wind speed, relative humidity, solar loading and variations in the ambient temperature were measured by a

weather station located on-site at the block. Thermal images were collected over a period of 89 days on a surface of the test block exposed to direct solar loading. The resulting data has been analyzed to identify optimum conditions for the inspection of concrete bridges using IR cameras. This report focuses on the study of environmental conditions and their effect on detection of subsurface deterioration using the IR technology. This led to determining favorable conditions to carry out an inspection using the IR thermography. In this study, exposure to full sunlight (i.e. solar loading) is considered. For shady conditions refer to thesis of R. Fenwick.(Fenwick 2009).

1.2 Nondestructive Evaluation

Nondestructive Evaluation (NDE), which is also known as non-destructive testing (NDT) is the evaluation or test of an object or material without damaging the material. These technologies frequently focus on the detection of defects in a material as a measure of damage. It can be an essential component for the inspection of a bridge or structure. Various methods have been used to find defects that decrease a structure's resistance to corrosion or its load carrying capacity. These include:

- Visual Inspection
- Chain Drag
- Hammer sounding
- Corrosion Potential- Half Cell Test
- IR thermography

- Ultrasonics
- Radiography

NDE techniques in general are characterized as active or passive, surface or volumetric. Active techniques are those in which considerable amount of energy, in some form, is imparted to the test specimen or object and corresponding changes in the output energy are studied to assess the presence of defects. For example, ultrasonic testing uses high energy pulses to pass through the concrete and their characteristics are studied which might be effected as a result of flaws such as cracks, delaminations and voids in the structure. Eddy current, Magnetics, Radiography and active Thermography can be cited as examples for active techniques. Passive techniques monitor the test object or specimen in its normal state or under the influence of typical environmental factors without imparting energy to the object. The reaction of the test object to its ambient environment or operating conditions is considered for detecting the defects in passive techniques. Acoustic emission, leak testing and visual inspection are some examples for passive techniques. Surface methods typically detect flaws pr damage at the surface of the material, *Volumetric* methods are used to detect subsurface defects located within a volume of material. Eddy current and Penetrants are chief examples of surface methods where as Radiography and Ultrasonics are good examples for volumetric methods. Selection of right NDE technique depends on various factors like the depth, size, location and orientation of the anticipated defect or flaw. IR thermography has characteristic

of both a surface technique and a volumetric technique, in that it measures the effect on the surface of a defect within the volume of material.

This report focuses on the application of themography for detecting subsurface features in concrete based on the variations in surface temperature at the concrete. Testing has been conducted on a large concrete test block to evaluate the effect of various environmental factors on the detectability of subsurface targets. Specific details of the equipment, data collection scheme, test block design and other experimental details are described fully in Chapter 3, EXPERIMENTAL SETUP. The methodologies used to analyze the data and render useful results are described in Chapter 4, ANALYSIS. Results of the analysis are reported in Chapter 5, RESULTS. The conclusions reached from the analysis of the results are documented in Chapter 6, CONCLUSIONS.

2

BACKGROUND

In this chapter a brief description of basic principles of IR thermography is given. This section provides an introduction to the theory behind thermographic inspections and an overview of various other NDE technologies. The challenges faced in various inspection techniques were also discussed in this chapter.

2.1 Infrared

This section explains infrared radiation and the basic principles of heat transfer along with a brief description of IR thermography method.

2.1.1 Infrared Radiation

The light we see is a very small portion of Electromagnetic Spectrum. Electromagnetic spectrum includes radiation which varies from short wavelength radiation like X- rays to long wavelength radiation, like radio waves. The wavelength of infrared radiation is slightly longer than that of radiation in the visible region. Short wavelength radiation like Gamma rays, X- rays are very dangerous because they carry high energy where as longer wavelength radiation like radio waves are less harmful as they carry less energy. The wavelength that

covers the range from close to 1 µm to 100 µm of the electromagnetic spectrum is typically referred to as infrared range (see Figure 2.1).

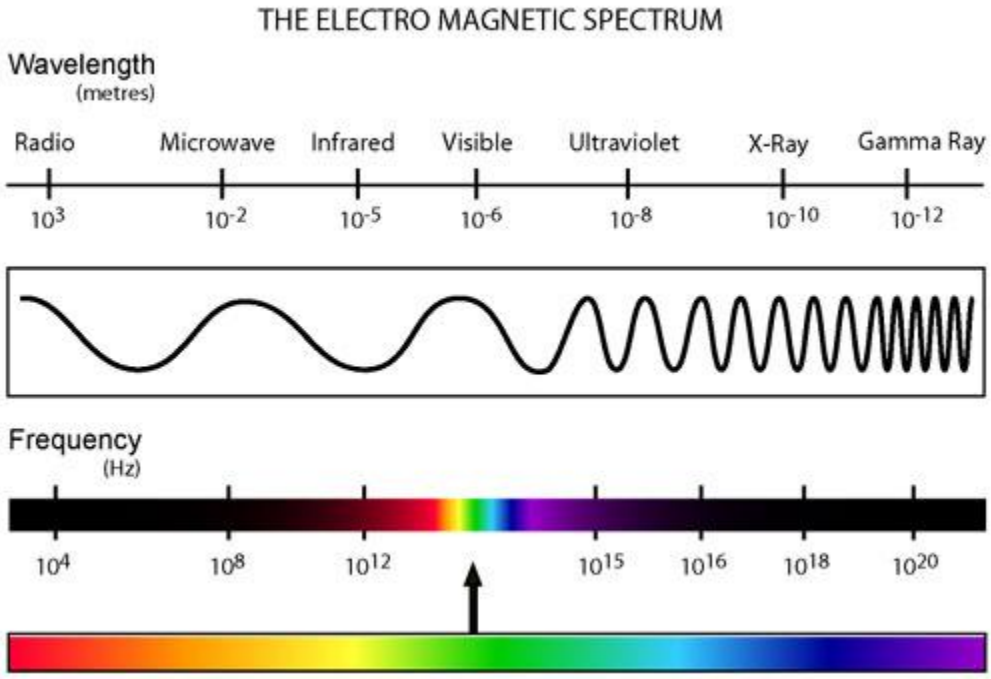

Figure 2.1 : Electromagnetic Spectrum.

2.1.2 Heat Transfer

Any object which is above absolute temperature (0 K or -273°C) emits some form of electromagnetic waves(Clemena G G and Wallace T. McKeel 1978). The amount of energy and the wavelength of waves emitted depend on the temperature and physical properties of the object. These physical properties of an object play an important role in heat transfer mechanisms. Thermal Conductivity and Emissivity are two such important properties. Emissivity of an object or body is defined as the ratio of actual emission from the body to that of a black body. The emissivity of a material is a surface property that expresses the

ability of the surface of an object to emit energy. In other words, the emissivity of an object is a relative measurement of rate at which the object emits radiation, one being a perfect emitter and zero being no emission at all. In general, concrete has relatively high emissivity values, between 0.9 and 1.0. Black body is an idealized object that absorbs all the incident radiation without reflecting thereby behaving as a perfect absorber. Emissivity values are generally available such that the Infrared radiation can be related to the temperature of the objects being observed. The surface roughness of a material will also have an effect of emissivity values, with rough surfaces generally having higher emissivity than smooth surfaces. Thermal conductivity is that property of material that shows its ability to conduct heat. When heat is applied to a portion of a material, that heat will move through the material. This movement of heat through a material is called the thermal current. Depending on the composition of the atoms of that material, the heat movement may happen very slowly, or it may move very quickly. This dependence is quantified by the coefficient of thermal conductivity.

The energy radiated by any object is given by Stefan-Boltzmann law. The Stefan-Boltzmann law describes the total energy radiated per unit surface area as

$$\mathbf{W = \varepsilon \sigma T^4} \qquad \text{.....} \mathbf{2.1}$$

Where W is the total energy radiated, ε is the emissivity of the material, σ is Stefan-Boltzmann constant (5.67×10^{-8} W/(m^2-K^4)) and T is the absolute temperature (K).

The transfer of energy between two bodies which is temperature in this case takes place in three ways: Conduction, Convection and Radiation.

Radiation is the process in which a body is heated up by using the energy radiated from other bodies. All objects radiate and absorb heat. The amount of heat an object radiates and absorbs depends on the temperature, surface condition of the object and the surrounding environment. Thermography uses this emitted radiant energy to measure the temperature of an object.

Conduction is transfer of energy by the collision of atoms with their neighboring atoms. The heat flow in a conductive medium is directly proportional to the temperature difference across the medium. The rate at which heat flows depends upon the object's thermal conductivity. Metals have high thermal conductivity and insulators have low thermal conductivity. The heat flowing through an object is given by

$$Q = \frac{kA(T_2 - T_1)}{L} \qquad \text{.....2.2}$$

Where Q is the heat flow, k is the thermal conductivity in W/(m-K), A is the cross sectional area and L is the object thickness in the direction of heat flow.

Convection is the process in which heat is transferred by the motion of air or fluid. The various processes through which heat transfer takes place in a body are shown in Figure 2.2. The processes are

- Radiant heating from sun
- Radiant heat transfer from object
- Convection via air
- Conduction through concrete

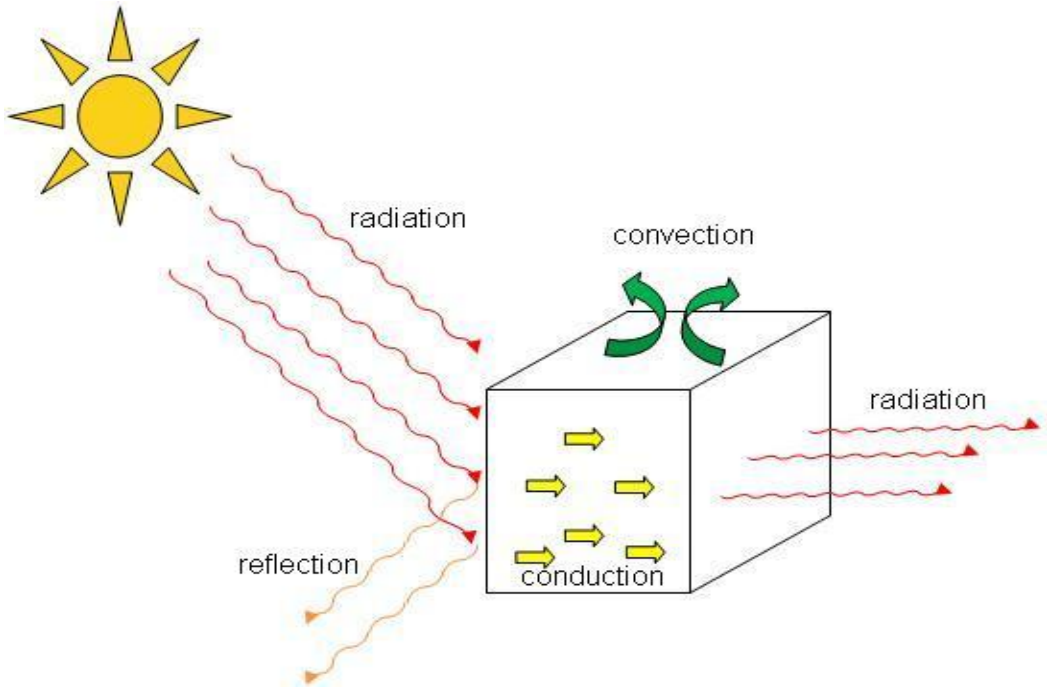

Figure 2.2 : Heat transfer properties for concrete test block.

2.1.3 Infrared Thermography

If infrared radiation measured is used to determine the temperature of an object, the technique is then termed as Infrared (IR) Thermography. Since infrared radiation is emitted by all objects proportionally to their temperatures, infrared thermography allows us to evaluate the variations in thermal condition of the object (i.e. hot or cold). As a result, IR thermography has wide range of applications in various fields. Its application in the field of civil engineering is growing in the recent years as an effective NDE tool. This technology is being used to detect the deterioration in the structures, especially bridges. Cracking, delaminations and spalling that can occur as a result of corrosion of embedded reinforcing steel can lead to pot holes and even punch-through of concrete bridge decks. Delaminations that develop in the concrete manifest in spalling that further

exposes the steel to the corrosive environment, accelerating the deterioration process(Clark et al. 2003). Delaminations typically initiate and develop at or near the level of the reinforcing bars in the concrete as shown schematically in Figure 2.3. The delaminations develop as a subsurface feature in the concrete that may not be observable through visual inspection until the deterioration is in its later stages, where spalling of the concrete has occurred(Maser 1990).

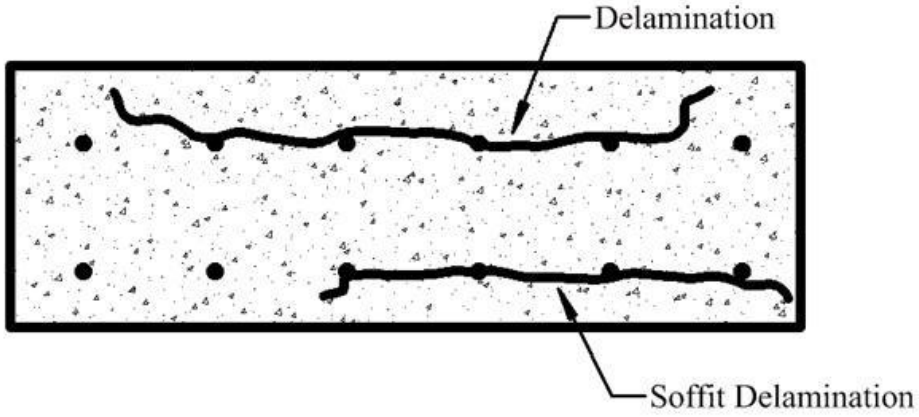

Figure 2.3 : Schematic diagram of delaminations in concrete.

These delaminations disrupt the path of heat flow through the material. The differences in heat flow are manifested as cold or hot spots depending on the temperature gradient in the concrete. These differences in temperature on the surface of concrete can be detected by using IR thermography. The use of IR thermography in civil engineering is mainly to detect corrosion-induced delaminations in reinforced concrete bridges (Carino 94) and early research into the subject was carried out in 1977 by Clemeña and McKeel at the Virginia Highway and Transportation Research Council. They highlighted that because of the immense differences in the volumetric heat of solid concrete and the air in the

delaminated area, the separated concrete was warmer than the sound concrete when exposed to solar heating (Clemena and McKeel Jr 1977). Their research found that more severely delaminated regions gives rise to a stronger thermal contrast. An interpretation of this phenomenon by Holt in 1979 was that the temperature difference at the surface correlates with the depth of the delaminations. In 1980s, Manning & Holt investigated the use of IR thermography for delamination detection, and compared the findings to results achieved with manual methods such as chain drag(Manning and Holt 1983). Concrete cores were utilized to establish delamination depth; thermocouples embedded 6 mm into the deck measured temperatures of sound and delaminated concrete. They determined their deck differentials both under daytime conditions and at night.

Their results suggested that IR thermography was not as accurate as the chain drag technique (ASTM D-4580) even though the thermography method had the capacity to quickly scan large areas, be vehicle mounted, or even attached to a helicopter. Additionally, they pointed out that thermal contrasts could occur at any ambient temperature, but were greatest during period of rapid heating and cooling. Furthermore, they suggested that the surface temperature changes were indicative of the depth of the flaw(Manning 1980), and larger temperature differences are therefore associated with shallower defects.

There has been for many years an ASTM standard test method that describes the condition assessment of bridge decks using vehicle-mounted cameras (ASTM 2007). This test method was first approved in 1988, and

appears to be based on research conducted in Canada and the United States. This research consisted of field testing several bridges with known delaminations, and evaluating the performance of thermography for those specific field conditions. Some data on the environmental conditions necessary for detection of subsurface delaminations are provided, and these conditions are summarized in Table 2.1. The standard test method notes that based on available data, infrared thermography can detect between 80 and 90% of delaminations found in an exposed concrete bridge deck and 80 to 90% in asphalt covered bridge decks. No data is provided for the detection of delaminations in areas not exposed to direct sunlight, i.e. in the shade or for the deck soffit. In spite of being available since 1988, the standard test method has not seen widespread application for the condition assessment of concrete bridge decks.

Table 2.1 : Environmental conditions for deck inspections according to ASTM D 4788-07

Time of Year	Direct Sunlight (hrs)	Change in Ambient Temp.	Wind Speed	Detection Limit (Δ_t)	Notes
Summer	3 hrs	None specified	<30 mph (50 km/hr	0.5° C (1.8°F)	Dry deck for 24 hrs prior to test
Winter	4 hrs	11°C (20°F)	<15 mph (24km/hr)	0.5° C (1.8°F)	Ambient Temp > 0° C (32°F)
Winter, asphalt covered deck	6 hrs	11°C (20°F)	< 15 mph (24km/hr)	0.5° C (1.8°F)	Ambient Temp > 0° C (32°F)

One limitation of this standard practice is that there is no consideration of the depth at which the delaminations are anticipated. Exploration of the reported research referenced in the document revealed that testing was conducted on relatively shallow delaminations between 10 mm (0.39 in.) and 24 mm (1.0 in.)

(Manning 1980), to a maximum depth of perhaps 44 mm (1.73 in.)(based on concrete cover) (Manning 1983). Given that typical concrete cover in a bridge deck is ~51 mm (2 in.), the delaminations on which the specifications are based may not be representative of typical bridge decks in the United States. This may contribute to the lack of widespread application of the test method; as performance in the field would not match that described in the test method if deeper delaminations are to be detected.

The thermal gradient in the concrete is an important factor in the detection of these defects. In order to create this thermal gradient, the structure is exposed to thermal radiance either from external sources or from direct sunlight. At least 4 hours of direct sunshine is needed to set up the thermal gradient according to ASTM standards(ASTM 2007). Thermal gradient in an object can be created by using an external source of energy, typically termed Active IR thermography; and if the thermal gradient in the object is created by the effect of surrounding environment the technique is typically referred to as Passive IR thermography.

In Passive thermography the objects are studied in their normal state for features of interest where as in active thermography an external source of energy is used to create the heat flow. Depending upon the application, method of the energy, active thermography is further categorized as pulsed thermography, step-heating, and lock-in thermography.

In *pulsed thermography* the specimen is heated for a brief period of time and the response temperature curve is observed. The thermal energy applied at the surface starts changing the temperature of the specimen volume through thermal

wave propagation. Once the thermal wave hits a delamination or defect, the diffusion rate decreases. This makes defects appear at a different temperature with respect to surrounding sound concrete. As a result deeper defects will be observed later and with a reduced contrast. In fact, the observation time t is function (in a first approximation) of the squared of the depth (z) and the loss of thermal contrast (c) is proportional to the cube of the depth(z) (Maldague 2000).

$$t = \frac{z^2}{\alpha} \quad and \quad c = \frac{1}{z^3} \qquad \textbf{2.3}$$

Where α is the thermal diffusivity of the material.

In step lock, also called as long pulse thermography the surface is monitored with the application of step heating. The variations of surface temperature are related to the specimen features. This technique is sometimes referred to as time-resolved infrared radiometry or TRIR. TRIR finds applications such as for coating thickness evaluation (including multi-layered coatings)(Aamodt et al. 1990). In the lockin thermography thermal waves are generated in the test specimen a the permanent regime. The specimen is exposed to sine modulation heating which introduces thermal waves of frequency ω inside the material. The resulting oscillating temperature field in the stationary regime is remotely recorded with the infrared camera. The lockin terminology refers to the necessity to monitor the exact time dependence between the recorded temperature signal and the reference signal *(i.e.* the sine-modulation heating) (Busse et al. 1992). For applications in civil engineering, variations in ambient temperature and

radiant heating from the sun provide the thermal excitation for the detection of subsurface defects.

2.1.4 Environmental Factors

For civil structures, several different factors affect the heat transfer in concrete exposed to the ambient environment. The important environmental factors that affect the ability of thermography to detect subsurface defects in concrete include solar loading, ambient temperature changes, and wind speed. Relative humidity has also been suggested in the literature as a factor (Manning 1983). This section briefly describes what each of these environmental parameters and why it affects the thermal contrast developed from a subsurface defect in concrete.

A primary driving force for the development of thermal gradients in concrete is radiant heating from the sun. Radiant energy from the sun imparts thermal energy into the surface of the concrete that causes the concrete to heat up (Figure 2.2). The surface heats up at a much higher rate than the core of the concrete, developing a thermal gradient with high temperatures at the surface and cooler temperatures at depths into the concrete. To achieve thermal equilibrium, the heat at the surface of the concrete is transferred (conducted) toward the core of the concrete. The amount of solar loading may be expressed as the radiant energy of the sun measured in Watts/m^2, which is the radiant energy at a given point in time. In this research, the *solar loading area* or amount of solar radiation energy was developed as a parameter for analysis of the

effects of direct sun exposure. The solar loading area was found by determining the area under a solar radiant energy curve over a given time period.

The temperature of the air surrounding the concrete will also impart a thermal gradient. In the daytime, when temperatures are typically rising over the course of a day, the ambient air temperature is higher than the temperature of the concrete, and as a result heat is transferred into the concrete to move the concrete toward thermal equilibrium with its surroundings. This will establish a thermal gradient in the concrete, as the surface warms faster than the core of the concrete. Obviously, the greater the difference between the ambient air temperature and the concrete, the larger the thermal gradient established. The temperature of the concrete lags in time relative to changes in the ambient environment, due to its large mass and low thermal conductivity. As a result, if there are large changes in the ambient environmental temperature, there will develop a large difference between the temperature of the air and the temperature of the concrete, therefore a greater thermal gradient. For this reason, the change in the ambient temperature over the course of the day is the parameter that controls the level to which a subsurface target will affect the surface temperature of the block, i.e. be detectable with a thermographic camera. The actual environmental temperature really plays no role at all; the thermal gradient would be the same if the air were maintained at 40°C (104°F) or if it were maintained at 0°C (32°F), if the concrete was in thermal equilibrium with its surroundings. However, if the air temperature were to change from 0 to 40°C (32

to 104°F) over a period of 10 hrs, the concrete temperature could not change fast enough and a thermal gradient results.

The rate of heat transfer between the ambient air temperature and the concrete is controlled by convection (Figure 2.2). The rate of convective heat transfer typically depends on a number of factors, including the ambient air temperature and wind speed. For a large difference in temperature between the concrete and the air, the rate of convective heat transfer can be large. If the wind speed is high, the convective heat transfer will be increased. This is analogous to blowing on a bowl of soup to cool it off. The result of these effects is that the high rate of convective heat transfer can reduce effects of radiant heating from the sun by cooling the surface of the concrete, making it more difficult to detect a subsurface defect in the concrete by reducing the thermal gradient. In other words, the wind blowing on the surface that is warmer than the ambient air due to radiant heating from the sun has the effect of cooling the surface, making the surface temperature closer to the core temperature and reducing the thermal gradient. However, if the air temperature were greater than that of the concrete, then increased convective heat transfer would warm the surface of block, and this would occur more rapidly if wind speeds were high than if wind speeds were low. Therefore, in the absence of radiant energy from the sun, high wind speeds could increase the thermal gradient, and therefore make subsurface features more readily detected than they otherwise would. Conversely, at night, when air temperatures are cooler than concrete temperatures, high wind speeds could increase the negative thermal gradient in the concrete. The effect of wind speed

on the detectability of subsurface features in concrete has been studied here for conditions when radiant energy from the sun is available to heat the concrete block.

Convective heat transfer properties are also affected by the relative humidity of the ambient air surrounding the concrete (Zhang et al. 2007). Increases in relative humidity increase the convective heat transfer coefficient, increasing the rate of heat transfer. As a result, it would be expected that humid air would transfer heat into the concrete more rapidly than dry air, increasing the thermal gradient and thus having a positive effect on the detectability of subsurface features in the concrete.

2.1.5 IR Cameras

A camera consists of three basic components the lens, the photographic film and the mechanical device. In digital cameras the film is replaced by a series of image sensors. Each image sensor is a charged-coupled device (CCD) which converts light into electric charges. Infrared camera works on the same basic principle of a camera except that it detects infrared radiation. The electric charges created by the incident infrared light are converted into a color image where a particular temperature is associated for each color in the image. There are wide varieties of infrared cameras available in the market for various applications. For the purpose of the research a FLIR S65 camera was used, shown in Figure 2.4. The specifications of S65 camera is shown in Table 2.2.

Table 2.2 : Table of Specification for S65

Characteristics	Specifications
Thermal Imaging Performance	
Field of View / min. focus distance	24°×18° / 0.3 m
Spatial Resolution (IFOV)	1.3 mrad
Thermal Sensitivity	0.08°C to 30° C
Image Frequency	50/60 Hz
Focus	Automatic / Manual
Detector type	Focal Plane Array (FPA), Uncooled microbolometer 320×240 pixels
Spectral Range	7.5 to 13 µm
Measurement	
Temperature Range	-40°C to +1500°C
Accuracy	+/-2° C, +/-2% of reading
Measurement Mode	Spot/Manual (up to 10 movable), Isotherm, Line profile
Image Storage	
Type	Removal Flash Card (256 MB) Built- in Flash Memory (50 images)
File Formats	Thermal Standard JPEG, 14 bit measurement data included and Visual Standard JPEG (including movable marker) linked with corresponding thermal image
Battery System	Li-Ion rechargeable, Field replaceable
Environmental Specifications	
Operating Temperature Range	-15°C to +50°C
Storage temperature range	-40°C to +70°C
Interfaces	
FireWire	IEEE-1394 FireWire output
USB / RS	232 Image (thermal and visual), measurement, voice and text transfer to PC

Figure 2.4 : FLIR S65 Camera.

2.2 Inspection Technologies

There are various other NDE inspection technologies available for use, depending upon the defect features and its location in a structure. This data is provided to establish the state of the practice for highway bridge inspection and compare alternative methods to IR thermography. The four most commonly used inspection technologies for delamination in concrete are described briefly along with their benefits and limitations.

2.2.1 Hammer Sounding

Hammer sounding of concrete is a tried and tested method of determining variations in the subsurface area of structure, and is a common tool to accompany visual inspection. If a hammer or tool is used to strike the delaminated area, a hollow tone is produces, in comparison to the high pitched ringing noise produced when sound concrete is struck. The limitations of this method include that each individual has a slightly different assessment of the sound produced and is further complicated by the likely presence of traffic noise.

2.2.2 Pulse Velocity Method

The velocity of compressional waves through a solid depends on the material elastic constants and density. This the principle on which pulse velocity method works. The compressional wave velocity *V* in a homogeneous solid medium is given by

$$\boldsymbol{V} = \sqrt{\frac{\boldsymbol{KE}}{\boldsymbol{\rho}}} \qquad \textbf{2.4}$$

Where $\boldsymbol{K} = (1-\mu)/\big((1+\mu)(1-2\mu)\big)$, μ is the Poission's ratio, $\boldsymbol{E}$ is the modulus of elasticity, and ρ is the density. The variations in E and ρ have more significant effect on $\boldsymbol{V}$ than variations in μ and $\boldsymbol{K}$ (Popovics 2003). The velocity of propagation is given by the relation between the frequency *f* (in Hertz) and wavelength λ (units of length) as $V = f\,\lambda$.

The defects in the concrete structure cause variations in velocity of pulse due to different densities. To measure the pulse velocity a pulse generator transmits waves and a receiver (sensor) at a distance L receives the pulse. The time T for the compressional pulse to travel through the concrete is noted. The pulse velocity is then given by

$$\boldsymbol{V} = \boldsymbol{L}/\boldsymbol{T} \qquad \textbf{2.5}$$

This method is good for detection of larger defects (> 10 cm), and uniformity of the material(Popovics 2003). But it has limitations in detecting surface cracks, condition of embedded steel, smaller defects and defects away from testing location.

2.2.3 Impact – Echo Method

This is a NDE technique in which the stress waves are generated using some impact on the concrete or masonry structures and characteristics of reflected waves are studied which might be a result of flaws such as cracks, delaminations and voids in the structure. A typical setup for an impact echo method is shown in the Figure 2.5.

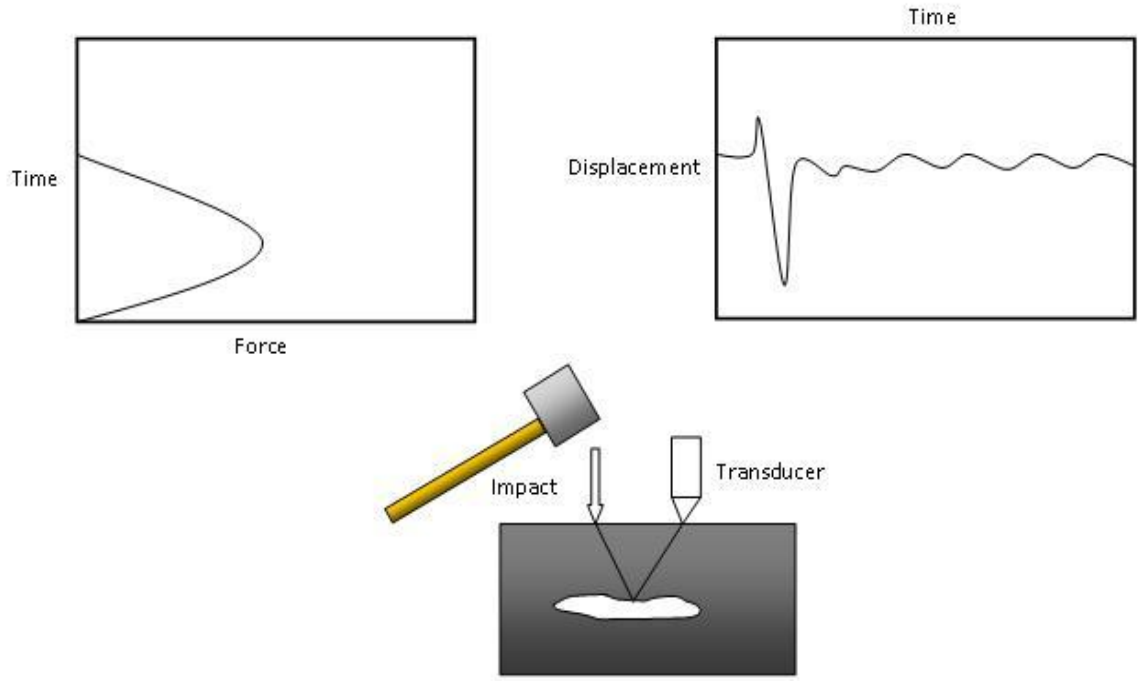

Figure 2.5 : Typical setup for an impact echo method.

The three basic components to carry out an impact echo test are as follows

- A mechanical impactor,
- A receiver to measure the response, and
- A data acquisition system

The compressional velocity of the wave V, the thickness t and the fundamental impact echo frequency F are related as shown in equation

$$\boldsymbol{F = \beta V / 2t} \qquad \textbf{2.6}$$

Where $\boldsymbol{\beta}$ defines the cross sectional shape of the structure(Popovics 2003).

In order to measure the surface motion correctly the transducer has to be effectively attached to the concrete surface. The other vital factor for the success of the test is duration of impact. As an approximation the highest frequency component of the significant amplitude of the input signal and the contact time are inversely proportional to each other(Carino 2001). The input pulse must contain the correct frequency to create resonant vibration corresponding to the thickness. Thus as the contact time increases, the amplitude of frequency components increases but range of frequencies decreases. The detection of flaws in a concrete structure using this method depends on several factors including the size of the flaw and its orientation, depth of the flaw, the contact time and the homogenity of structure.

This technique is very useful when there is only access to one surface and proves to be very effective if the flaws are parallel to the surface. The results can be difficult to interpret and require some technical proficiency.

2.2.4 Ground Penetrating Radar

Ground Penetrating Radar (GPR) is one of the inspection technologies being employed for condition assessment of concrete. In this technique, high frequency electromagnetic waves (in the range of 0.5 to 5 GHz) are launched

into a concrete deck, and reflections caused by the differences in electromagnetic properties of the subsurface features are detected and analyzed to determine where deterioration exists. GPR results are based on the measurements of time delay and the amplitude of the reflected signal. When the wave hits a buried object or a boundary with a different dielectric constant, the receiving antenna records variations in the reflected return signal. Using GPR technology for bridge decks can require a considerable amount of lane closure. The results obtained are complex in nature and often requires experienced personnel to interpret the results (Yehia et al. 2007).

3

EXPERIMENTAL APPROACH

In this section, the experimental setup both for the lab and the field are discussed. A detailed explanation of how the data is collected and processed is given in later sections of this chapter. The development of infra units for transferring the bridge data in the field to a central database for further processing is discussed. The development of the web page to retrieve the past weather data at a place is also discussed.

3.1 Lab Test Setup

This section describes the preparation of lab test and the equipment used in this test. The laboratory test was conducted prior to the field test to serve as a mock up of field test design and proof of concept test. Some information about how the data is collected is also explained. The lab test was carried out prior to field test. The main purpose of conducting the lab test was to prepare for any unforeseen problems that may arise from the materials we used to create the targets and from the procedure adopted to acquire data from the test block in the field.

To carry out this test, a concrete block with dimensions 91.4 × 91.4 × 15.2 cm was constructed. Nominal reinforcement was used in the block. To create the effect of defects in the block, two Styrofoam pieces 12.7 × 12.7 cm were placed at 25 mm and 51 mm (1 and 2 inch) deep on the opposite corners of the block. Styrofoam was used because its thermal conductivity is close to that of air. Six thermocouples were placed in the concrete block through the thickness to get the internal block temperatures. Figure 3.1 shows the casting of block along with the thermocouples, Styrofoam pieces and reinforcement.

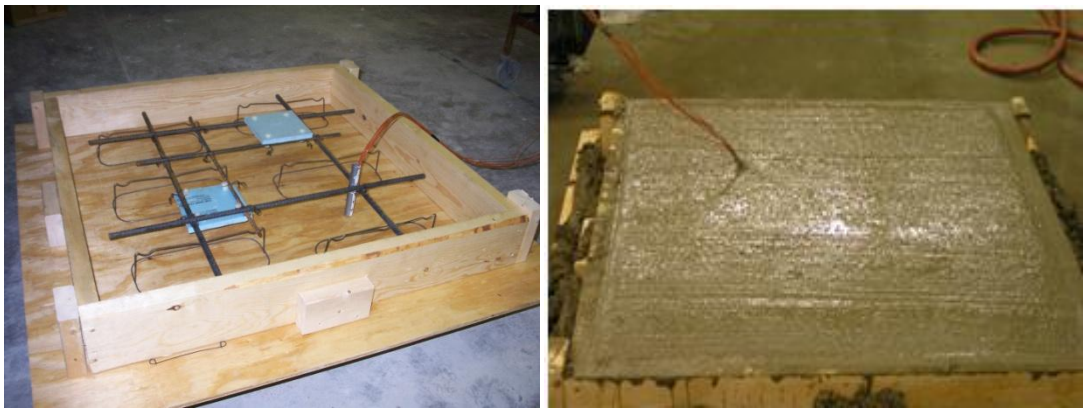

(a) (b)

Figure 3.1 : Test block built for the Lab test (a) before and (b) after pouring concrete.

3.1.1 Heat Source

A radiant heater was used as a heat source. The heater was placed at a height 6 ft vertically above the block. The radiant heating provided a uniform heat input at the surface of the block.

3.1.2 IR Camera

The infrared camera, FLIR S 65 was used to collect images of the test block. The camera was connected to the computer and was operated by ThermaCAM Research Professional Software. The camera was configured to takes image of the block for every minute. The properties of camera were shown in Table 2.2.

3.1.3 Thermocouples

Standard thermocouples were cast into the test block to monitor the actual temperature gradient through the concrete. A small thermocouple array was built. Using a 25 mm inside diameter PVC pipe, 6 Type J Teflon coated fused thermocouples were mounted through drilled holes at 0, 25, 51, 76, 102, and 127 mm depths. Temperatures were monitored at 1 minute intervals at the same time as the thermal images. The thermocouples were linked to computer program to collect data at intervals of one minute. An additional thermocouple was used to monitor room temperature during the test.

3.1.4 Tests

Six tests were carried on the block with different heating times of 1, 2, 4, 8, 16 and 32 minutes. The heating times indicates the time for which the block is exposed to radiant heating. The block was then allowed to cool down to the room temperature before carrying out the next test. The thermocouple data and the infrared data was collected and stored in the computer every minute during both the heating and cooling periods of the block. The results from these tests are shown in Chapter 5.

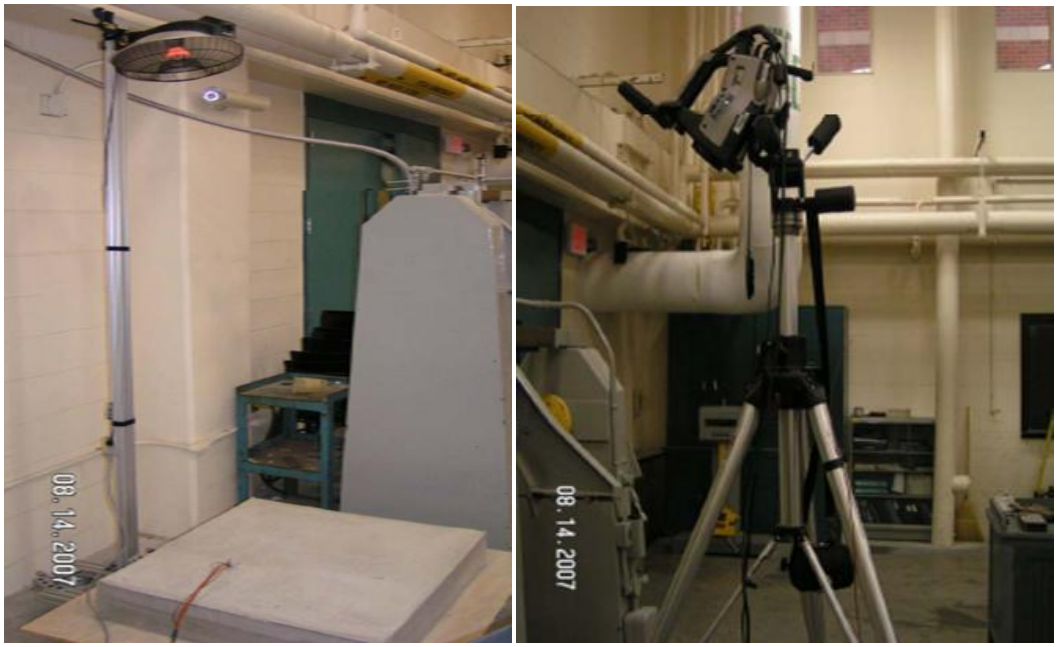

Figure 3.2: Lab Test set up with the heater and IR camera.

3.2 Test Block

This section explains the experimental design for the field test and the equipment used for collection and processing of the data. This field data was used in developing the desired guidelines for thermographic inspection. The data that was acquired over a period of 89 days on the sunny side was used to analyze the effect of environmental variables.

3.2.1 Test Block

A concrete block of dimensions 2.4 m x 2.4 m x .914 m was built in Columbia, Missouri. The concrete block was built at University of Missouri Columbia (UMC) dairy farm which is 3.5 miles north from I – 70 (exit 121). The location of the block is shown in Figure 3.3

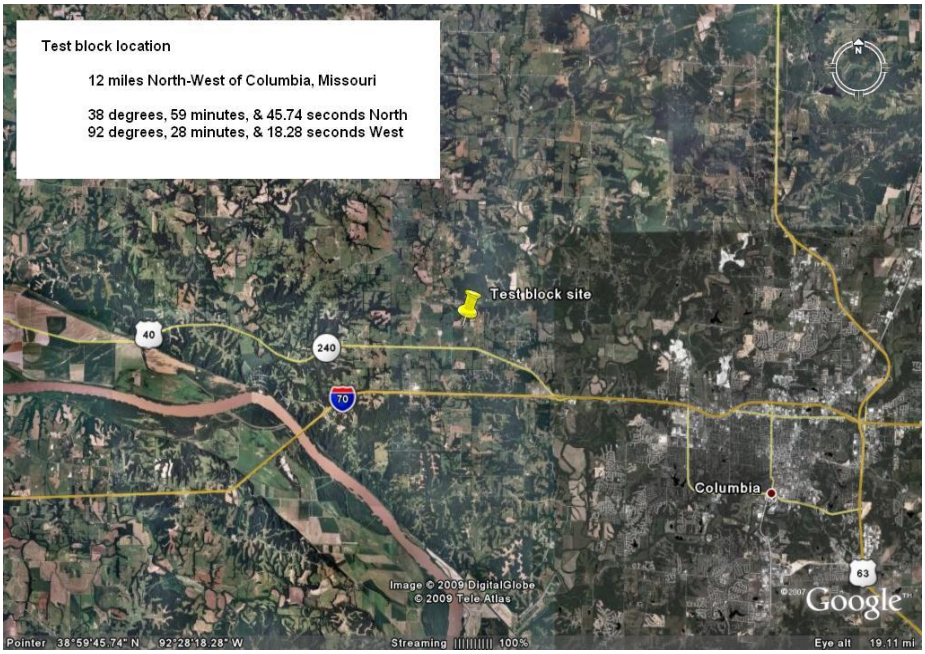

Figure 3.3 : Location of Field Test Block.

Styrofoam pieces 305 mm x 305 mm x 13 mm thick were placed at different depths from the surface on all faces of the block to model subsurface defects (delaminations). Styrofoam placed on both faces of the block simulates the delaminations in concrete on both sides of the bridge deck (the solar exposed surface and the soffit of the bridge). The south face of the block represents bridge surfaces exposed to direct sun light (top surface of the bridge) and the North face of the block represents the shady side, which is similar to the underside or shaded portion of bridge. The Styrofoam targets were placed at depths of 25, 51, 76 and 127 mm. There were also Styrofoam pieces of same thickness on east and West face of the block at 25 and 76 mm deep from the surface. The location of these Styrofoam pieces is shown in Figures 3.4, 3.5 and 3.6. The location of the Styrofoam targets is the same on the East side and West

side. The details of the Styrofoam targets on all faces of the test block are shown in Table 3.1.

Table 3.1 : Depth and location of embedded Styrofoam targets for all test block surfaces

Surface of Block	Embedded Target (Styrofoam) Label & Depth (in mm)			
	A	B	C	D
	25	**51**	**76**	**127**
North	X	X	X	X
East	X		X	
South	X	X	X	X
West	X		X	

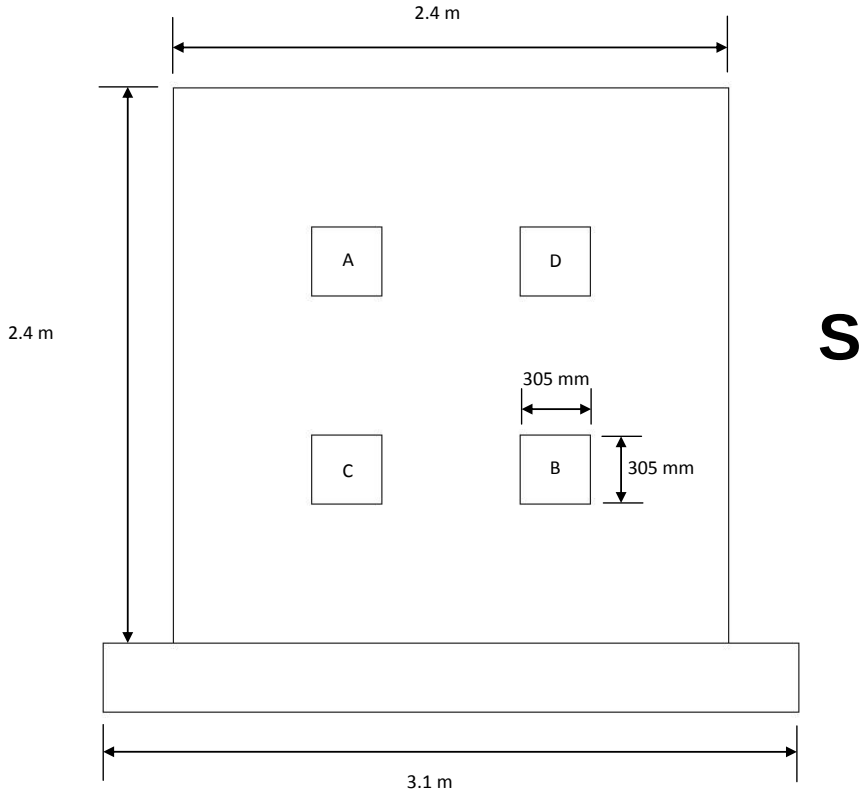

Figure 3.4 : South Face of the Test Block with location of Styrofoam targets.

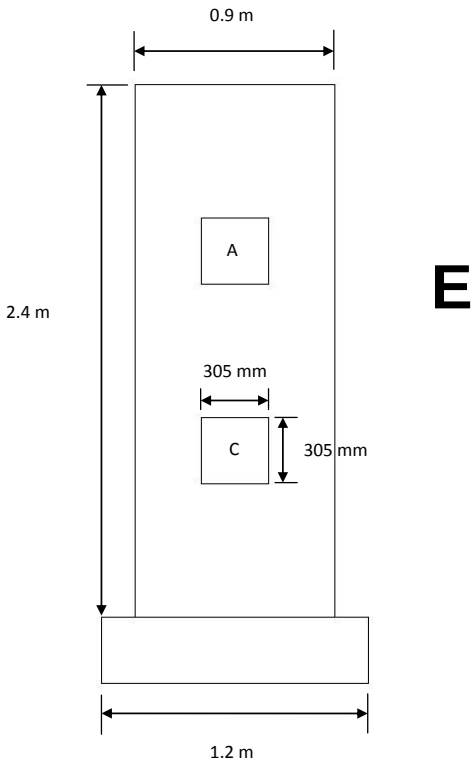

Figure 3.5 : East Face of the Test Block with location of Styrofoam targets.

Figure 3.6 : Photograph showing the North face of the block with Styrofoam targets and Thermocouple Arrays in PVC tubes.

3.2.2 Thermocouple Array

To monitor the thermal gradients in the test block, arrays of thermocouples were mounted in the test block. There were two arrays for both the width and depth of the block. Each thermocouple array runs parallel to an identical array. Two arrays were used in case one failed. Sensors were closer together for near surface locations, and more spread out toward the center of the block. Thermocouple depths for the South-North array were at 0, 25, 51, 76, 102, 127, 152, 305, 457, 610, 762, 787, 813, 838, 864, 889, and 914 mm (mirrored at the 457 mm midpoint). Thermocouples depths in the East-West array were 0, 25, 51, 76, 152, 305, 1219, 1676, 2134, 2286, 2362, 2388, 2413, and 2438 mm (mirrored at the 1219 mm midpoint). Figure 3.7 shows the layout of thermocouple array of east half of the test block.

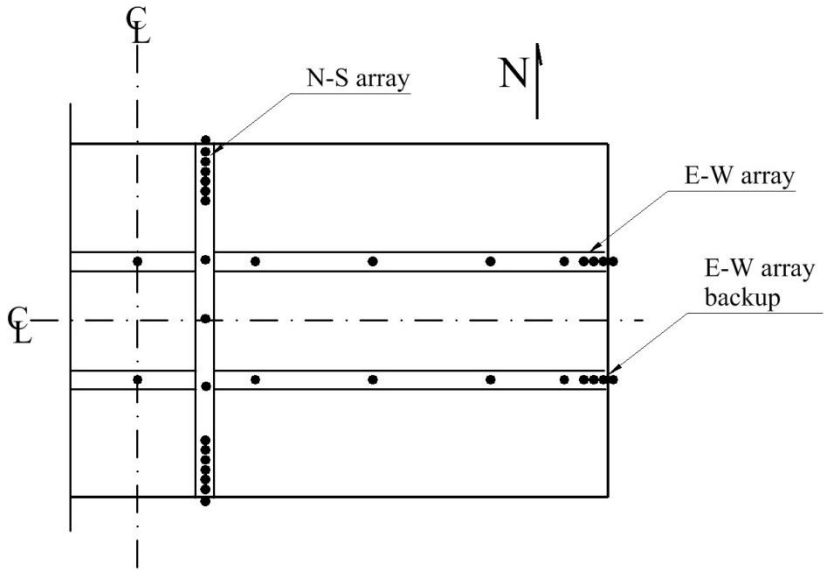

Figure 3.7 : Layout of Thermocouple Array in Test block.

3.2.3 Thermal Camera

To collect the infrared images of the block, a research grade camera, ThermaCam S65 from FLIR, was used. The specifications for the S65 were given in Table 2.2. The infrared image of the block can be viewed through a LCD monitor that is attached to the camera. The camera is connected to the computer and is operated using ThermaCam Researcher Professional 2.8. The images of the block were stored at 10 min intervals on to the hard drive attached to the computer.

A snap shot the software displaying a live image is shown in the Figure 3.8. The captured image can be adjusted using this software. An infrared image is basically a normal image except that each pixel in the image corresponds to a particular temperature which is represented using a color scale. The color scale depends upon the type of palette selected. The most important feature in adjusting the image is the Span. The span is difference between the maximum and minimum temperature on a particular infrared image. The span has to be selected carefully so that the points of interest can be clearly visualized. In Figure 3.8, the span is set at 20.7°C and 26.2°C. With this span the details can clearly seen.

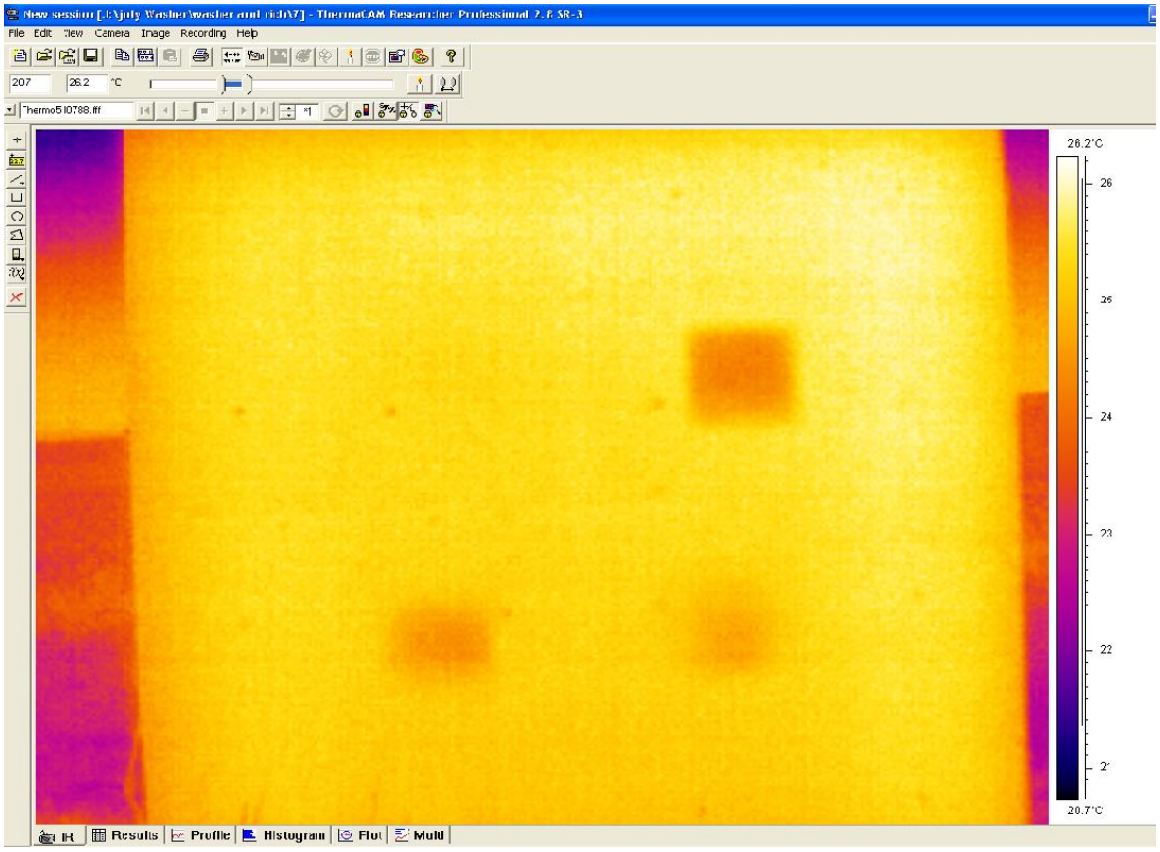

Figure 3.8 : Snapshot of ThermaCam Researcher Pro 2.8.

3.2.4 WeatherHawk

In order to get the real-time data on various environmental factors a WeatherHawk™ weather station shown in Figure 3.9 was installed at the test site. The weather station was mounted onsite on top of a 4.3 m extended tripod frame approximately 9.1 m from the test block.

Figure 3.9 : WeatherHawk Weather Station.

Table 3.2 displays the parameters measured by the WeatherHawk system.

Table 3.2 : Various Environmental Factors measured by WeatherHawk along with units

Variable	Sensor Type	Units
Air Temperature (Ambient)	Thermistor	°C
Barometric Pressure	Piezoresistive transducer	kPa
Solar Radiation	Silicon pyranometer	W/m^2
Rain gauge	Tipping bucket Tipping bucket	mm
Wind Speed	Cup anemometer	m/s
Wind Direction	Vane	360° mechanical
Relative Humidity	Precision, temperature corrected, bulk polymer	Percentage

3.2.5 Data House

To store and shelter the data acquisition equipment, camera, and computer, a secure and temperature controlled data house was built, as shown in Figure 3.10. It was made as a small insulated work station (internally about 0.9 m x 0.9 m x 2.3 m high) with a roof sloping away from the viewing aperture,

and thermostatically controlled air conditioning and heating units to deal with the extremes of mid - Missouri weather.

Figure 3.10 : Data House with inside layout.

The computer and vital equipment were powered through surge protection and an Uninterruptible Power Supply (UPS) to account for short power failures and surges in the area. The UPS could run the vital equipment for up to 30 minutes in the case of a power failure.

The collection of thermocouple data requires specialized equipment for signal conditioning of the raw data, which converts, displays and stores the necessary information. Figure 3.11 shows the conceptual diagram of the field test setup. Figure 3.12 shows the weather station in between the test house (left side in the figure) and the test block.

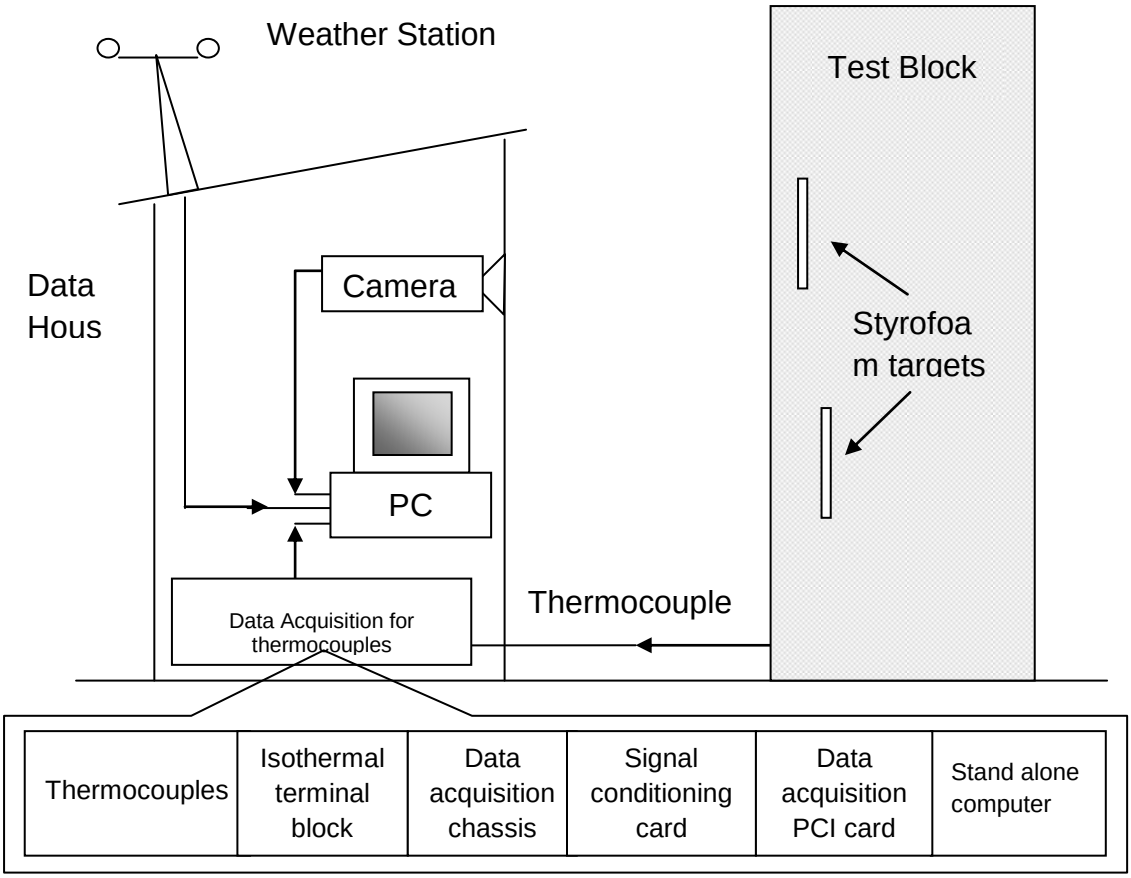

Figure 3.11 : Schematic diagram of test setup.

National Instruments data acquisition equipment was used, and LabVIEW was employed as the hardware/software interface. A snapshot of the Labview program is shown in the Figure 3.13. LabVIEW is used to display and store thermocouple temperature data along with the WeatherHawk data every minute. On the left is the list of 32 channels collected from the embedded thermocouples, next to the respective temperatures. A wave form per second (lower plot) and per minute (upper plot) is also shown in Figure 3.13.

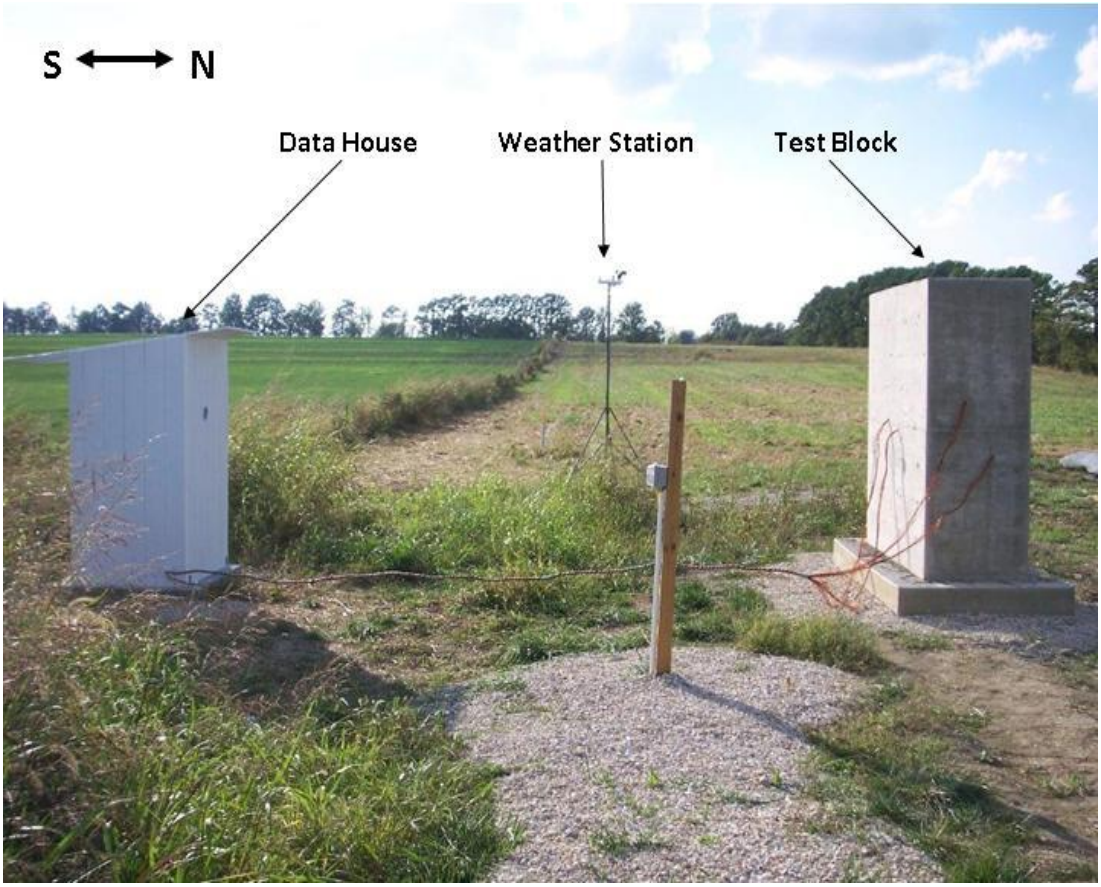

Figure 3.12 : Research site layout.

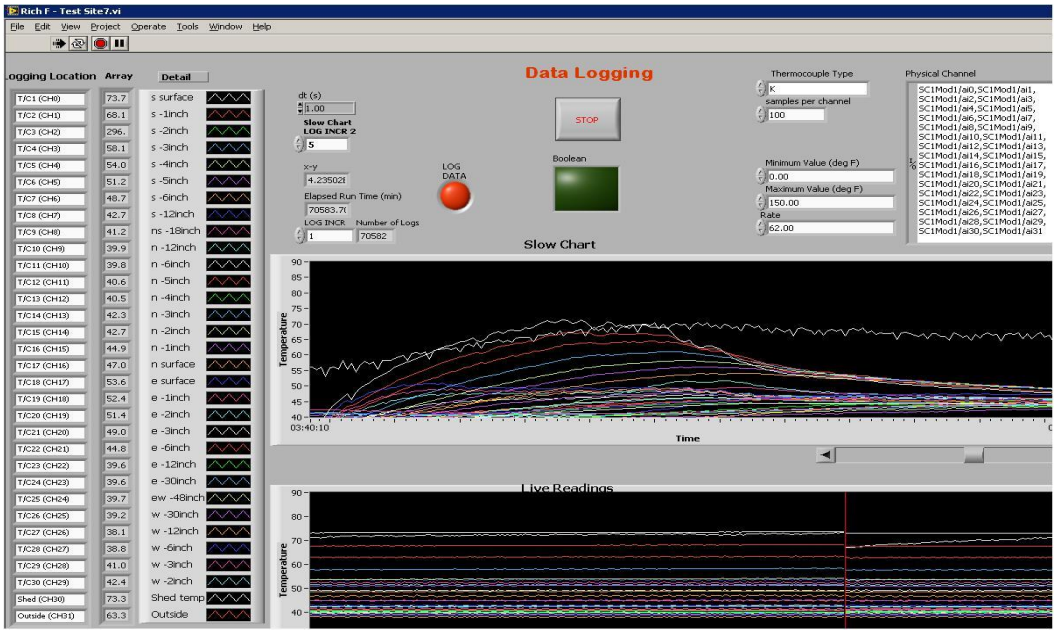

Figure 3.13 : Snapshot of LabVIEW Program.

3.3 Data Processing

This section explains how the data from various sources like WeatherHawk, Thermocouples and ThermaCam S65 is collected, processed and reduced.

3.3.1 Data Recording

Once the experimental set up was complete, each system was configured to synchronously record and display the necessary data. Each minute, all 32 thermocouple measurements were stored in a continually updated LabVIEW data file, which could be converted to a Microsoft Excel file when necessary. The data for all the environmental variables was stored for every minute and could be retrieved and converted from a .csv file to excel file when necessary using the WeatherHawk software. The thermal images were captured and stored on the hard drive every 10 minutes, since it would have taken up too much space for images to be stored every minute. Also, during pre-tests it was noted that negligible changes occurred between one minute images, and such that a 10 minute interval for images of the block was sufficient to characterize the thermal behavior.

3.3.2 Thermal Data Processing

The IR data which was collected in the form of images needed to be represented as numeric values for further analysis. Most importantly, surface temperature differentials are needed for quantitative analysis. To extract the surface temperature at the targets and at the sound concrete a template was developed using the researcher software. In this template a location was

selected close to the center on each target area, for example location A in Figure 3.14 and one area is selected in between the four delaminated areas on sound concrete like location B in Figure 3.14. The embedded targets appear as white areas on the figure, indicating a different temperature from sound concrete

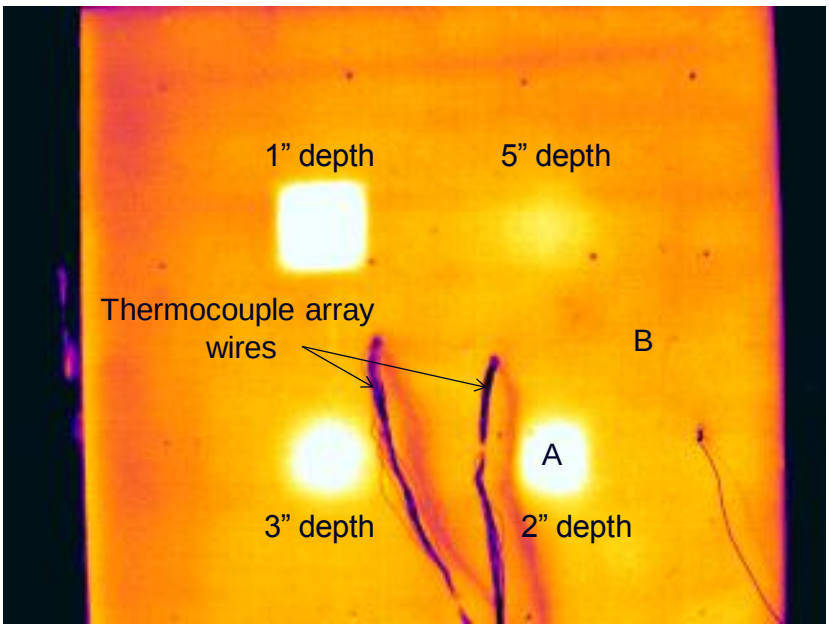

Figure 3.14 : Template showing the 4 target locations and measurement points on South Face of the test block.

Location B measures the temperature of the sound concrete. Using these surface temperatures of sound concrete, thermal contrast for each target area(relative to sound concrete) was calculated. The equation 3-1 shows the equation used to calculate the thermal contrasts.

$$T_{contrast} = T_A - T_B \qquad \textbf{3-1}$$

The result is four thermal contrasts (temperature differentials) that represent the temperature difference between a defective area (target area) of

concrete relative to sound concrete in the same image. This provides a numerical value for the color contrast that can then be used to process data more effectively than simply comparing multiple images.

The camera was configured to capture a thermal image every 10 minutes. These images were then processed using consistent locations for determining the thermal contrast at each target. The process is shown schematically in Figure 3.15. The same locations were selected for analysis in every image, as shown in the figure. This provided a thermal contrast value for each target location as a function of time, such that the thermal behavior could be assessed and compared with environmental variables that vary with time.

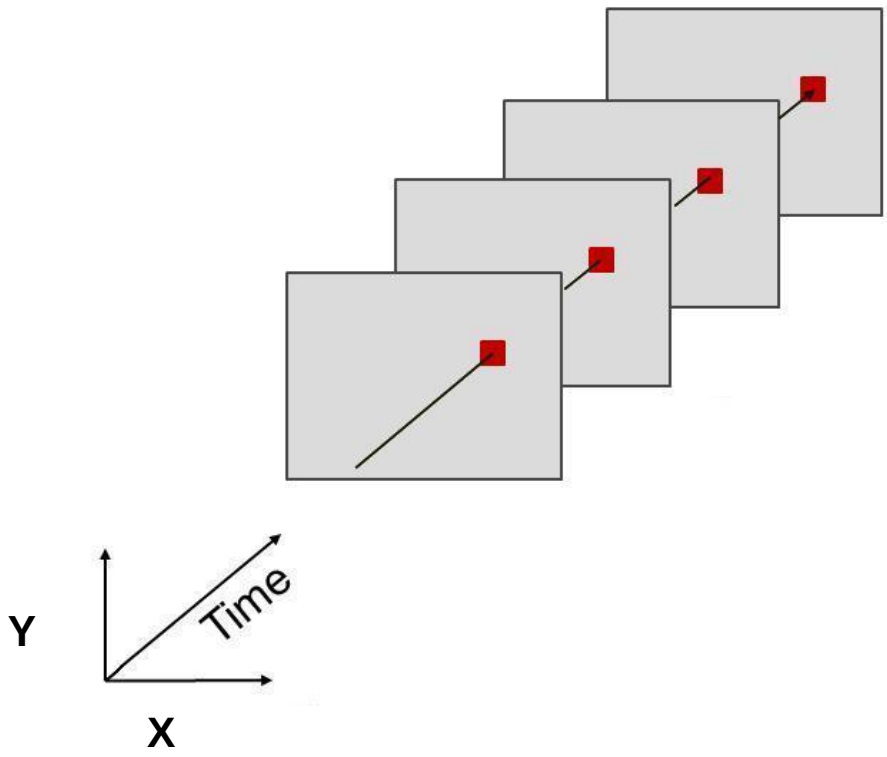

Figure 3.15 : Thermal contrast taken from image pixel every 10 minutes.

Figure 3.16 shows an example of thermal contrast for each of the four targets over a typical 24 hr time period. The horizontal axis is Time over a 24 hour period. As can be observed in this figure, the thermal contrast for each of the targets develops at different times of the day, with deeper targets developing thermal contrast later in the day. Additionally, the magnitude of the thermal contrast, that is the peak contrast value, is reduced as the target depth increases. This is the behavior anticipated based on fundamental heat transfer theories.

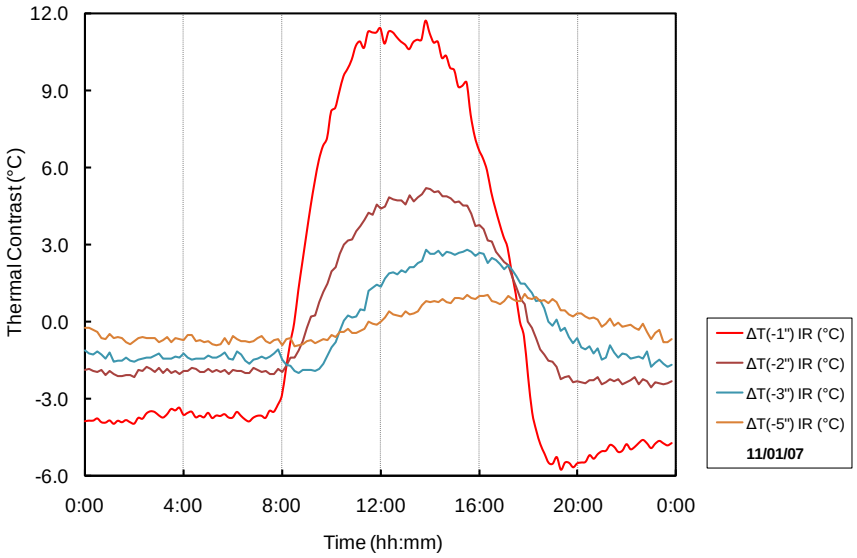

Figure 3.16 : Thermal contrast for a 24 hr time period.

3.3.3 Data Reduction

To reduce data and support analysis we have taken 10 minutes as base interval and applied the same to process other data including thermocouple data and WeatherHawk data. The 10 minute interval was chosen as it was sufficient

to represent the changes in the recorded environmental data. A MATLAB code was used to reduce the 1 minute data to 10 minute data which takes tenth minute data point to correspond to the IR data. Table 3.3 shows the summary of the data reduction.

Table 3.3 : Summary of Data Reduction

Variable	**Sampling Frequency**	**Measurement Frequency**	**Analysis Frequency**
Thermocouples	1 second	1 minute	10 minutes
Weather Station	1 second	1 minute	10 minutes
Thermal Camera	N/A	10 minutes	10 minutes

3.4 Other Developments

In addition to the test site, two resources for inspectors were developed as part of the research effort. These are a weather website, which provides real time information for inspectors and the other resource is Infra unit which consists of computer and cellular modem to retrieve the weather data from any place.

3.4.1 Weather Website

To provide access to real time weather data for the inspectors in the field a webpage was developed using data from Meteorological Assimilation Data Ingest System (MADIS). MADIS is dedicated toward making value-added data available from the National Oceanic and Atmospheric Administration's (NOAA)

Earth System Research Laboratory (ESRL) Global Systems Division (GSD) (formerly the Forecast Systems Laboratory (FSL)) for the purpose of improving weather forecasting, by providing support for data assimilation, numerical weather prediction, and other hydro meteorological applications. MADIS also includes an Application Program Interface (API) that provides users with easy access to the observations and quality control (QC) information. The API allows a user to specify station and observation types desired. A program was developed to show weather trends over the previous 14 day period at a specific bridge location. The website http://madis.noaa.gov/ was used to get the weather data by using the GPS coordinates. The website displays the weather data recorded at a weather station nearest to the given coordinates. A server was setup in MU campus which constantly updates every hour and stores the weather data. This page develop for this research displays the ambient temperature, wind speed and relative humidity of a particular location. The location has to be defined by entering the latitude and longitude. The page provides the name of the nearest station to the location and also displays the most recent ambient temperature, wind speed and relative humidity values. Figure 3.17 shows the login page for the website. After entering the appropriate credentials the next webpage would be displayed which is shown in the Figure 3.18.

Figure 3.17 : Login page of the Weather Website

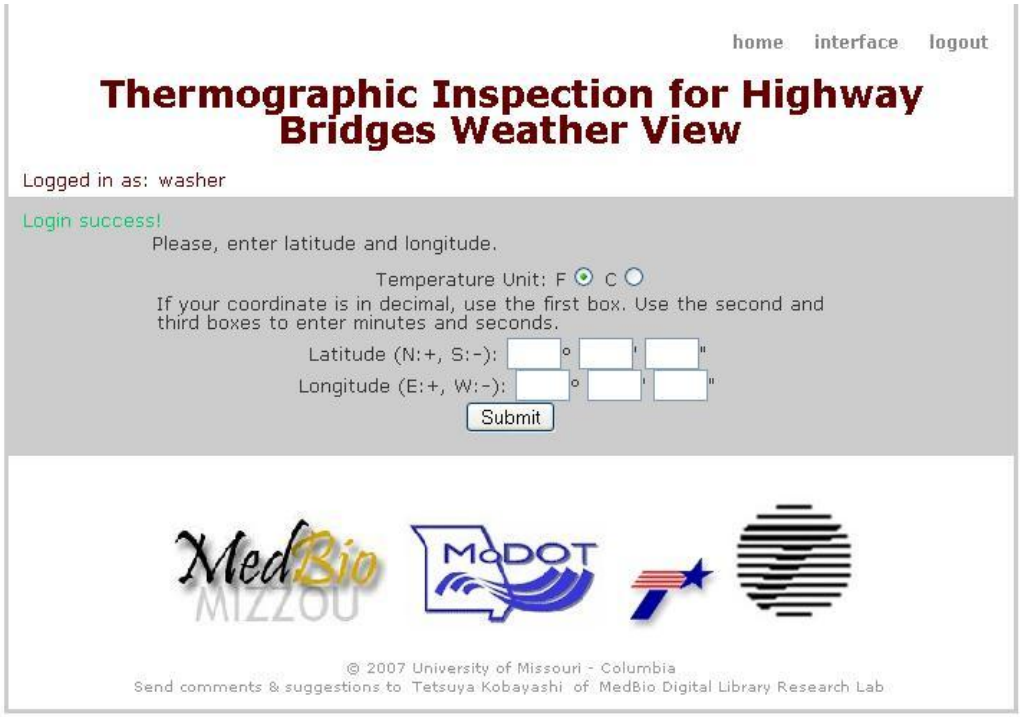

Figure 3.18 : Data Input page for Weather Website.

In this page there is an option to choose a unit Celsius or Fahrenheit for temperature. The latitude and longitude of your desired location is entered. If

latitude or longitude has a negative sign it has to included while entering the data. For example, Columbia MO is located at 38°57′9″N 92°19′35″W. Negative sign is used for West location. After entering the data the next webpage would be displayed and is shown in the Figure 3-19. In this webpage there is information about the weather station closest to the input latitude and longitude along with its location and elevation. This page also displays the recent measurement of Wind speed, Humidity and Ambient Temperature. There are two graphs displayed on the page. The top graph has the ambient temperature on primary Y axis and Relative Humidity on secondary Y axis plotted against 14 days. The graph in the bottom shows the Wind speed of past 14 days from the present date in meters per second.

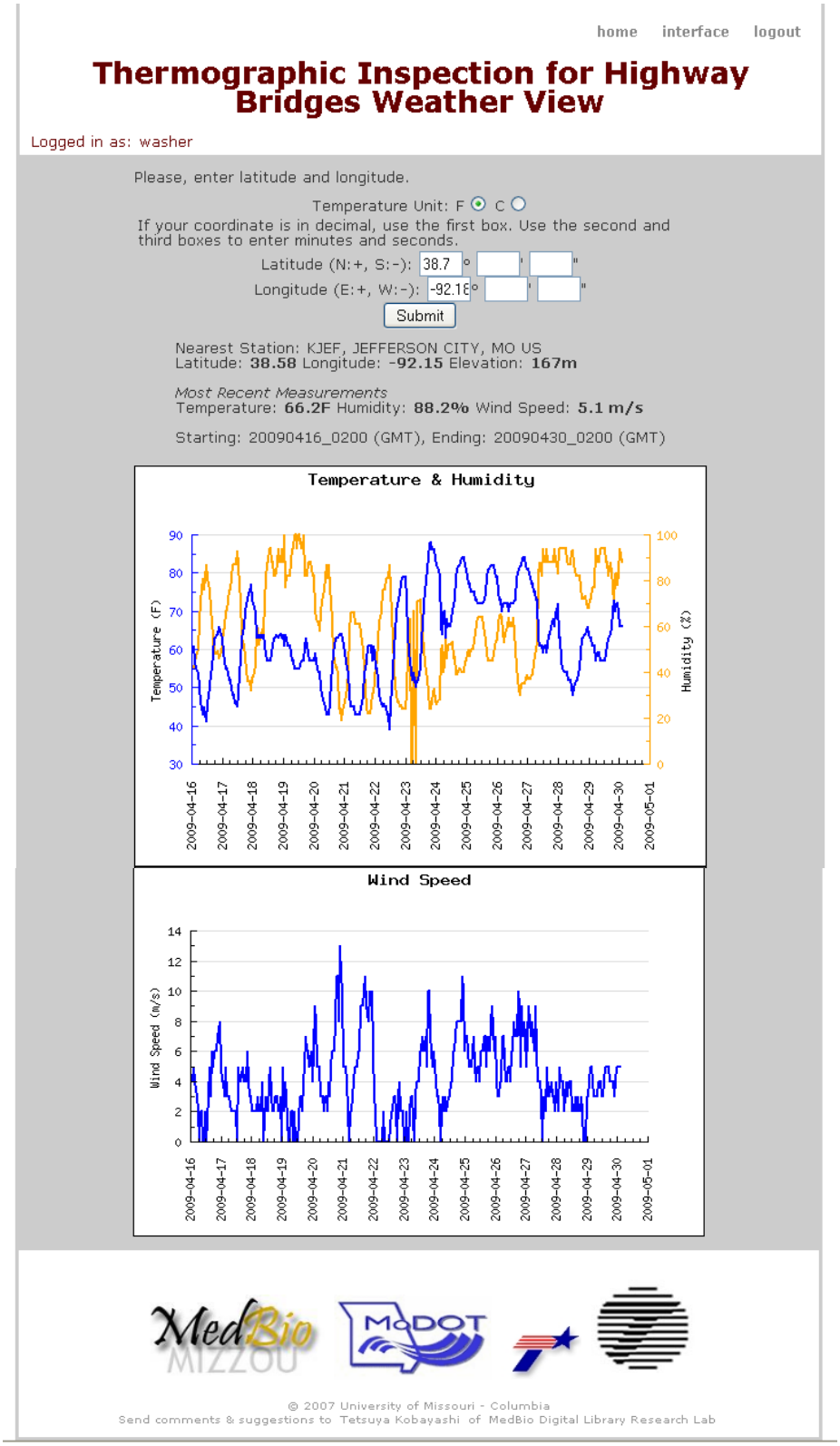

Figure 3.19 : Results Page for the Weather Website.

4

ANALYSIS

This chapter summarizes the various analyses that were done on the south side of the block. The graphical representation of the data is also clearly explained. The effect of rain on the analyses is also explained. The results from these analyses are discussed in Chapter 5 RESULTS.

4.1 Preliminary Analysis

A total of 89 days were examined for the south side of the block which is the face of the block exposed to direct solar loading. The 89 days were from 1st of November 2007 to 29th January 2008. All the data from various sources like thermography data from IR images, thermocouple data and environmental data from the WeatherHawk were reduced to 10 minute sampling intervals, such that each day has 144 data points of the environmental parameters, thermocouple values and IR values. For much of the analysis, this data collected at 10 minute intervals was analyzed to determine single values that would represent behavior of specific parameters on a given day, to be compared with the thermal contrast achieved on that day. For example, one might wish to compare the maximum

thermal contrast achieved on a particular day with the maximum ambient temperature on that day. As such, the parameter of temperature is reduced to a single value, maximum temperature, and compared with a single value for the thermal contrast for that day. Such reduction of data led to the simplification of 89 days of data for the south face for each parameter that could represent the entire day. The data points were then used to correlate various parameters with the thermal contrast produced on the same day.

4.1.1 Graphs

All the basic graphs have two Y axes, typically primary and secondary. On primary Y axis the thermal contrast of the targets is shown. This temperature contrast has been calculated from the IR images. Celsius has been used as the unit for the temperature. On the secondary Y axis an environmental parameter is shown. This environmental parameter may be maximum Solar loading in watt/m^2, Solar loading area in Kwatt-hr/m^2, wind speed in m/sec, core temperature in Celsius or ambient temperature in Celsius. There will be always two set of curves in basic graphs; one set consists of four curves showing the thermal contrasts of the targets embedded in the block at 25, 51, 76 and 127 mm (1, 2, 3 and 5 in.) depths and the other one has only one curve of an environmental parameter.

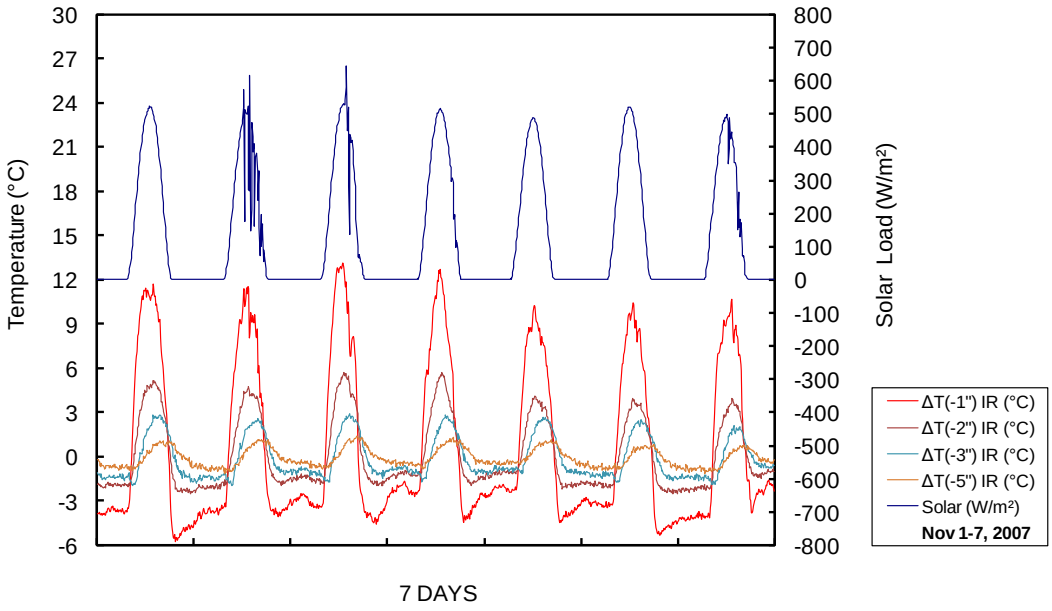

Figure 4.1 : Graph showing thermal contrast for various depths and solar load for 7 days.

Time is shown on the X axis depending upon the time frame being used, for example, a day, a week, or a month. For example a sample basic graph for a week is shown in Figure 4-1. All weekly graphs for the three months for five variables are shown in Appendix.

4.2 Bins Analysis

Division of data into separate “Bins” was used in some cases to provide analysis of typical average values for one parameter within a selected range of a second parameter. Most commonly the range parameter was thermal contrast, and the average parameter was an environmental variable. For example, thermal contrast value might be in separate “bins” or ranges such as 0 to 1°C (0 to 1.8°F), 1 to 2°C (1.8 to 3.6°F), 2 to 3°C (3.6 to 5.4°F) etc. The average value

for an environmental parameter, for example wind speed, for each of the defined bins was calculated along with the standard deviation for the parameter (within the particular bin). This analysis provided for assessment of characteristic values for the environmental parameters at different levels of thermal contrast, to determine what values were typically measured (and their variation) for each bin.

4.3 Wind Speed Analysis

Initial assessment of the wind speed data collected on the south side of the block indicated that although wind speeds varied over the course of a typical day, sudden changes in wind speed (over minutes) did not have a strong effect on the thermal contrast developed in the test block, particularly for targets at depths of 51, 76 and 127 mm. It was also observed that isolated high wind speeds did not typically occur; the winds were generally high on some days, and generally low on others. To characterize the effects of wind, it was necessary to determine time periods over which wind speeds could be characterized in a meaningful way, such that wind speeds could be evaluated by an inspector in the field to guide inspections. Figure 4.2 shows wind speed data for a typical day. The wind speed values shown in the figure are wind speeds sampled every 10 minutes at the on-site weather station. The figure shows that wind speeds vary over the course of the day, but there are time periods of a day that may be “windy” and time periods that are “calm.” In general, night times have lower wind speeds than daytimes due to the lack of radiant heating from the sun and resulting thermal conditions.

It was determined that an effective way to characterize wind speeds was to break down each 24-hour period into four quarters of 12:00 midnight to 6 AM, 6 AM till 12:00 noon, 12:00 noon till 6:00 PM, and 6:00 PM till 12:00 midnight as shown in Figure 4.2. These time periods were selected for two reasons. First, they provide a general measure of the wind speed during times of high ambient temperature change that is separate from time of more sustained thermal conditions. For example, the morning was separated from the afternoon. In this manner, the influence of wind speed during the development of thermal contrast at the targets could be evaluated separately from the influence of the wind speed at the time maximum or sustained thermal contrast were occurring. Second, it was assumed that inspections would typically be conducted during the normal business day when possible. As such, it could be useful to understand the effect of morning wind conditions vs. afternoon wind conditions in terms of determining if a particular day was a “good day” for thermography or a “bad day.” For example, if it was determined that high winds in the morning reduced the thermal contrast observed in the afternoon; this may be useful in decision-making regarding use of a thermal camera.

Other forms of wind speed data, such as daily average, maximum, and average from sunrise to sunset were also assessed during the course of the research. Overall, it was decided that the 2nd and 3rd quarter wind speeds were most critical to thermal contrast development, in particular 2nd quarter (2nd quarter wind speed takes place between 6:00 AM and 12:00 noon). The second quarter wind speeds are important because these are the time periods when thermal

contrast is being developed, and the rate of heat transfer from the environment to the concrete was thought to be most significant in terms of the resulting thermal contrast. Figure 4.2 shows the wind speed for a 24 hour period. The graph shows the four quarter separated by vertical lines. This graph also shows the averages for each quarter by thick red lines.

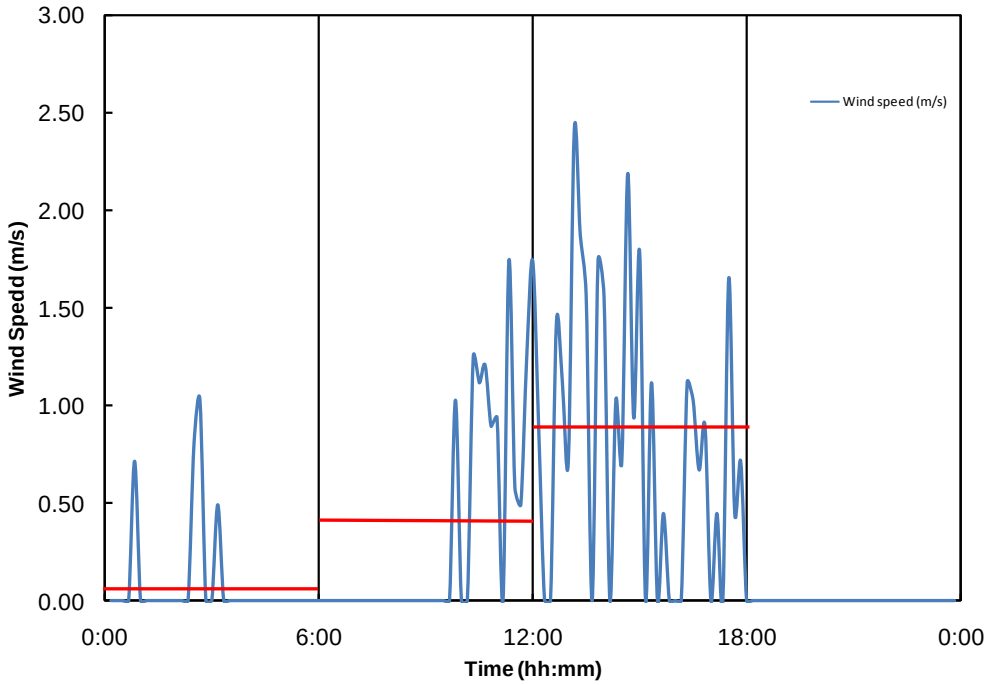

Figure 4.2 : Wind speed with quarter averages for 24 hours (11/01/07).

4.4 Inspection Times

One of the main steps in analysis was to determine a period of time which could be used by inspectors to capture the surface changes which highlighted subsurface defects. Major importance was given to 2 in. (51 mm) deep target. However, “real” delaminations do not have well-defined characteristics; they vary in depth in the concrete, surface texture, size and shape etc., all of which could

be expected to affect the thermal contrast produced. Consequently, there is not a defined transfer function that relates the behavior of an idealized model such as the foam target in concrete and a real defect. Therefore, it was necessary to select a threshold value for the thermal contrast in the test block that could indicate when a real delamination was likely to be detectable in the field. The 1°C threshold was selected for three reasons

- 1°C (1.8°F) at least an order of magnitude (12.5 times) higher that the sensitivity of the camera (0.08°C, 0.14°F), such that much smaller variations in surface temperature were easily detectable by the equipment.
- This value is 20 times the sensitivity of the cameras typically used during field testing (0.05°C, 0.09°F)
- The ASTM specification indicates that 0.5°C (0.9°F) is the necessary contrast between sound concrete and a defect. 1°C (1.8°F) is twice the requirement.

The threshold value selected was intended to be sufficiently high to generally consider modeling effects to provide representative values for conditions when thermographic inspection was likely to be effective in the field.

For each day of analysis, the data points were related to the time at which contrast exceeded its 1°C threshold, and these times were noted. This was similarly carried out for each month of south side analysis until all 89 days were accounted for. The results gained from the 1 °C constraint included; the time it took for contrasts to exceed 1 °C, and the time the contrast drops below 1 °C.

Times relative to sunrise were used to generate the data. This was an important step to delineate quantitative guidelines to be applied by bridge inspectors to routine inspections, and was a necessary step to specify the use of sunrise as a base time from which observation times may be established.

4.5 Effects of Rain

The occurrence of rain is a factor that could bias or affect the results. Rain has a different emissivity than that of dry concrete such that a wet surface will appear differently in a thermal image. Water on the surface also changes the rate of heat flow in concrete by (possibly) the cooling caused by evaporation and also by conduction from cold water into hot concrete. The process of rain removal from the data points requires the knowledge of precipitation characteristics, including the amount of rainfall, and the time of day that it occurred. Some of the graphical results were the first sign of the effects of rain, however, the results were not enough to negate days of data on that basis alone. Therefore, all the 10 days that recorded any precipitation from on-site weather station were eliminated from the data set for certain analysis, as noted in the text.

The Weather Hawk weather station has a built-in tipping bucket measuring device which triggers a switch producing an electrical pulse for each millimeter of rain which falls. The time and frequency of the occurrence was recorded in raw data form and a set of Excel calculations summarized this data into useable daily rainfall information. This information provides the basis for the process of elimination that is used here. There were a total of 10 rainy days out of 89 days. Figure 4.3 gives a basic idea how bad a rainy day is for IR inspection. This figure

shows the good IR image on a dry day on the left and a bad IR image on a rainy day on the right.

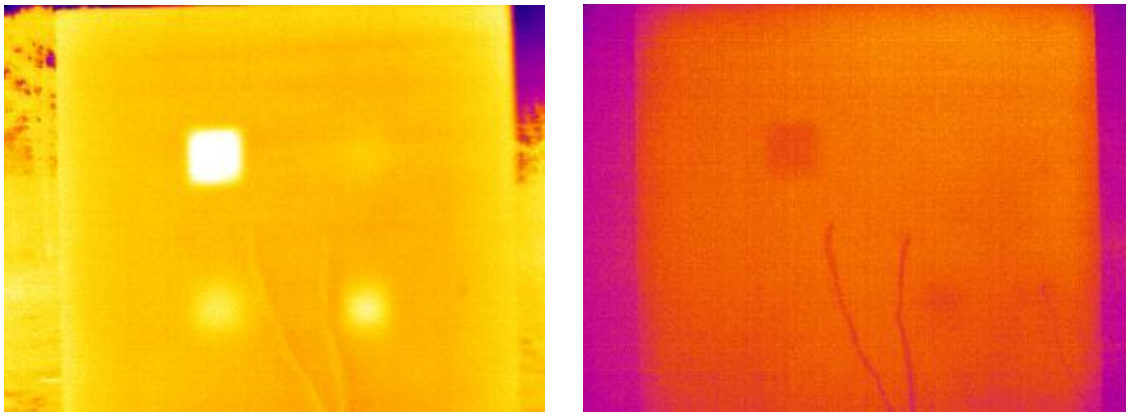

Figure 4.3 : IR Images showing a dry day and a rainy day.

The image on the left shows the image of the block taken on a sunny day where we can see the defects at 25, 51 and 76 mm depth clearly and 127 mm depth defect (partially). The image was taken on a sunny day where there is no interference of clouds. The image on the right was taken on a rainy day which clearly shows only the 1 inch depth defect due to lack of enough solar loading and the rain which took of the heat from the concrete due to conduction. The reason why the image showed only 1 inch depth defect is that it is too close to the surface to dissipate the heat quickly.

5

RESULTS

In this chapter the results from the laboratory and field testing will be discussed. This chapter also includes the results from the various analyses performed on the data along with their graphical representation.

5.1 Lab Results

Results for the controlled testing of the concrete slab yielded data for the 1, 2, 4, 8, 16, and 32 minute heating periods. The test slab had Styrofoam embedded at 1 and 2 inch (25 mm and 51 mm) below the surface to represent 1 and 2 inch (25 and 51 mm) deep delaminations as described in section 3.1. A radiant heater was applied to the test slab surface which was monitored by a thermal imaging camera, and results were recorded by thermocouples and IR images until the concrete temperatures had returned back to room temperature. Figure 5.1 shows the temperatures measured by the thermocouples for the 32 minute test. The duration of the entire test was 88 minutes.

The temperature response of the concrete test slab shows the immediate rise of the surface temperature from the first minute until the heat source was removed 32 minutes later. The temperature of the surface peaked after 32 minutes with an increase of 2.5 °C from initial temperature at 20°C. After 2 minutes, a temperature increase was detected at the 25 mm deep thermocouple; an increase was detected after 6 minutes at a depth of 51 mm. After 14 minutes the temperature at 76 mm below the surface began to rise and at 19 minutes the temperature at a depth of 102 mm. It wasn't until 27 minutes into the test that the concrete temperature 127 mm below the surface began to increase. This is shown in Table 5-1.

Table 5.1 : Temperature increase and its detection time against the depth of the defect from thermocouples

Depth (mm)	Temp. Increase Detection (Time in Minutes)	Temp. Increase (˚ C)
25	2	2.5
51	6	1.7
76	14	1.1
102	19	0.7
127	27	0.6

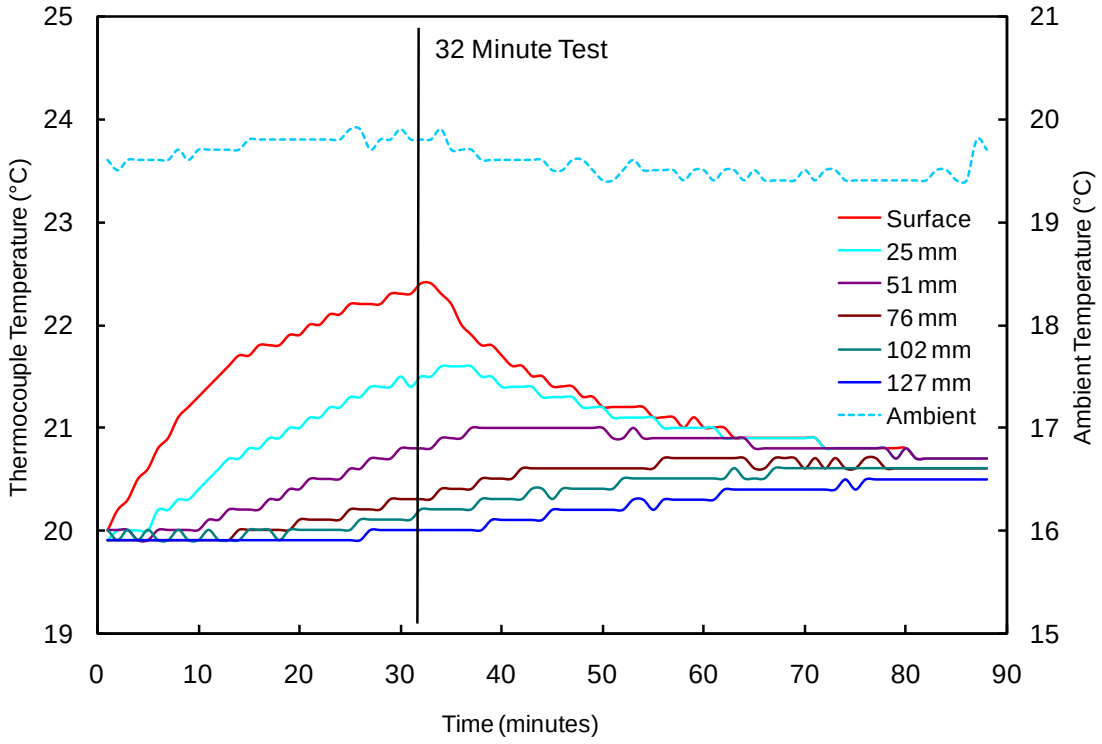

Figure 5.1 : Thermocouple results for a 32 minute laboratory test.

The surface, 25, 51, 76, 102 and 127 mm temperatures reached a maximum temperature at later times with increasing depth, showing a temperature increase of 2.5, 1.7, 1.1, 0.8, 0.7 and 0.6 °C from the initial slab temperature. To have clear understanding of the heat flow through the block Figure 5.2 was developed. It can be clearly seen from this figure that the rise in temperature at deeper depth occurred later when compared to shallow depth. The IR results for the same test are shown in Figure 5.3 which shows the surface temperature measured by the camera. The rise in temperature at 25 and 51 mm deep targets with the increase in time of heating is clearly seen. Figure 5.4 show the thermal contrast for 25 mm and 51 mm deep targets.

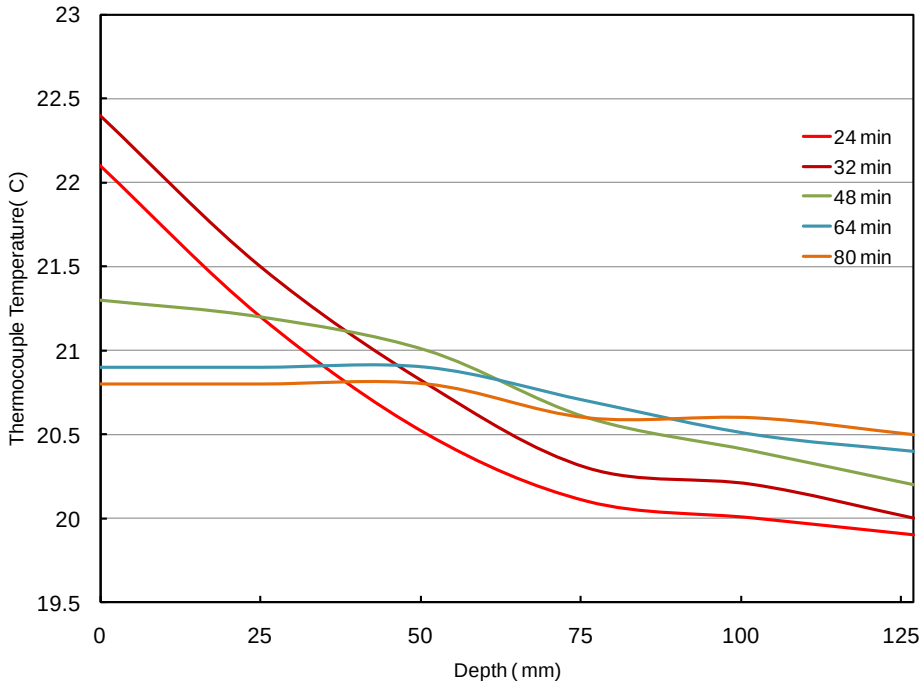

Figure 5.2 : Thermocouple temperature against different depth for different time periods for a 32 minute test.

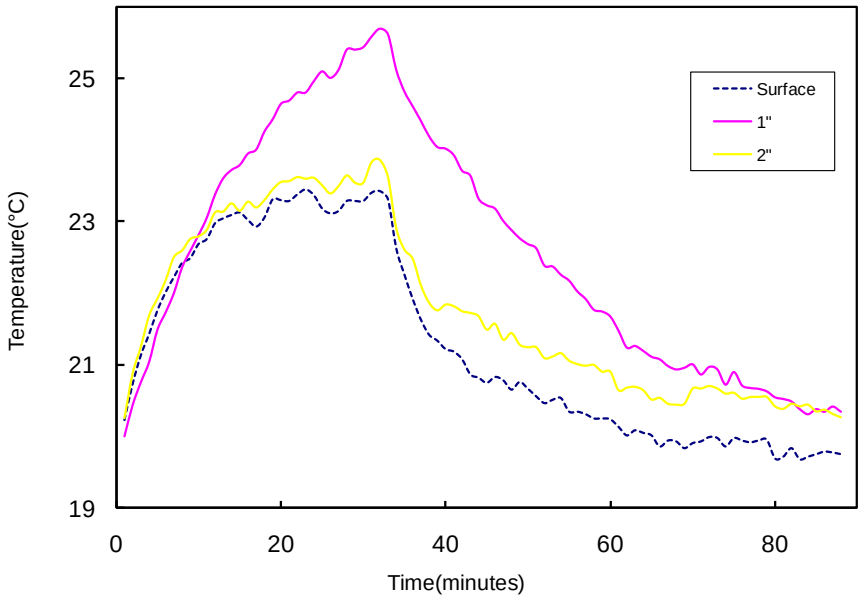

Figure 5.3 : IR results for 32 minute laboratory test.

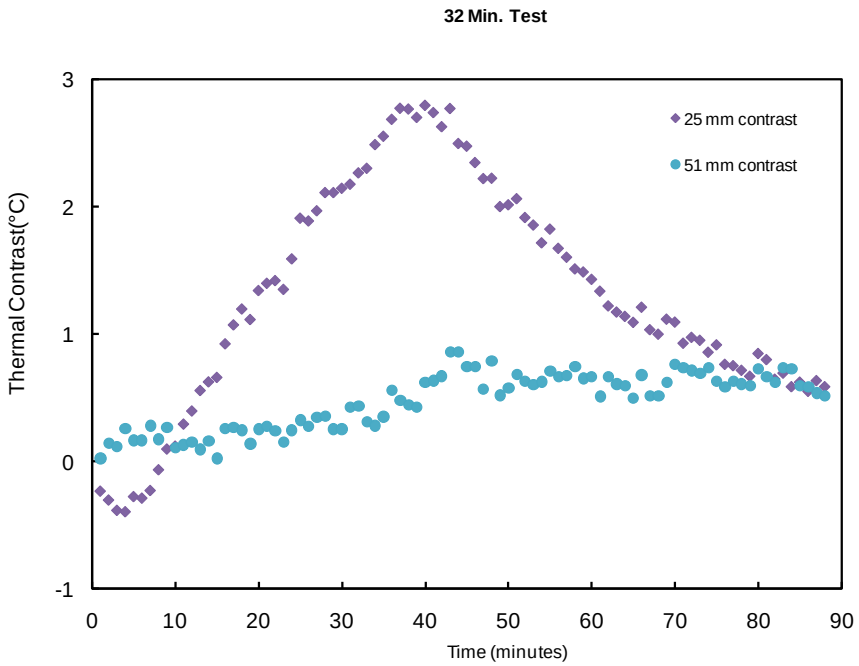

Figure 5.4 : Thermal contrast from IR images for a 32 minute laboratory test.

5.2 Basic Statistics

To understand wide range of data for different variables in the entire 89 days of data collected at the test block, some statistical values are necessary. These statistics are obtained from 10 minute data points. Table 5.2 gives some of the basic statistics about the environmental parameters of ambient temperature, average wind speed, and relative humidity observed at the test block.

Table 5.2 : Basic Statistics of different variables for three months

Month	Variables	Mean	Maximum	Minimum	Std.Deviation
November	Ambient Temp.(°C)	6.6	25.0	-7.2	6.5
	Wind speed (m/s)	1.7	9.3	0.0	1.7
	Relative Humidity (%)	66.6	100.0	13.0	24.5
December	Ambient Temp (°C)	0.0	16.4	-13.2	4.7
	Wind speed (m/s)	1.6	9.6	0.0	1.7
	Relative Humidity (%)	85.8	100.0	33.0	17.9
January	Ambient Temp.(°C)	-0.8	22.3	-18.1	8.7
	Wind speed (m/s)	3.1	12.0	0.0	1.9
	Relative Humidity (%)	68.0	100.0	13.0	21.9

Statistics for thermal contrast for each of the targets, the surface temperature and the ambient temperature were also calculated. The calculations were done individually for each month and are shown in both tabular and graphical forms. Tables 5.2 to 5.4 show the statistical values for the months November to January. A total of 30, 31 and 28 data points would be available for each target for the month of November, December and January respectively. The positive contrast in the table represent warming trend (daytime) and the negative values are derived from cooling trends in the overnight hours. These data points are the maximum, minimum and standard deviations for each variable for each day and then means were calculated for each month. The surface temperature was calculated from the pixel selected in between the four delaminated areas. The procedure was clearly explained in section 3.3.2

Table 5.3 : Statistics of targets for the month of November

November	Surface Temp.(° C)	1" contrast (° C)	2" contrast (° C)	3" contrast (° C)	5" contrast (° C)	Ambient Temp. (° C)
Max. Mean	19.60	8.60	3.32	1.84	0.87	12.79
Max. Std.	7.00	3.81	1.72	0.92	0.40	6.24
Min. Mean	2.88	-3.38	-1.77	-1.34	-0.79	0.18
Min. Std.	4.26	1.25	0.50	0.41	0.22	4.71

Table 5.4 : Statistics of targets for the month of December

December	Surface Temp. (° C)	1" contrast (° C)	2" contrast (° C)	3" contrast (° C)	5" contrast (° C)	Ambient Temp. (° C)
Max. Mean	8.22	5.87	2.24	1.15	0.63	4.42
Max. Std.	6.03	5.14	2.19	1.06	0.52	5.07
Min. Mean	-4.25	-2.19	-1.36	-1.00	-0.73	-4.62
Min. Std.	3.31	1.12	0.37	0.25	0.20	3.27

Table 5.5 : Statistics of targets for the month of January

January	Surface Temp. (° C)	1" contrast (° C)	2" contrast (° C)	3" contrast (° C)	5" contrast (° C)	Ambient Temp. (° C)
Max. Mean	9.61	7.58	2.56	1.55	0.73	5.11
Max. Std.	7.23	3.44	1.48	0.90	0.40	8.25
Min. Mean	-6.05	-2.99	-1.64	-1.11	-0.87	-6.18
Min. Std.	8.16	1.32	0.58	0.41	0.35	8.44

All the values shown in table are units are in °C. The maximum mean for the month of November along with the standard deviation is shown in the Figure 5.5. The depth of the targets in mm was used on X axis. Secondary Y axis was used so that the mean temperature values can be seen in both °C on primary axis and °F on secondary axis.

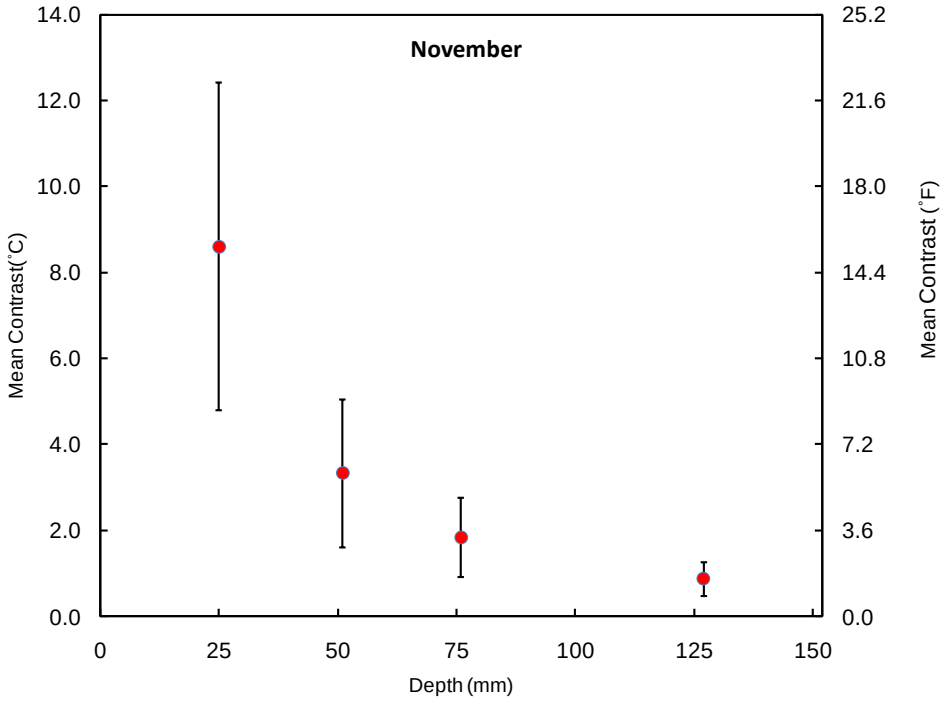

Figure 5.5 : Graph with error bars for targets maximum mean contrast against different depth for November.

Similar graph with minimum mean temperature for the month of November is shown in the Figure 5.6.

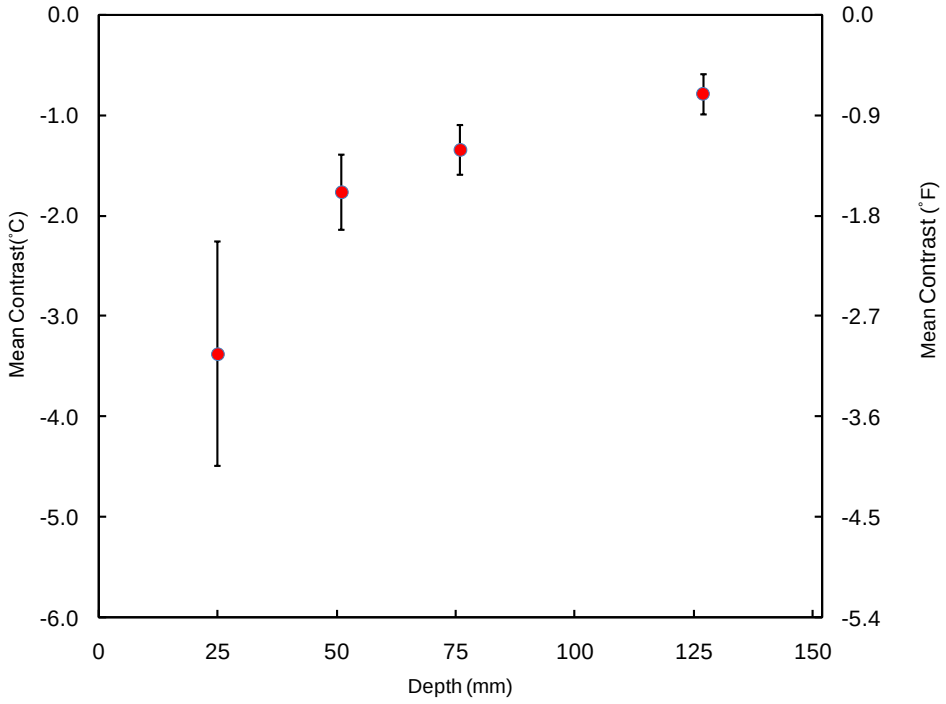

Figure 5.6 : Graph with error bars for targets minimum mean contrast against different depths for November.

Figures 5.7 and 5.8 show the maximum mean temperature and minimum mean temperature for various targets in the month of December along with their standard deviation values. Same is the case with Figures 5.9 and 5.10 which are for the month of January. One more interesting point is that the maximum mean temperatures for different months for a particular target is almost same with lesser standard deviation in the month of November.

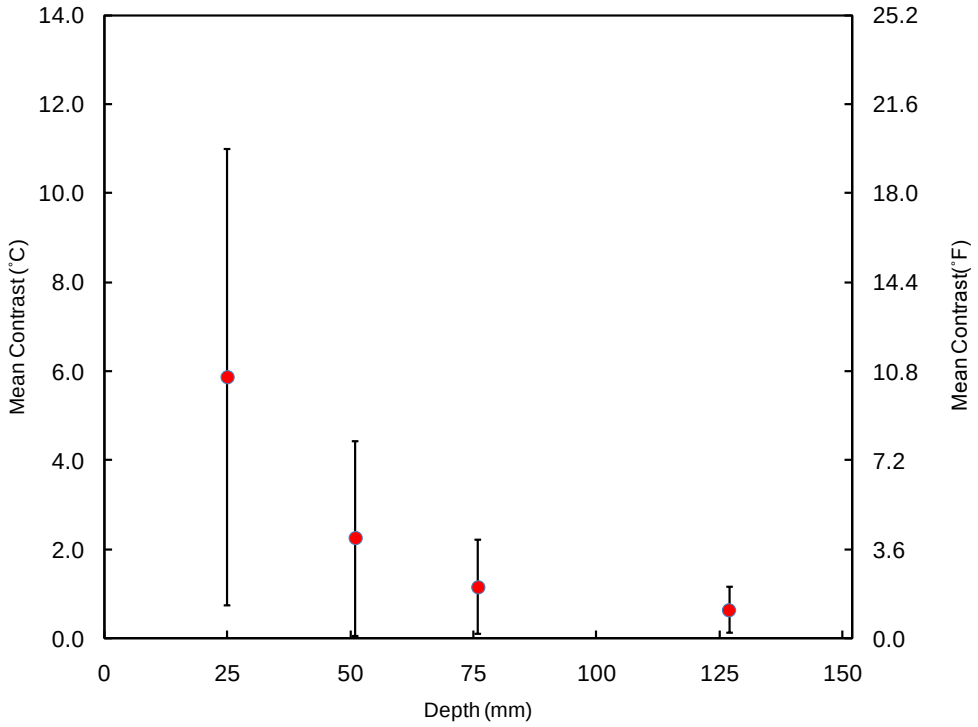

Figure 5.7 : Graph with error bars for targets maximum mean contrast against different depths for December.

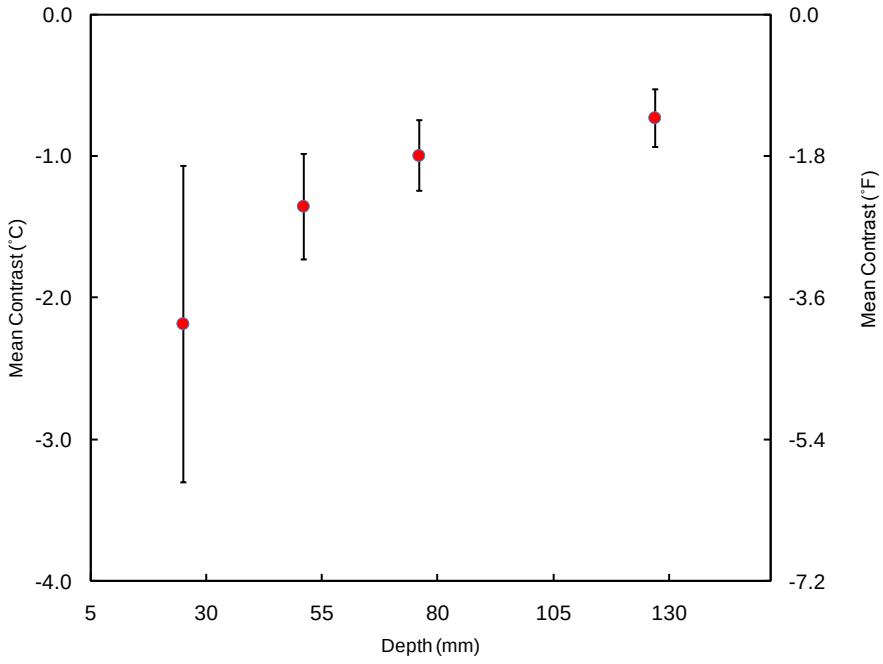

Figure 5.8 : Graph with error bars for targets minimum mean contrast against different depths for December.

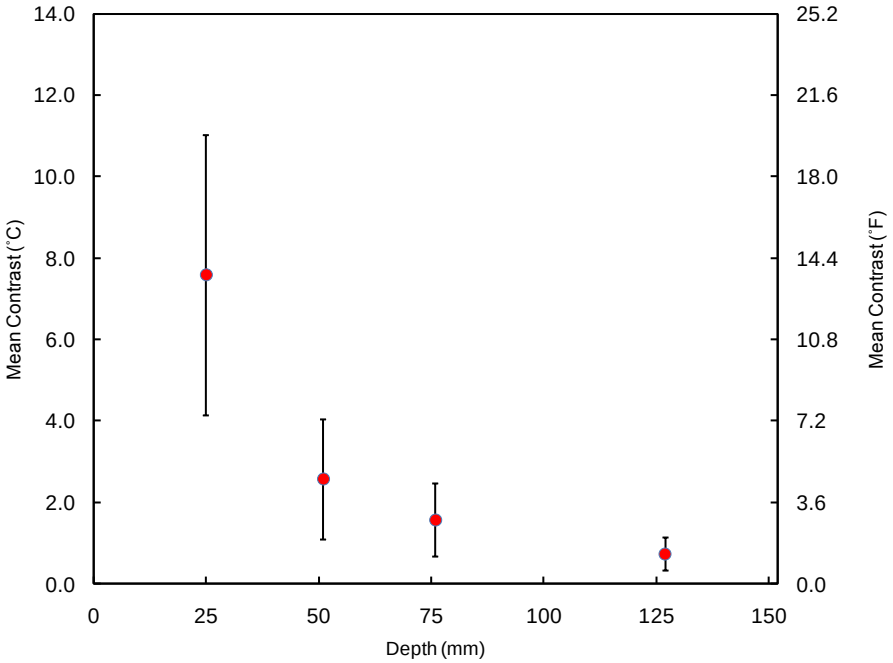

Figure 5.9 : Graph with error bars for targets maximum mean contrast against different depths for January.

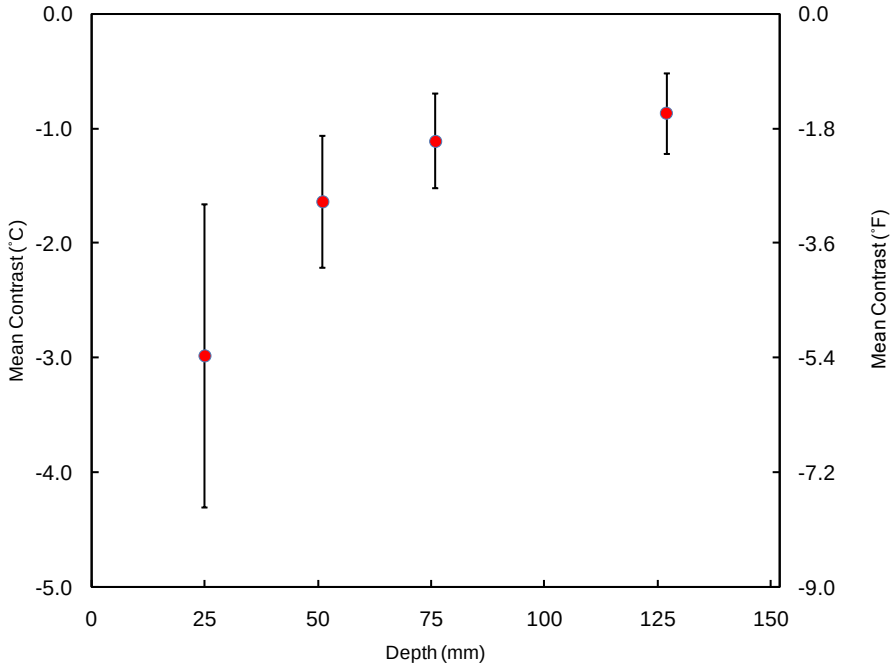

Figure 5.10 : Graph with error bars for targets minimum mean contrast against different depths for January.

In order to have a clear picture of weather trend in each month each month has to be assessed for the “good days” in terms of applying IR thermography. As earlier said 1°C was taken threshold for determining inspection times, similar threshold was followed in observing the typical days for each month and for the total 89 days.

Figure 5.11 shows the thermal contrast behavior for a typical day on the south side of the block. Thermal contrast on the south side of the block during the day typically developed in a sinusoidal shape that mirrored to some extent the solar loading on the surface of the block. The shape of the thermal contrast curve was predictable and consistent, such that selecting a maximum value on the curve to represent the overall behavior was representative, especially with respect to the targets at depths of 51, 76 and 127 mm (2, 3 and 5 in.). The shape of the contrast curve for the 25 mm (1 in.) deep target was more sensitive to short term effects, such as periodic cloud cover, and as a result was typically more varied than the deeper targets. This can be observed in Figure 5.10, when cloud cover occurs in the afternoon, the contrast for the 25 mm (1 in.) deep target is reduced almost immediately. This cloud cover has some effect on the 51 mm (2 in.) deep target, but the effect is much smaller. Analysis generally focused on the 51 mm (2 in.) and 76 mm (3 in.) deep targets, which are at more realistic depths for defects in real concrete bridges and structures. For the south side of the block the thermal contrast behavior for a single day could be characterized by the maximum thermal contrast observed on that day.

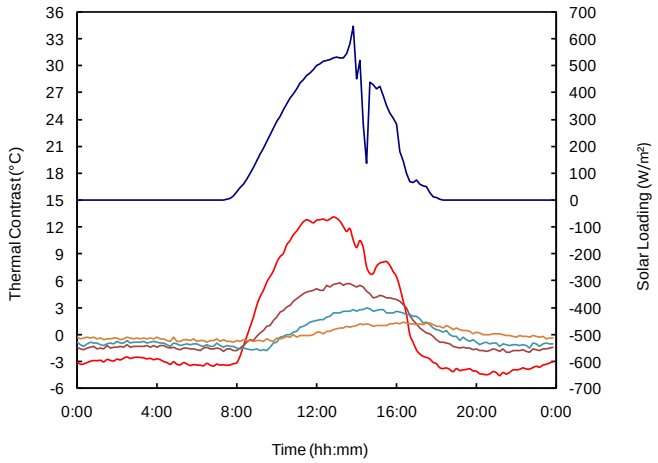

Figure 5.11 : Thermal contrast for a typical day on the south side.

The number of days when the targets contrast crosses a predetermined threshold values of 1°C and 2°C were counted and expressed as a percentage to the total number of days in each month and to total number of 89 days. These values were tabulated as shown in Table 5.6.

Table 5.6 : Table showing percentage distribution of days for different months on threshold contrast limits for all targets

	Percentage of Days				
	Depth	**25 mm**	**51 mm**	**76 mm**	**127 mm**
November	Greater than 1°C (1.8°F)	90 %	83 %	80 %	43 %
	Greater than 2°C (3.6°F)	87 %	80 %	57 %	0 %
December	Greater than 1°C (1.8°F)	84 %	52 %	45 %	29 %
	Greater than 2°C (3.6°F)	58 %	45 %	29 %	0 %
January	Greater than 1°C (1.8°F)	96 %	82 %	68 %	36 %
	Greater than 2°C (3.6°F)	86 %	64 %	39 %	0 %
Total	Greater than 1°C (1.8°F)	90 %	72 %	64 %	36 %
	Greater than 2°C (3.6°F)	76 %	63 %	42 %	0 %

From the Table 5-5 it can be clearly seen that the 127 mm target never reached 2°C in the 89 day period, although the 1° C threshold was reached on roughly one third of days. The percentage of days when the targets contrast was greater than 2°C is less in the month of December when compared to January and November. November has the highest percentage of days when the thermal contrast of the targets was greater than 1°C or 2°C. The data from the Table 5.6 is represented in graphs to give a clear picture of the three months share in providing good days. Figure 5.12 to Figure 5.15 shows the percentage of days when the thermal contrast of the targets were greater than 1°C and 2°C for November, December, January and total 89 days respectively. X axis has depths of the targets in mm.

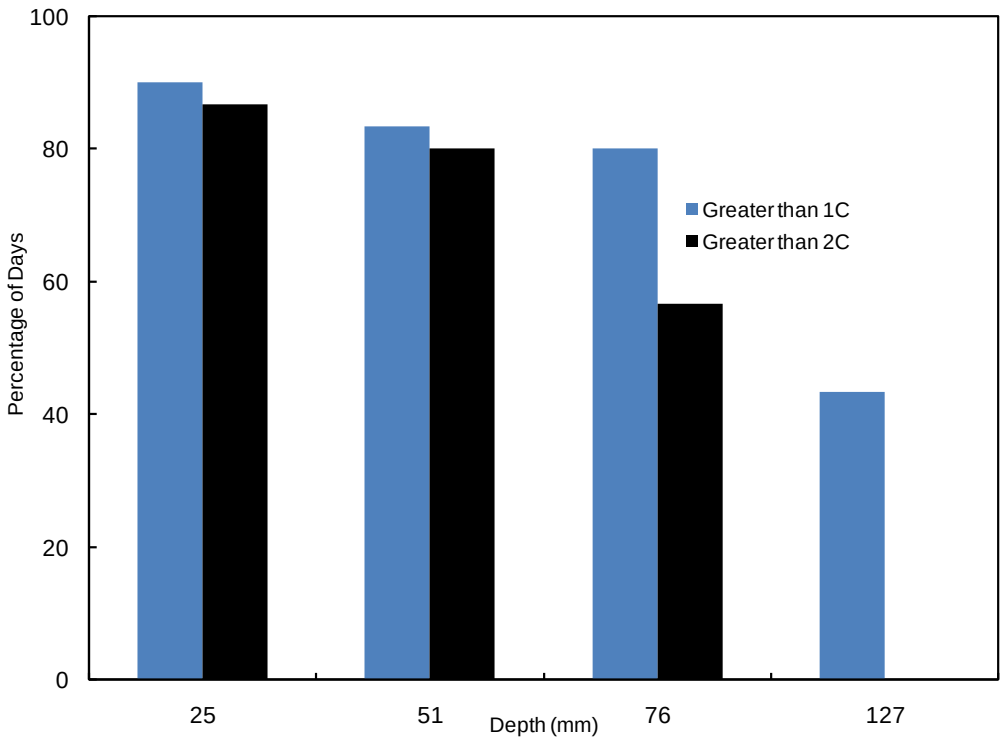

Figure 5.12 : Percentage of Days for November for various threshold values.

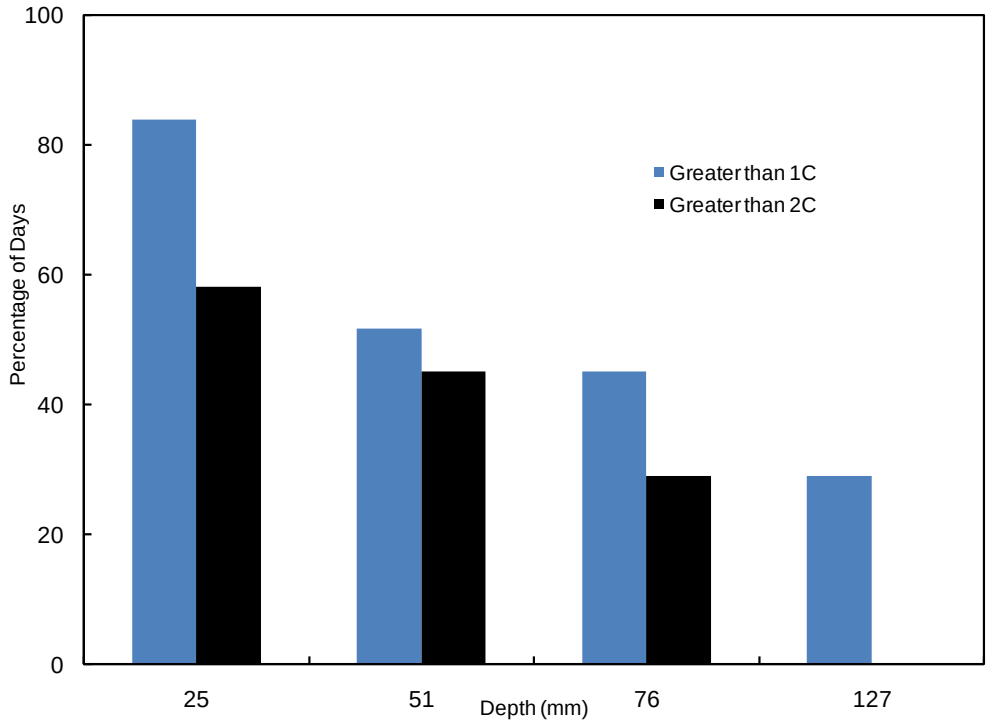

Figure 5.13 : Percentage of Days for December for various threshold values

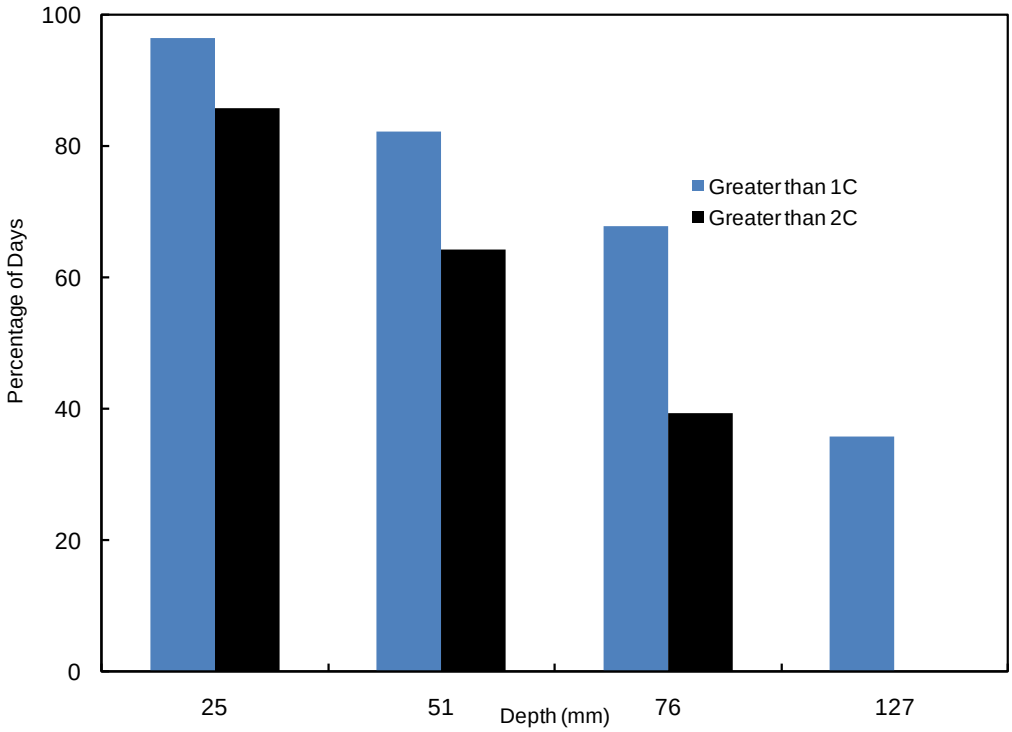

Figure 5.14 : Percentage of Days for January for various threshold values.

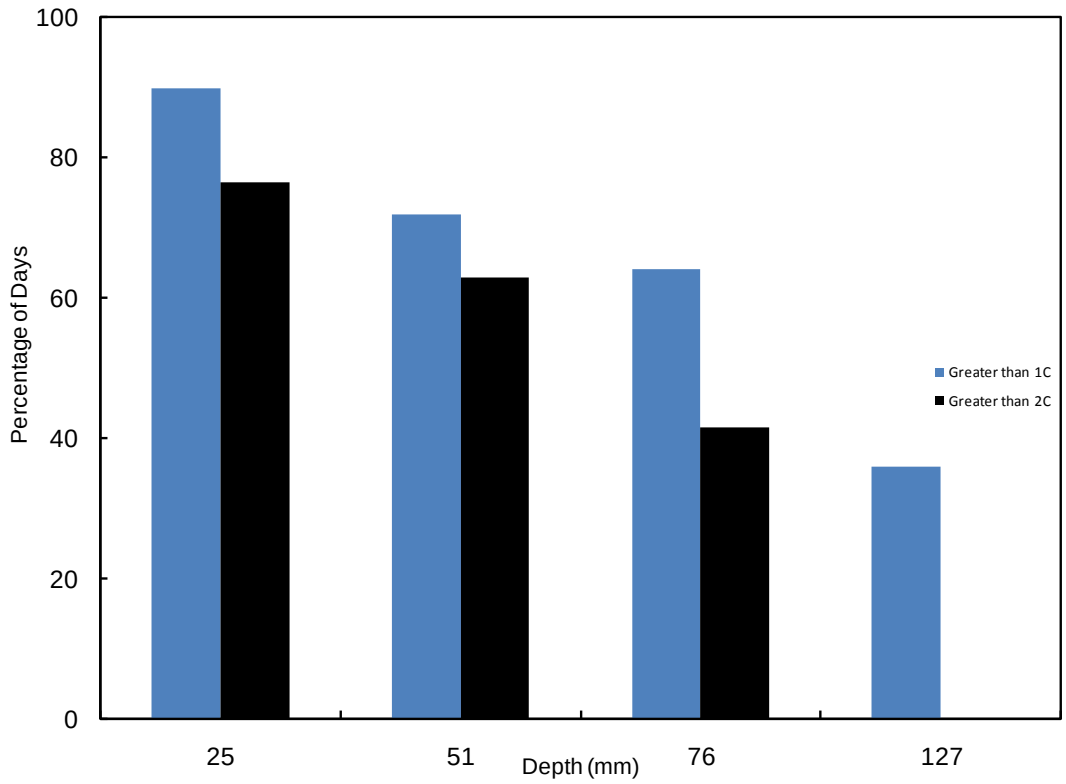

Figure 5.15 : Percentage of Days for total data set (89 days) for various threshold values.

5.3 Trend lines

To study the relationship between environmental parameters and the development of thermal contrast for the targets, scatter plots were developed. Four parameters were evaluated:

1. Difference between the maximum and minimum ambient temperature (ambient temperature change),
2. Average wind speed,
3. Maximum solar loading and
4. Solar loading area.

To clearly understand how these plots were drawn a detail explanation for each graph is provided. Figure 5.16 shows the scatter plot of ambient temperature change versus the thermal contrast for 51 mm deep target. The vertical axis indicates the thermal contrast in units of °C. A best-fit line was calculated for the data points and the equation of the trend line is in the graph along with coefficient of determination (R^2 value), which shows the degree of correlation of the data, on a range of 0 to 1. The data in this Figure was derived by taking the range of ambient temperature changes for a given day, and plotting that against the maximum thermal contrast for that day. As shown in the Figure and by the relatively low R^2 value (0.22), there was poor correlation between the ambient temperature change and the resulting thermal contrast in the test block. However, the trend line does have a positive slope, which indicates that higher ambient temperature changes correlated with increased thermal contrast that developed for the 51 mm deep target. However from 89 days, it can be observed that on certain days, even though there was relatively high ambient temperature change, significant thermal contrasts were not developed.

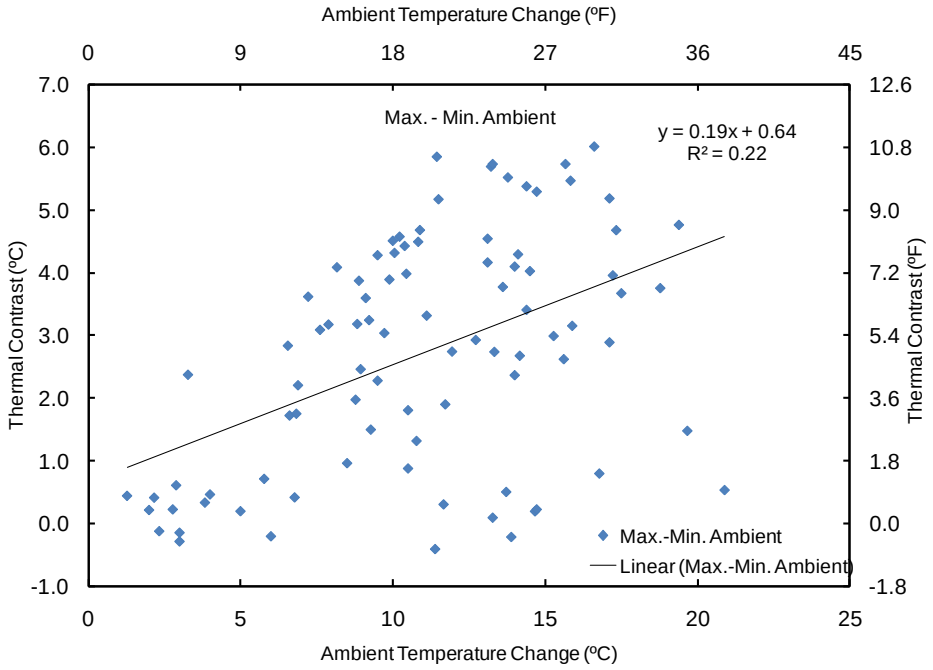

Figure 5.16 : Scatter plot with trend line for ambient temperature change versus thermal contrast

Figure 5.17 shows the scatter plot of average wind speed versus the thermal contrast for 51 mm deep target. Primary X-axis has average wind speed in m/s and the primary Y-axis contains the thermal contrast (°C). The equation shown here is not the best fit curve for the data. This implies that no linear relationship exists between the development of thermal contrast and wind speed. R^2 value also suggests this average wind speed values for each day may not be a good representation of the day to correlate to the thermal contrasts. Analysis of portion of the day rather than average 24 hour analysis was carried out that will be explained in the later section of this chapter.

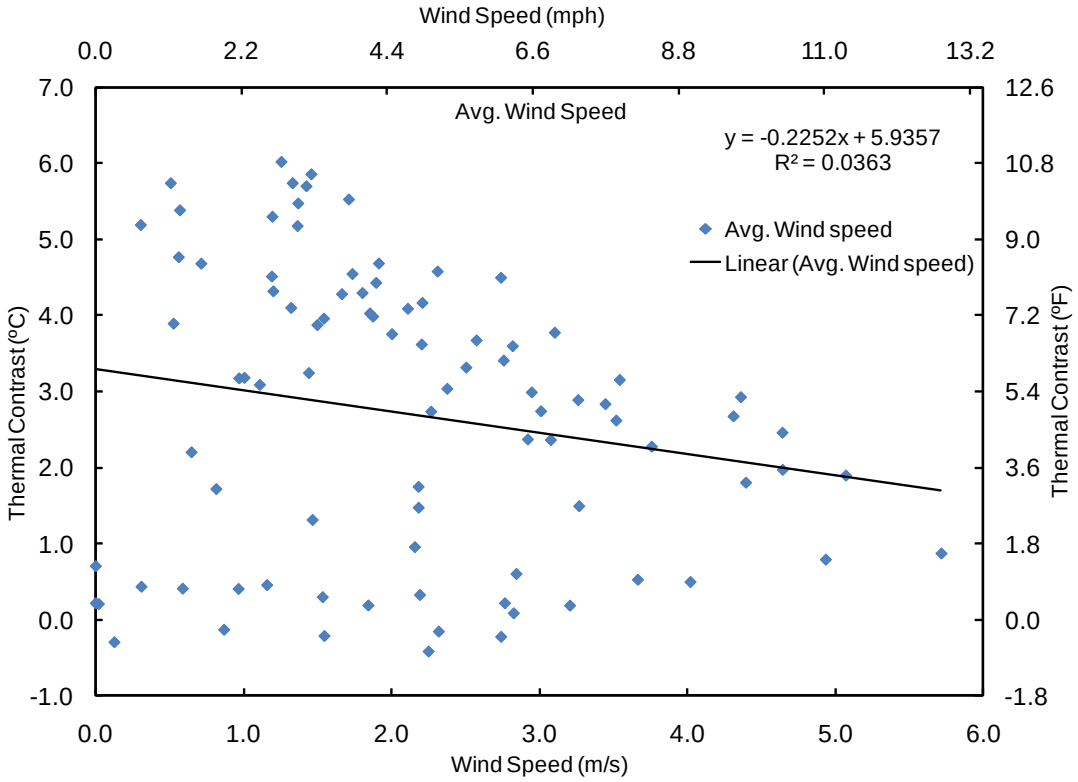

Figure 5.17 : Scatter plot with trend line for average wind speed versus thermal contrast.

Figure 5.18 shows the correlation between the Solar loading (radiation) vs. the thermal contrast for 51 mm deep target. Solar radiation was measured at the on-site weather station. Because the South side of the block is exposed to direct sunlight, measurement of the solar radiation provides a quantitative description of the intensity of sunlight for a given time period on the surface of the block. The maximum solar loading represents the most intense sun period of the day. This may occur for only a short period as there are periodic clouds that block the sun. As the Figure indicates, there was a correlation between the maximum solar loading and the thermal contrast developed. However, the R^2 value for this correlation is relatively low, only 0.55. It can be observed in the data that the days with the most intense sunlight, over 700 watt/m^2, did not correspond to the

highest thermal contrast values. This indicates the maximum solar load may not be the most effective measure when characterizing the quality of a day for thermographic inspection. Other factors such as periodic cloud cover, which interrupts the solar loading, need to be considered.

To evaluate this data further, analysis was made of the data to consider the solar loading imparted into the concrete over the course of the entire day. To calculate this value, the area under the solar loading curve was calculated for each day, and this value was then correlated with the observed maximum thermal contrast.

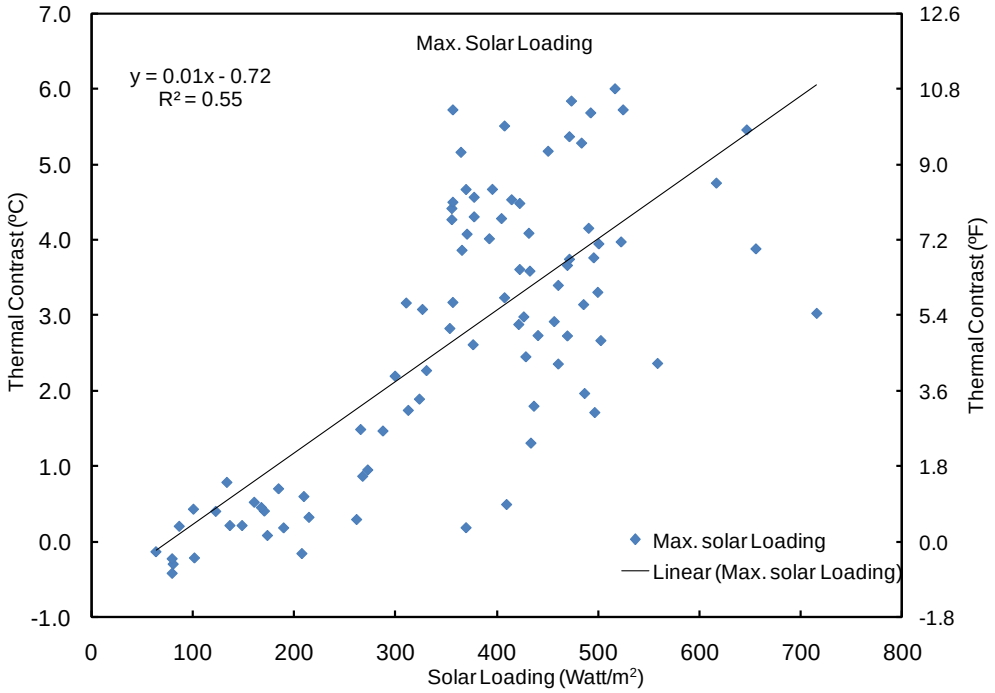

Figure 5.18 : Scatter plot with trend line for maximum solar loading versus thermal contrast.

Figure 5.19 shows the results of this analysis, which showed a strong, linear correlation between the level of developed contrast and the amount of solar loading for a given day. This implies that strong linear relationship exists

between the development of thermal contrast and total solar loading. The high R^2 value (0.75) suggests the area of solar loading had very good correlation with the development of thermal contrasts. Applying a minimum threshold or 1 °C for usable thermal contrast, it was found that for 90 % days with at least 0.7 kW-hr/m^2 also had at least 1 °C of contrast. This is was calculated by determining the intercept of a horizontal line, drawn at 1 °C , with the trend line in the Figure, and calculating the percentage of days remaining above 0.7 kW-hr/m^2 and 1 °C of contrast as a portion of all days with solar loading of at least 0.7 kW-hr/m^2. The significance of this in terms of inspection is that periodic cloud cover that reduces the intensity of sunlight for short periods has a negative impact on the thermal contrast developed, and that the solar loading over the course of the day may be more important than the intensity of sunlight at any particular time. This is consistent with the importance of the radiant heating from the sun to develop thermal contrast in a concrete structure. Additionally, because the relationship between the area of solar loading and the thermal contrast was found to be linear, longer periods of intense sunlight are proportionally better than shorter time periods. In other words, inspection conducted during longer days (summer) will provide improved results over inspections conducted on shorter days (winter).

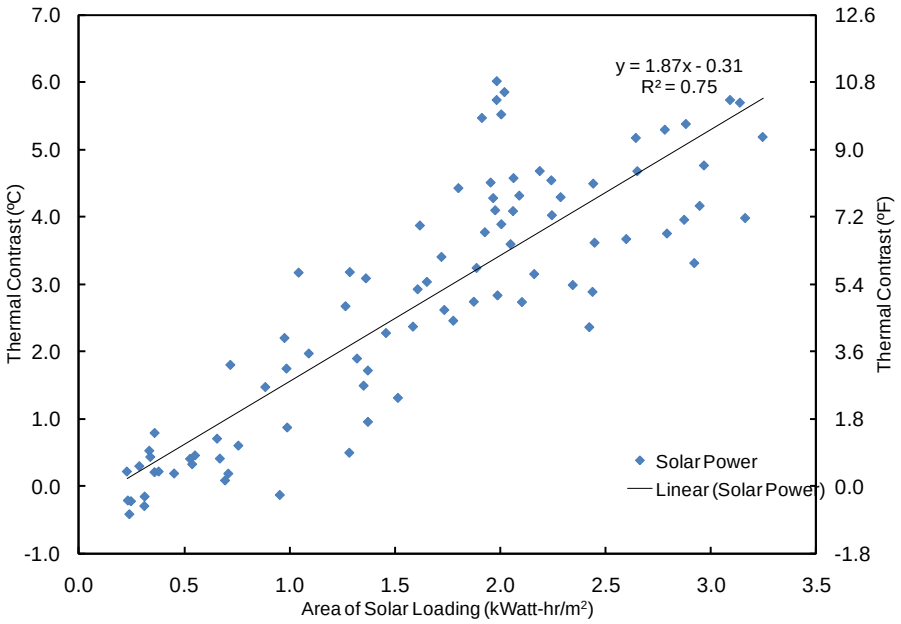

Figure 5.19 : Scatter plot with trend line for area of solar loading versus thermal contrast.

5.4 Wind Quarters

As we discussed in the earlier section that an average wind speed value for a day may not be a good representation, and as such the day was represented by using four quarters. The development of the wind quarters for each day was discussed in the section 4.3. Using the average wind speed values from each quarter and by using the bins analysis more illuminating graphs were developed. The other reason for considering these two quarters is sun being the primary source for creating the thermal contrast on the sunny side and these quarters divide the daily sun exposure. Additionally, sunrise and sunset takes place in these two quarters. Two graphs were developed using the 51 mm (2 in.) deep target thermal contrast bins and the second and third quarter wind speeds. Once limits of the bins were selected, data from days with maximum contrast (for 51

mm target) were sorted into their respective bins. Then the average values for wind speed during the second and third quarters were calculated for those particular days in the bins. Figure 5.20 shows the graph with average and standard deviation for second quarter wind speeds for each bin. Figure 5.21 shows the graph with average and standard deviation for third quarter wind speeds for each bin.

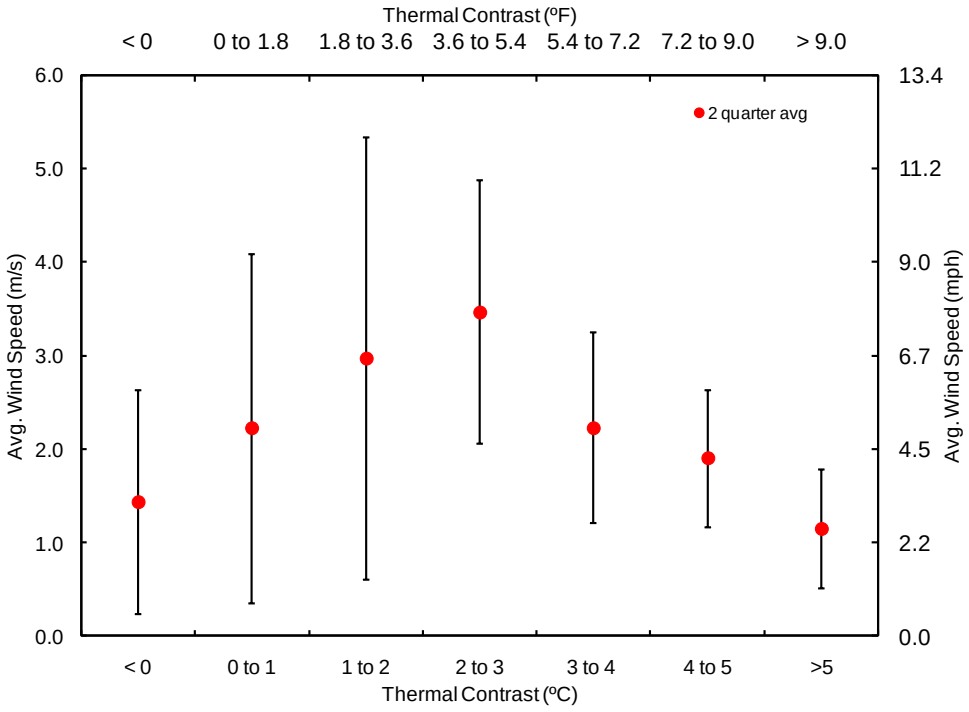

Figure 5.20 : Graph of second quarter wind speed versus thermal contrast for 2 in. (51 mm) deep target with error bars.

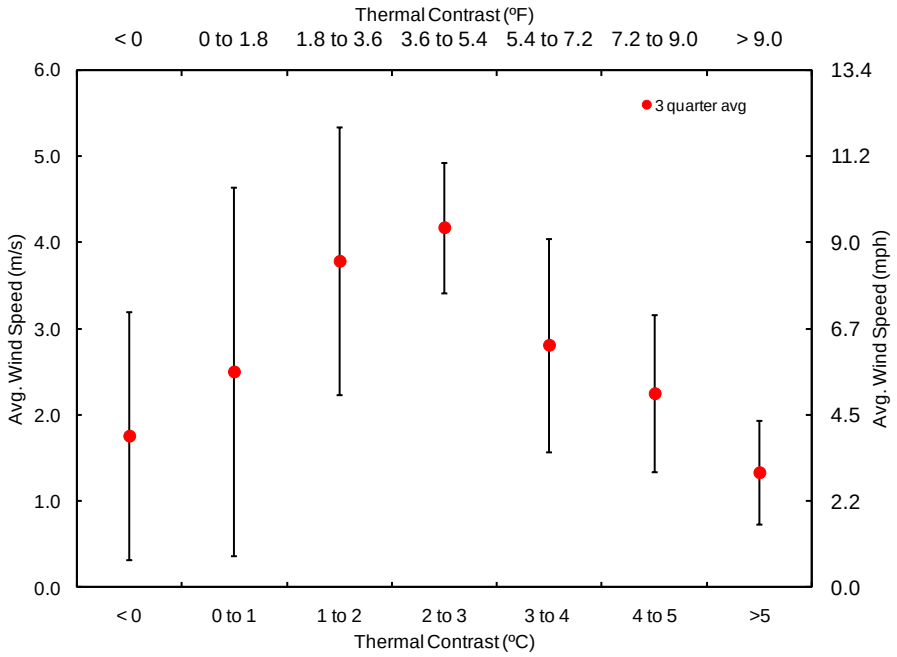

Figure 5.21 : Graph of third quarter wind speed versus thermal contrast for 51 mm (2 in.) deep target with error bars.

If the Figures 5-20 and 5-21 are studied closely you can see the average wind speed and standard deviation are reduced for the higher contrast relative to lower contrast. It is also shown that the average values for very poor thermal contrasts have low average wind speeds. This corresponds to days in which the solar loading is not adequate to develop thermal contrast, but may be calm conditions in terms of wind. This finding from Table 5.7 suggests that days with optimum conditions for thermographic inspection have low wind speeds, as would be expected, and also have adequate solar loading to develop thermal contrast. The average values in the table for each quarter are the average of 6 hour wind speed data points that fall in a particular contrast bin. The maximum and minimum averages are the maximum and minimum of average 6 hour wind speed data points. It is difficult to define specifically a limiting value for wind

speed, but the data indicates that days with the best thermal contrast, say greater the 3°C typically were characterized by winds of less than ~ 3 m/s (7 mph) to ~ 4 m/s (9 mph) based on 2nd and 3rd quarter analysis, respectively. These values consider +1 standard deviation of the average wind speeds in the 2nd and 3rd quarter.

Table 5.7 : Wind speed data for each quarter for each thermal contrast bin

		Thermal Contrast Bins						
		<0°C	**0-1°C**	**1-2°C**	**2-3°C**	**3-4°C**	**4-5°C**	**>5°C**
1st Quarter	**Average**	1.6	1.8	2.0	2.4	1.5	1.4	1.1
	Max. Average	2.9	4.9	4.3	5.4	3.7	4.6	3.0
	Min. Average	0.0	0.0	0.1	0.0	0.0	0.1	0.1
	Standard Deviation	1.1	1.6	1.9	1.8	1.1	1.3	1.1
2nd Quarter	**Average**	1.4	2.2	3.0	3.5	2.2	1.9	1.1
	Max. Average	3.0	5.9	5.9	5.6	3.5	3.0	2.2
	Min. Average	0.0	0.0	0.6	0.07	0.4	0.7	0.3
	Standard Deviation	1.2	1.9	2.4	1.4	1.0	0.7	0.6
3rd quarter	**Average**	1.8	2.5	3.8	4.2	2.8	2.3	1.3
	Max. Average	3.8	7.6	5.9	5.1	5.5	3.8	2.3
	Min. Average	0.0	0.0	1.7	2.4	0.4	0.6	0.8
	Standard Deviation	1.4	2.1	1.6	0.8	1.2	0.9	0.6
4th quarter	**Average**	1.8	1.9	3.2	3.0	1.4	1.1	1.0
	Max. Average	3.8	5.8	4.8	4.9	3.9	3.3	2.7
	Min. Average	0.0	0.0	0.0	0.2	0.0	0.1	0.0
	Standard Deviation	1.5	1.8	1.6	1.4	1.2	1.17	1.1

One more noticeable point is that the values of average wind speeds for third quarter were greater than the values for same contrast for the second quarter. This might be due to greater solar loading during the third quarter. To explore this point more the second and third quarter wind speed data was categorized as low wind (0 - 4 mph), medium wind (4 - 8 mph) and high wind (> 8 mph). These wind speeds are the average wind speeds during the respective quarters. Analysis of this data using a scatter plot of the solar loading and the maximum thermal contrast showed that the trend for thermal contrast was lower for days with high winds (>8 mph or ~ 4 m/s) relative to the trend for all days combined, and much lower than the trend when winds were low.

Figure 5.22 shows the scatter plot for maximum thermal contrast vs. the solar loading area (kW-hr/m^2), with the three wind categories, low, moderate and high shown as different markers. Also shown on the plot are trend lines drawn by linear regression for high winds (long dash lines), low winds (short dashed lines), and all of the data as one group (solid line). As can be seen, the trend of the correlation for days with low wind speeds is much higher than days with high winds. Figure 5.23 shows the same relationships for the 3rd quarter wind speeds. The third quarter is from the hours of 12:00 noon to 6:00 pm., which is envisioned as the primary time for inspections, due to the time delay for the concrete to warm over the course of the day.

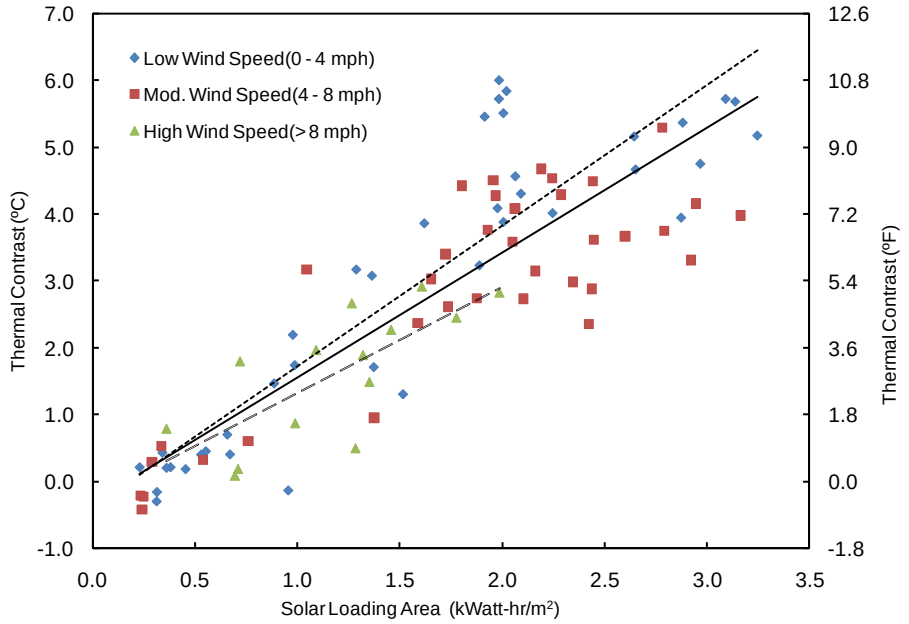

Figure 5.22 : Scatter plot of solar loading vs thermal contrast, with low, moderate and high wind speeds, 2nd quarter.

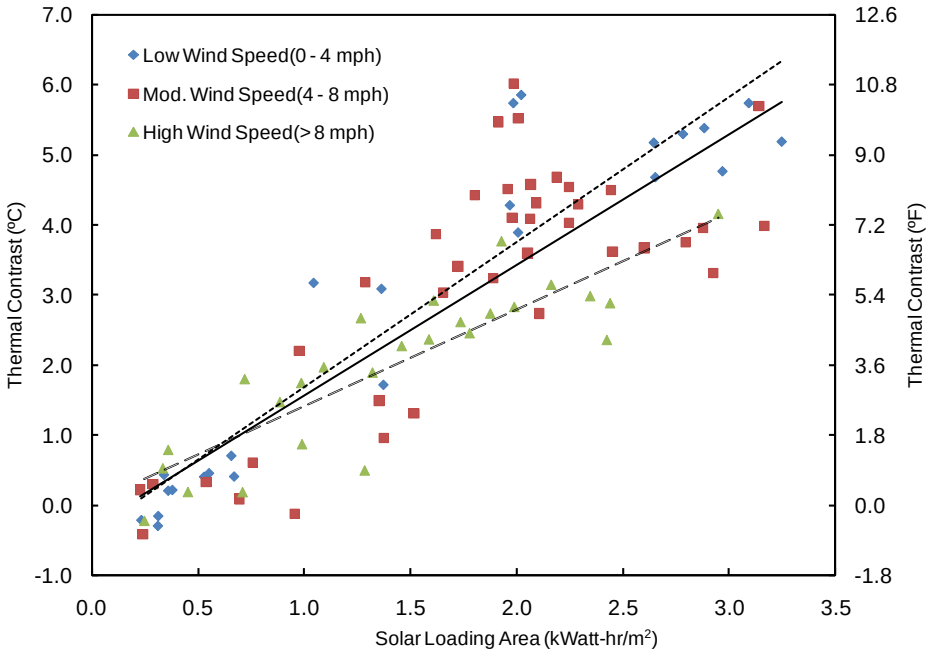

Figure 5.23 : Scatter plot of solar loading vs thermal contrast, with low, moderate and high wind speeds, 3rd quarter.

The analysis of the effects of wind speed on the south side of the test block showed that average wind speeds had an effect on the thermal contrast for two reasons. First, the trend of the correlation plots for low wind speeds was much higher than trends for high wind speeds. In other words, for the same amount of solar loading, days with lower wind speed developed higher thermal contrast than days with high wind speeds, on average. Table 5.8 shows the regression parameters from the analysis of wind speeds. This data indicates that the thermal contrast for days with low wind speeds is greater than days with high wind speeds. Additionally, the R^2 values are much lower for high wind speeds, indicating that this data is more scattered. Second, it was observed that days with higher solar loadings had the characteristic of being days with low to moderate winds. Therefore, based on the fact that trends were higher and the observation that the highest solar loading was observed on days with low to moderate wind speeds, applying a threshold of 3.6 m/s (8 mph) for the maximum average wind speed will result in improved conditions for detection of subsurface features. This "threshold" is not a fixed limit value for wind speed, but is suggested by the data as a useful general guideline based on the results of the study.

Table 5.8 : Regression parameter data from analysis of 2nd and 3rd quarter wind speeds

Regression Parameters	Slope		Intercept		R^2	
Wind Category	2nd Quarter.	3rd Quarter	2nd Quarter	3rd Quarter	2nd Quarter	3rd Quarter
Low Wind	3.79	3.74	-0.69	-0.71	0.81	0.88
High Wind	1.59	1.38	-0.27	0.04	0.55	0.75
All Data	1.87	1.87	-0.31	-0.31	0.75	0.75

It should also be noted that this wind speed is calculated as a 6-hr average wind speed, to characterize an overall condition for a particular time period of six hours. Most data reported by various weather stations is over a much smaller time interval. Therefore, when applying this threshold consideration of the overall wind condition is necessary. Such data can be determined from the web site developed under this research, though this feature has not yet been implemented.

5.5 Thermal Gradients in the Concrete Test Block

To achieve an understanding of the thermal behavior of the test block, this section focuses on the results of thermocouple measurements. The data presented focuses on the thermal behavior of the test block through the 3 ft. thickness of the block (N-S direction) to provide a better understanding of what is occurring over the course of a 24 hour period in concrete that is exposed to direct solar loading verses concrete not exposed to solar loading.

Figure 5.24 shows the thermal gradients established in the test block over the course of a day from 9:00 am to 4:00 pm. Thermocouple-based temperature measurements are shown on the vertical axis (°C) and the depth through the block is shown on the horizontal axis, with 0 being located at the south face of the block. The Figure shows that the temperature at the surface of the block is high and temperature in the block decreases with depth. This is the positive thermal gradient that results from the warming of the day. As can be seen in the Figure, the thermal gradient on the south side of the block is significantly larger than that of the north side of the block, which is consistent with the lower contrast

values found for targets on the North face of the block (Fenwick 2009). The Figure also illustrates the lag in thermal change through the thickness of the block, with the core of the block being significantly cooler than either surface. At the core of the block (near the center of the block) it can be observed that temperature actually decreases during the course of the day, indicating that the core of the block is out of phase with the warming of the ambient environment

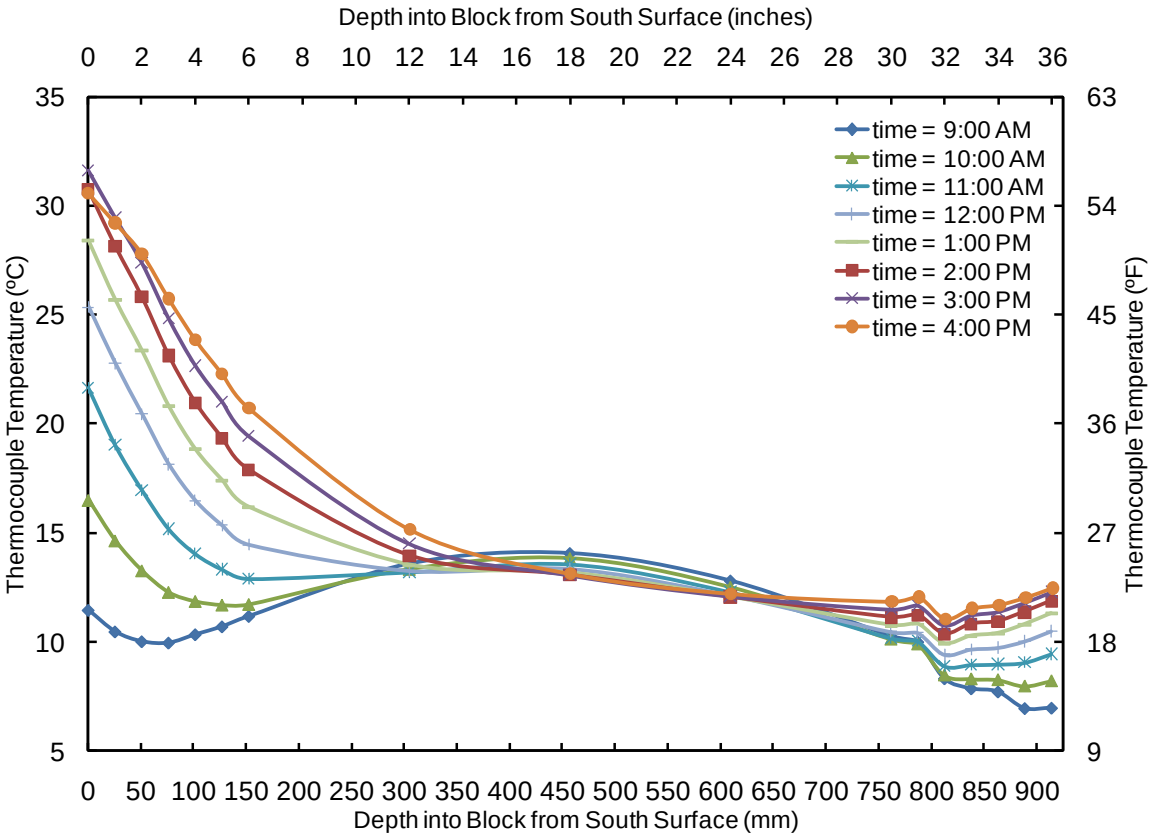

Figure 5.24 : Thermocouple temperature measurements through the test block (S-N) showing positive thermal gradient.

This effect is sometimes referred to as a “thermal wave,” propagating through the material, and results from the cold temperature from the previous nighttime period propagating through the block over the course of time. The significance of

this in terms of thermographic inspection is that it illustrates the thermal behavior of the block that results in deeper defects appearing later in the day than more shallow targets. That is, there is a lag in the thermal changes that occur that increases with depth through the block, such that when the day is warming, the effect of that warming decreases with depth through the block, such that the effects of deeper defects are not observed until later in the day. This also illustrates why that as the day is cooling, deeper targets may appear with higher thermal contrast than shallower targets, as the effect of the daytime warming is still effecting those deeper targets, while shallower targets are diminishing in contrast or beginning negative contrast. Figure 5.25 shows temperature measurements through the thickness of the block as the ambient temperatures are decreasing. In this figure, a negative thermal gradient is shown in which the surface of the block is cooler than temperatures 51-76 mm below the surface. Again it can be seen that the core temperature of the block is increasing while the ambient temperature is decreasing, as a result of the thermal wave from the warmer daytime temperatures. It is also shown in the figure that both the north and south sides of the block develop a negative thermal gradient, though it occurs more rapidly on the south side of the block due to the loss of radiant heating from the sun.

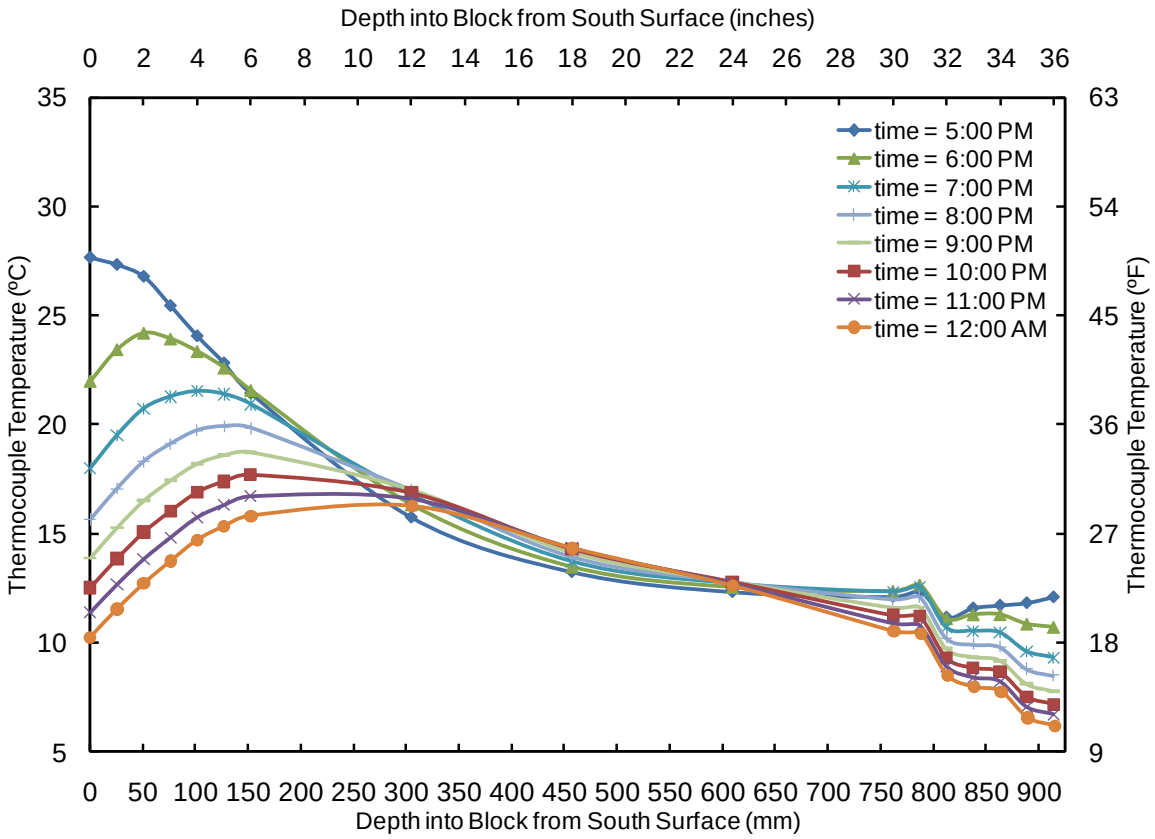

Figure 5.25 : Thermocouple temperature measurements through the test block (S-N) showing negative thermal gradient.

5.6 Inspection Times

The determination of appropriate inspection times is of significant importance for applying thermography to bridge inspection. Determining the appropriate time of day for inspection to be conducted was one of the primary goals of the research, to enable the development of specific guidelines for applying thermography in typical inspection scenarios. This section will describe the determination of “inspection periods” based on the application of the thresholds of 1 and 2°C (1.8 and 3.6°F).

Data from the south side of the block was evaluated to determine the inspection periods for surfaces expose to direct sunlight. In this analysis, 10 days out of the 89 days in which rainfall occurred were omitted, due to the potential influence of rainfall on the timing of thermal contrast development. The results for the warming trend (day time) and cooling trend (night time) periods are shown in Table 5.9. The table presents the time of day at which the threshold contrasts of 1°C and 2°C (1.8°F and 3.6°F) were reached, the average differential between this time and sunrise for the warming trend or day time measurement (based on the sunrise for individual day), and the period of time in which contrast was maintained above that threshold. In the same way the time of the day at which the threshold contrasts of - 1°C and - 2°C (- 1.8°F and - 3.6°F) were reached is recorded and the average differential between this time and sunset for the cooling trend or night time measurement (based on the sunset for individual day) is tabulated. As indicated in the table, for the deep 51 mm deep target, the contrast exceeded the 1°C (1.8°F) threshold at 3:30 (hrs:min) after sunrise, and this contrast was maintained on average for 6:00 hrs. To exceed the threshold of 2°C (3.6°F), the sunrise differential was 4:00 hrs, and contrast was maintained above the threshold level for 5:00 hrs. This data is rounded to the nearest ½ hour. In general, due to the solar loading from the sun, the thermal contrasts were much higher during the inspection intervals than indicated by the threshold values selected. The optimum time for inspection, when thermal contrast was greatest, was calculated and is discussed in section 5.7.

The useful inspection intervals were also calculated for the night time, when thermal contrast were negative. This data may be somewhat less relevant, since surfaces exposed to sunlight would likely be inspected during the day, since the contrasts observed for a given defect would be much greater. However, it was also considered for cases where a nighttime inspection was necessary for some reason, such as access could not be gained during the day, or that an inspector may want to inspect both solar-exposed surfaces and surfaces not exposed to sunlight at the same time, with constant environmental conditions for each. This only occurs at night. It can be noted from Table 5.8, it takes much longer for negative thermal contrast to develop at the targets. This is due to the carry-over of heat developed at the targets during the day. It should also be noted that in contrast to the north side of the test block, the 127 mm (5 in.) deep targets reach the threshold level of 1°C (1.8°F) for both the daytime and the nighttime (Fenwick 2009). For the case of the daytime, this is not unexpected, as the radiant heating from the sun provides a significant driving force for the development of thermal gradients in the block that leads to thermal contrast, even as deep as 127 mm (5. in.). For the nighttime, the increased thermal contrast for the deepest target is the result of the thermal mass of the block reducing the change in surface temperature relative to the target area. Above the target area there is very little concrete between the target and the surface that needs to be cooled, and hence this area cools much faster than the intact areas of the block, leading to increased thermal contrast. This phenomena also

occurs on the north side of the block, but because the overall variations in temperature of the block are small, it’s simply not observable.

Table 5.9 : Observation times, sunrise differentials and useful inspection times for targets for the daytime and nighttime, with contrast limits of 1 and 2°C (1.8 and 3.6°F), South side of test block

Warming Trend (Day Time)												
Target Depth	1 in. Deep Target			2 in. Deep Target			3 in. Deep Target			5 in. Deep Target		
Contrast Threshold	Time (hh:mm)	Sunrise Diff. (hh:mm)	Inspection Period (hh:mm)	Time (hh:mm)	Sunrise Diff. (hh:mm)	Inspection Period (hh:mm)	Time (hh:mm)	Sunrise Diff. (hh:mm)	Inspection Period (hh:mm)	Time (hh:mm)	Sunrise Diff. (hh:mm)	Inspection Period (hh:mm)
Contrast > 1°C (1.8°F)	10:00	2:30	6:30	11:00	3:30	6:00	12:30	5:00	5:00	15:00	8:00	3:00
Contrast >2°C (3.6°F)	10:00	3:00	6:30	11:30	4:00	5:00	13:30	6:30	3:00	x	x	X
Cooling Trend (Night Time)												
Contrast Threshold	Time (hh:mm)	Sunset Diff. (hh:mm)	Inspection Period (hh:mm)	Time (hh:mm)	Sunset Diff. (hh:mm)	Inspection Period (hh:mm)	Time (hh:mm)	Sunset Diff. (hh:mm)	Inspection Period (hh:mm)	Time (hh:mm)	Sunset Diff. (hh:mm)	Inspection Period (hh:mm)
Contrast < -1°C (-1.8°F)	18:00	1:30	13:30	20:00	3:30	12:00	23:30	6:30	8:30	2:30	10:00	5:00
Contrast < -2°C (-3.6°F)	19:30	2:30	10:00	20:30	4:00	8:00	x	x	x	x	x	x

A graphical representation of the suitable inspection periods for the south side of the test block was also developed. This is shown in Figure 5.26, which shows graphically the inspection times for each of the targets. In addition to the 25, 51 and 76 mm (1, 2, and 3 in.) deep targets, data for the 127 mm (5 in.) deep targets is shown (1 °C (1.8 °F) threshold).

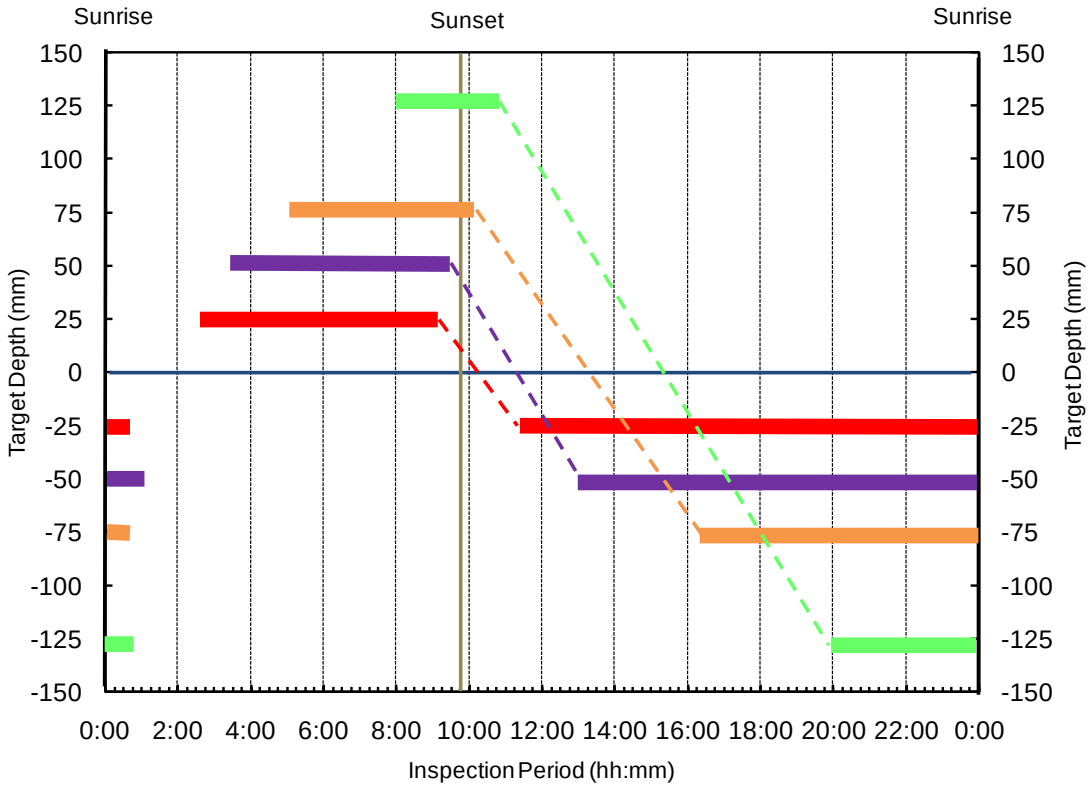

Figure 5.26 : Inspection periods for different target depths of 25, 51, 76 and 127 mm on the south side of the block.

5.7 Optimum Inspection Time

Thermal contrast for the subsurface targets in the test block on the south side of the block varied over the course of a day in a sinusoidal manner, meaning that thermal contrast had a specific peak value during the day that could be identified consistently. This maximum contrast value was evaluated to determine

the optimum time of day for an inspection. It was found that the optimum time of day to conduct inspections varied as a function of the depth of the target, as would be expected, with deeper target developing their maximum contrast very late in the day, after sustained solar loading. Figure 5.27 shows a scatter plot for the development of the optimum contrast for targets at 51, 76 and 127 mm depths (2, 3 and 5 in.). The vertical axis displays the level of maximum contrast, and the horizontal axis shows the time relative to sunrise that the maximum contrast occurred. As the figure shows, the shallower targets develop a much higher contrast over the course of the day, greater than 5°C (9°F) in some cases, and this typically occurs at 6 hours or more after sunrise.

To develop a relationship between the depth of the target and the timing of an optimum inspection, this data was analyzed using only those days when the thermal contrast for the 51 mm target developed at least 1°C or 2°C (3.6°F) of thermal contrast, to omit days when conditions are less optimal for the use of IR thermography.

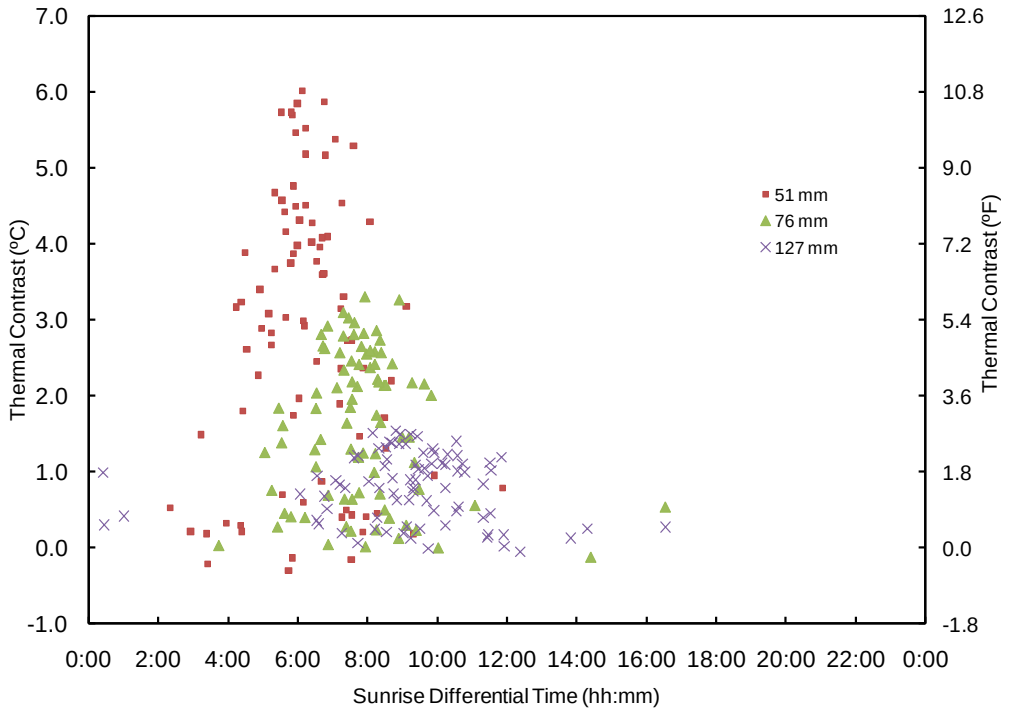

Figure 5.27 : Scatter plot of sunrise differentials against maximum contrast for 51, 76 and 127 mm (2, 3 and 5 in.) targets.

From 89 days of data the sunrise differentials for the four targets were calculated. Three cases were considered for the calculations. Sunrise differentials is the difference between the time at which the maximum contrast occurred and the sunrise time. In case 1 all 89 days were considered. In Case 2, only the days that had greater than 1°C contrast for 51 mm deep target were considered. In Case 3, the days that have greater than 2°C for 51mm deep target were considered. The results for all the three cases are shown in Table 5.10.

Table 5.10 : Sunrise Differentials for the four targets

Targets depth		Case 1		Case 2		Case 3	
		Mean	Std. Deviation	Mean	Std. Deviation	Mean	Std. Deviation
25 mm	Time (hh:mm)	12:47	2:10	12:54	1:05	12:55	1:02
	Sunrise Diff.(hh:mm)	5:32	2:12	5:40	1:06	5:42	1:03
51mm	Time (hh:mm)	13:12	2:22	13:30	1:07	13:30	1:01
	Sunrise Diff.(hh:mm)	5:57	2:23	6:16	1:09	6:17	1:04
76 mm	Time (hh:mm)	14:19	3:41	14:56	1:01	14:58	1:01
	Sunrise Diff.(hh:mm)	7:04	3:39	7:41	1:02	7:44	1:02
127mm	Time (hh:mm)	15:29	4:17	16:21	1:21	16:23	1:21
	Sunrise Diff.(hh:mm)	8:14	4:16	9:07	1:21	9:09	1:21

The results of this analysis are shown in Figure 5.28. This figure shows the relationship between the target depth and the optimum inspection times. The optimum inspection time for the 51, 76, and 127 mm (2, 3 and 5 in.) deep targets were found to be 6:17, 7:44 and 9:09 hrs, respectively. These values differed on the order of a few minutes if all days with at least 1°C (1.8°F) were considered. The standard deviations for this measure were on the order of 1 hr.

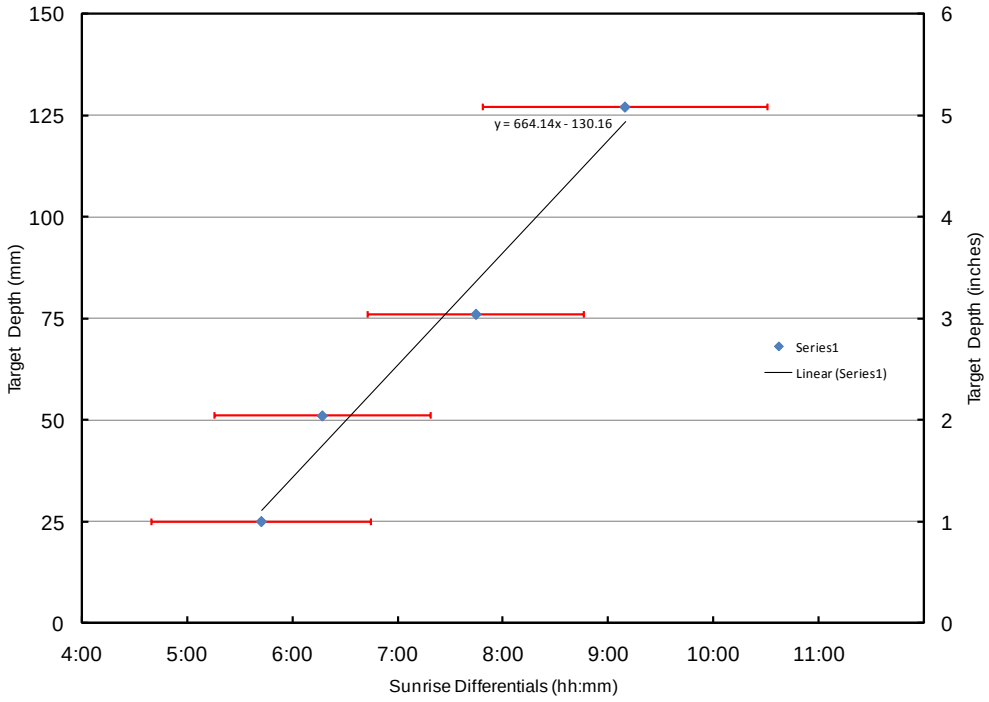

Figure 5.28 : Sunrise differential as a function of target depth with error bars for optimum inspection conditions, south side of test block.

The significance of this finding in terms of application of thermography for bridge inspection is twofold: first, there is a significant delay between sunrise and the optimum time for conducting inspections, and second, that knowledge of the expected depth of the defect can help guide an inspector to the appropriate time to conduct an inspection. For example, if the suspected area of delaminations is between a 51 mm (2 in.) overlay and the concrete deck, then waiting 5 or 7 hrs after sunrise would likely provide the optimum conditions. If the suspected area of delamination is at the level of rebar and the cover is 76 mm (3 in.), than waiting until 7 or 8 hrs after sunrise would provide the optimum conditions.

6

CONCLUSIONS

The objectives of this research were to:

1. Determine environmental conditions that enable detection of subsurface defects in concrete
2. Develop written guidelines for applying IR in the field

This section of the report indicates the conclusions of the research. The results from the south side of the test block, which is exposed to direct solar loading, are as follows:

1. There is a linear relationship between the total solar loading area and the thermal contrast developed for subsurface targets in concrete
    a. Direct, uninterrupted radiant heating from the sun provides the strongest thermal contrast
    b. Clear skies throughout the day will provide stronger thermal contrast relative to days with periodic cloud cover
    c. Longer days (summer) will provide higher thermal contrast than shorter days (winter)

2. High wind speeds were associated with lower thermal contrasts for targets in the test block
    a. Days with the highest solar loading area tended to have low to moderate wind speeds
    b. High winds speeds reduce thermal contrast relative to low wind speeds
3. A practical guideline for maximum average wind speeds during thermographic inspections is 3.6 m/s (8 mph), based on a 6 hour average
4. Optimum times for inspection under solar loading varied linearly as a function of depth of the target in the test block, ranging from a little greater than 6 hrs after sunrise for the 51 mm deep (2 in.) target to more than 9 hrs for the 127 mm (5 in.) deep target.
5. Inspection periods were calculated based on the thresholds of 1 and 2°C (1.8 and 3.6°F) for each of the targets in the test block. For daytime inspections of targets at 51 mm, the inspection periods based on 1 and 2°C (1.8 and 3.6°F) were 6:00 hrs and 5:00 hrs, respectively.

References

Aamodt, L. C., Spicer, J. W. M., and Murphy, J. C. (1990). "Analysis of characteristic thermal transit times for time-resolved infrared radiometry studies of multilayered coatings." *Journal of Applied Physics*, 68, 6087.

ASTM. (2007). "Standard Test Method for Detecting Delaminations in Bridge Decks Using Infrared Thermography." Standard ASTM D4788 - 03(2007), ASTM International, West Conshohocken, PA, United States.

Busse, G., Wu, D., and Karpen, W. (1992). "Thermal wave imaging with phase sensitive modulated thermography." *Journal of Applied Physics*, 71, 3962.

Carino, N. J. "The Impact-Echo Method: An Overview."

Clark, M. R., McCann, D. M., and Forde, M. C. (2003). "Application of infrared thermography to the non-destructive testing of concrete and masonry bridges." *NDT & E international*, 36(4), 265-275.

Clemena G G, and Wallace T. McKeel, J. (1978). " Detection Of Delamination in Bridge Decks with Infrared Thermography." *Transportation Research Record No. 664*, Volume 1, 180-182.

Clemena, G., and McKeel Jr, W. (1977). "The applicability of infrared thermography in the detection of delamination in bridge decks." *Virginia Highway and Transportation Research Council, Charlottesville Report* No. VHTRC-78R27,, 35 pp.

Fenwick, R. G. (2009). "Environmental Effects on Subsurface Defect Detection in Concrete Without Solar Load." *MS Thesis University of Missouri*.

Maldague, X. (2000). "Applications of infrared thermography in nondestructive evaluation." *Trends in Optical Nondestructive Testing*, 591-609.

Manning, D., and Holt, F. (1983). "Detecting deterioration in asphalt-covered bridge decks." *Transporation Rsearch Record 899*, 10-20.

Manning, D. G., and Holt, F.B. (1980). "Detecting Delaminations in Concrete Bridge Decks." Concrete International, 34, 41.

Manning, D. G., and Holt, F.B. (1983). "Detecting Deterioration in Asphalt-Covered Bridge Decks." *Transportation Research Record*, 899.

Maser, K. R. (1990). "Principles of Thermography and Radar for Bridge Deck Assessment." *Journal of Transportation Engineering*, 116, 583.

Popovics, J. S. (2003). "NDE techniques for concrete and masonry structures." *Progress in Structural Engineering and Materials*, 5(2), 49-59.

Yehia, S., Abudayyeh, O., Nabulsi, S., and Abdelqader, I. (2007). "Detection of Common Defects in Concrete Bridge Decks Using Nondestructive Evaluation Techniques." *Journal of Bridge Engineering*, 12, 215.

Zhang, J., Gupta, A., and Baker, J. (2007). "Effect of Relative Humidity on the Prediction of Natural Convection Heat Transfer Coefficients." *Heat Transfer Engineering*, 28(4), 335-342.

APPENDIX A

The following are suggested guidelines for the thermographic inspection of highway bridges, based on the results of the research.

1.1 Solar loading

1.1.1 Conduct inspections on days when there is direct, uninterrupted solar loading. Cloud cover should be minimal.

1.1.2 Due to the more intense and longer solar exposure, summer days are preferred over winter days.

1.1.3 The total solar loading area can be used to further define adequate solar loading, though this likely is not necessary in general. Solar loading, if determined, should be greater than 1.4 kW-hr/m^2 for the day. This can be estimated based on the solar radiation measured at midday, multiplied by the anticipated length of sunlight for the day. Direct solar loading in summer is approximately 1 kW/m^2.

1.1.3.1 Commentary: This value is based on conservatively estimating the total solar loading curve to occupy ½ the area of a rectangle defined by the approximate maximum solar load and the length of solar loading for that day.

1.2 Wind Conditions

1.2.1 Average wind speeds should be less than 8 mph prior to and during the inspection period. The average wind speed should be calculated based on a 6 hr average.

1.2.2 In general, lower wind speeds will result in improved thermal contrast for surfaces exposed to solar loading.

1.3 Inspection Period

1.3.1 Inspections should be conducted starting no sooner than 4 hrs after sunrise to allow for thermal contrast to develop when anticipated depth of the delamination is approximately 25 mm from the surface of the concrete. The useful inspection period is expected to last approximately 6 hrs. If the anticipated depth is 76 mm, inspection should be conducted starting 5 to 6 hours after sunrise. The useful inspection period will last approximately 5 hours.

APPENDIX B

In this appendix all the graphs with the ambient temperature against the thermal contrast for different target depths on a weekly basis for the three months are shown periodically. The first four weeks of each month are shown in chronological order.

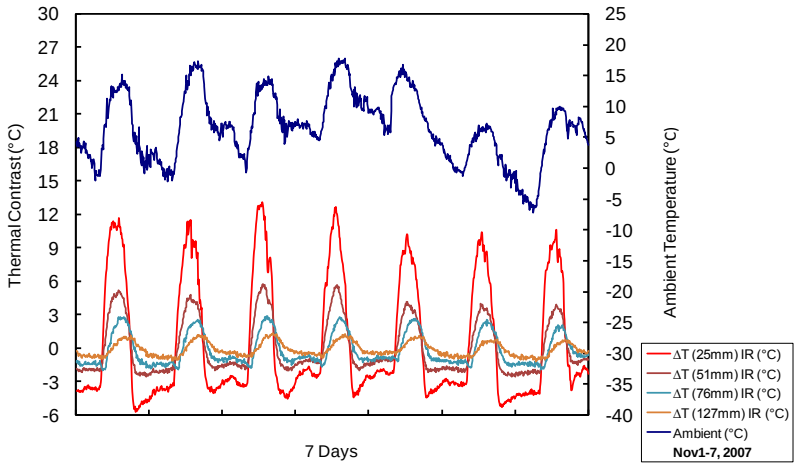
Thermal Contrast (°C)
Ambient Temperature (°C)
7 Days
ΔT (25mm) IR (°C)
ΔT (51mm) IR (°C)
ΔT (76mm) IR (°C)
ΔT (127mm) IR (°C)
Ambient (°C)
Nov1-7, 2007

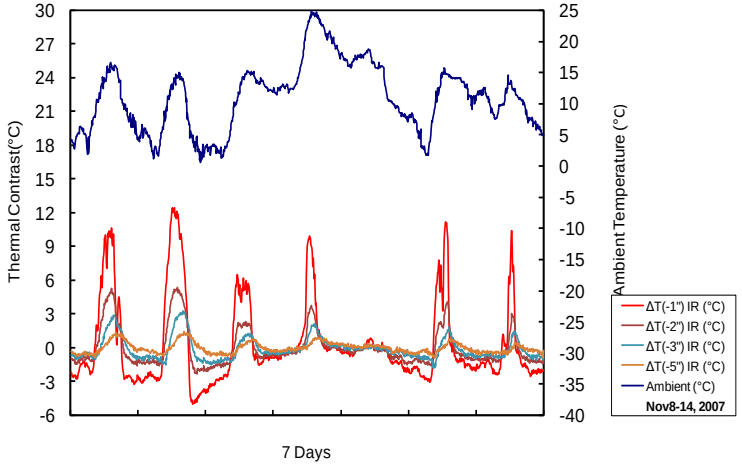
Thermal Contrast(°C)
Ambient Temperature (°C)
7 Days
ΔT(-1") IR (°C)
ΔT(-2") IR (°C)
ΔT(-3") IR (°C)
ΔT(-5") IR (°C)
Ambient (°C)
Nov8-14, 2007

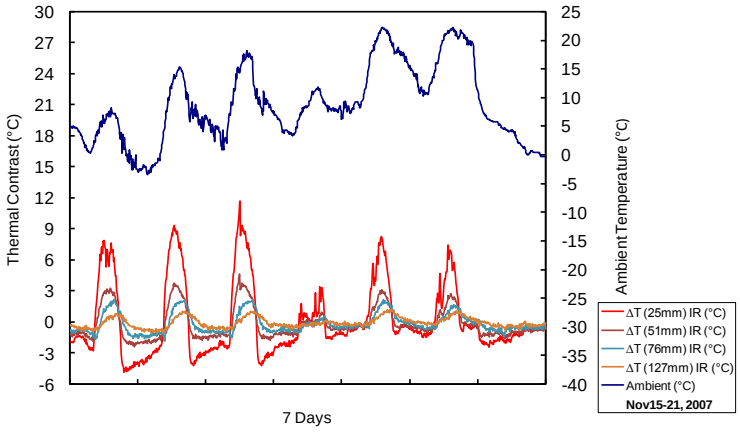
Thermal Contrast (°C)
Ambient Temperature (°C)
7 Days
ΔT (25mm) IR (°C)
ΔT (51mm) IR (°C)
ΔT (76mm) IR (°C)
ΔT (127mm) IR (°C)
Ambient (°C)
Nov15-21, 2007

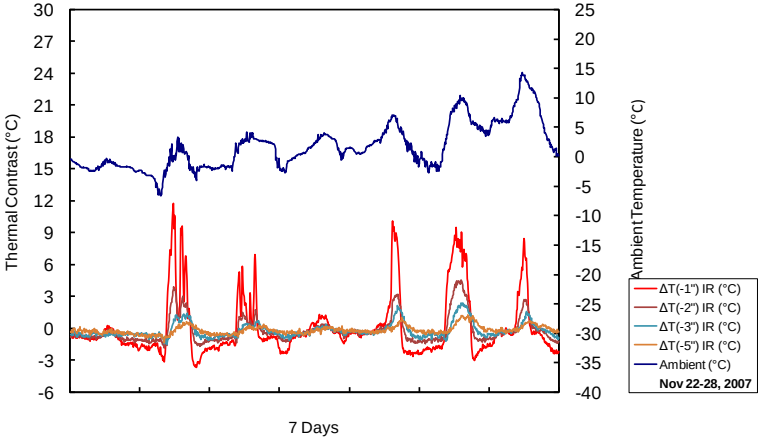
Thermal Contrast (°C)
Ambient Temperature (°C)
7 Days
ΔT(-1") IR (°C)
ΔT(-2") IR (°C)
ΔT(-3") IR (°C)
ΔT(-5") IR (°C)
Ambient (°C)
Nov 22-28, 2007

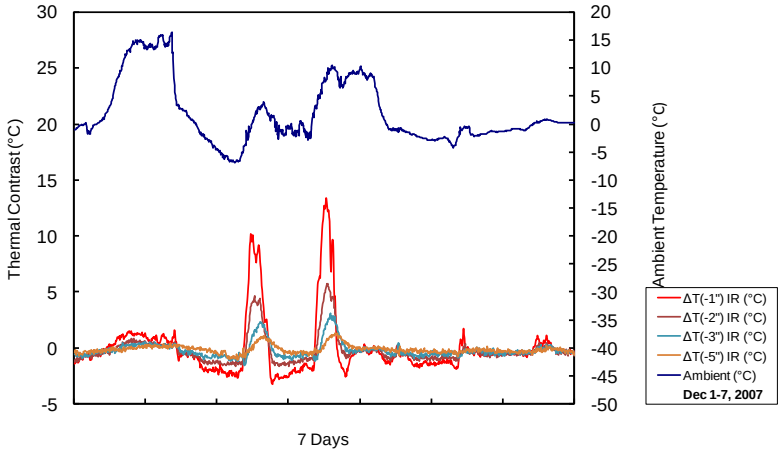
Thermal Contrast (°C)
Ambient Temperature (°C)
7 Days
ΔT(-1") IR (°C)
ΔT(-2") IR (°C)
ΔT(-3") IR (°C)
ΔT(-5") IR (°C)
Ambient (°C)
Dec 1-7, 2007

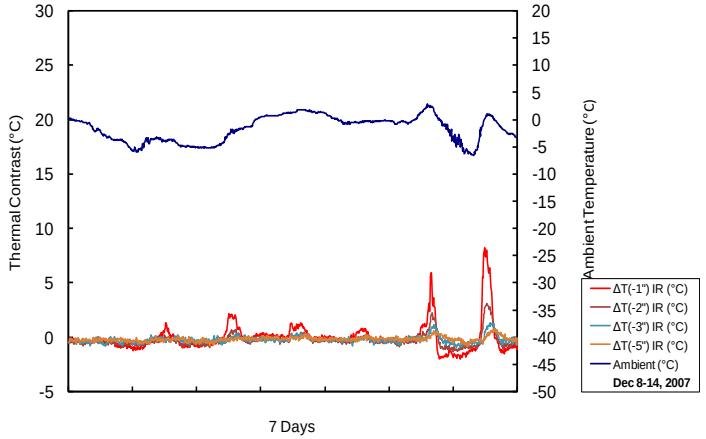
Thermal Contrast (°C)
Ambient Temperature (°C)
7 Days
ΔT(-1") IR (°C)
ΔT(-2") IR (°C)
ΔT(-3") IR (°C)
ΔT(-5") IR (°C)
Ambient (°C)
Dec 8-14, 2007

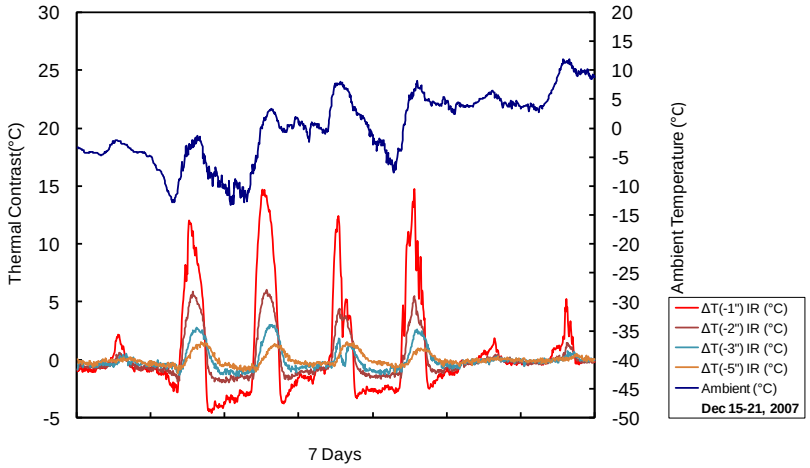
Thermal Contrast(°C)
Ambient Temperature (°C)
7 Days
ΔT(-1") IR (°C)
ΔT(-2") IR (°C)
ΔT(-3") IR (°C)
ΔT(-5") IR (°C)
Ambient (°C)
Dec 15-21, 2007

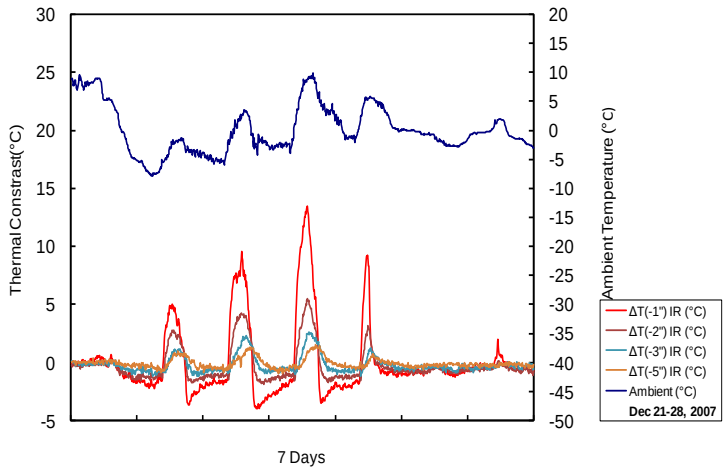
Thermal Constrast(°C)
Ambient Temperature (°C)
7 Days
ΔT(-1") IR (°C)
ΔT(-2") IR (°C)
ΔT(-3") IR (°C)
ΔT(-5") IR (°C)
Ambient (°C)
Dec 21-28, 2007

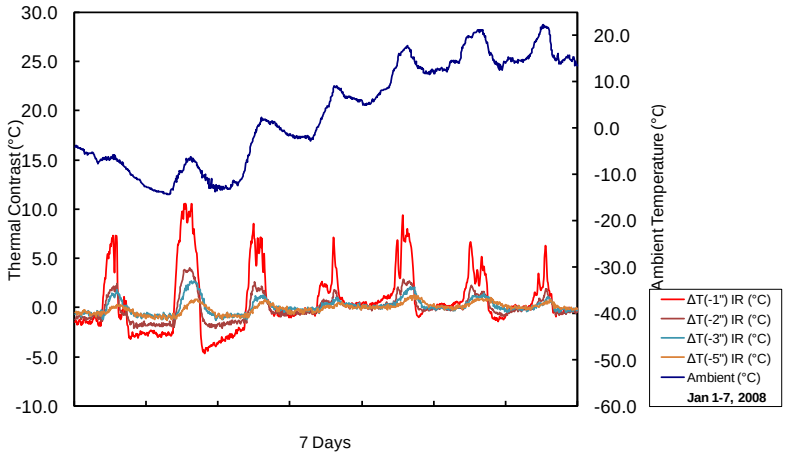
Thermal Contrast (°C)
Ambient Temperature (°C)
7 Days
ΔT(-1") IR (°C)
ΔT(-2") IR (°C)
ΔT(-3") IR (°C)
ΔT(-5") IR (°C)
Ambient (°C)
Jan 1-7, 2008

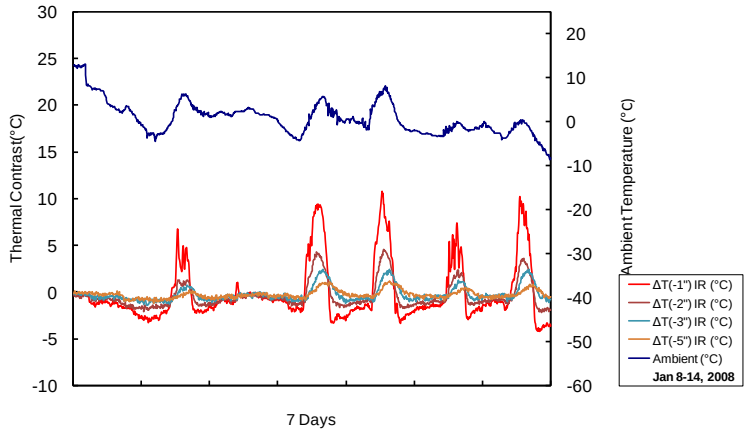
Thermal Contrast(°C)
Ambient Temperature (°C)
7 Days
ΔT(-1") IR (°C)
ΔT(-2") IR (°C)
ΔT(-3") IR (°C)
ΔT(-5") IR (°C)
Ambient (°C)
Jan 8-14, 2008

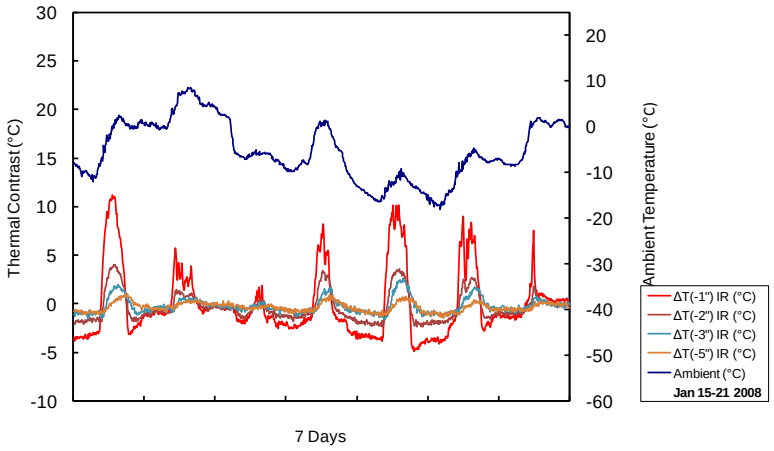
Thermal Contrast (°C)
Ambient Temperature (°C)
7 Days
ΔT(-1") IR (°C)
ΔT(-2") IR (°C)
ΔT(-3") IR (°C)
ΔT(-5") IR (°C)
Ambient (°C)
Jan 15-21 2008

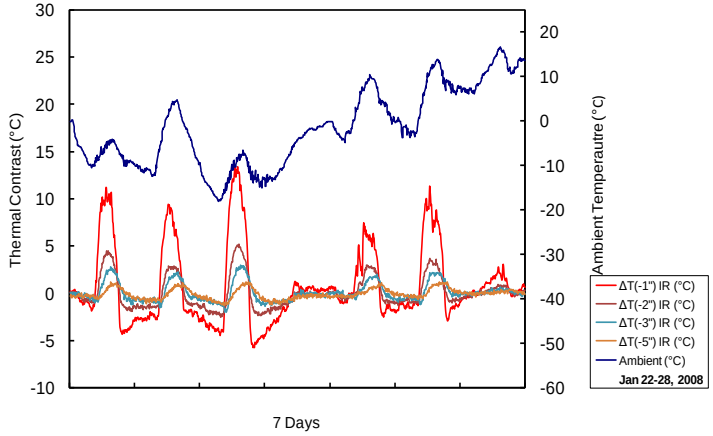
Thermal Contrast (°C)
Ambient Temperautre (°C)
7 Days
ΔT(-1") IR (°C)
ΔT(-2") IR (°C)
ΔT(-3") IR (°C)
ΔT(-5") IR (°C)
Ambient (°C)
Jan 22-28, 2008

APPENDIX C

In this appendix all the graphs with the Solar Load against the thermal contrast for different target depths on a weekly basis for the three months are shown periodically. The first four weeks of each month are shown in chronological order.

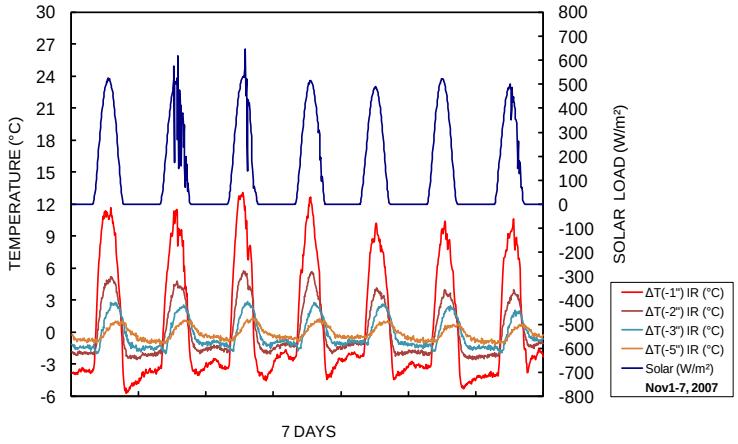
TEMPERATURE (°C)
SOLAR LOAD (W/m²)
7 DAYS
ΔT(-1") IR (°C)
ΔT(-2") IR (°C)
ΔT(-3") IR (°C)
ΔT(-5") IR (°C)
Solar (W/m²)
Nov1-7, 2007

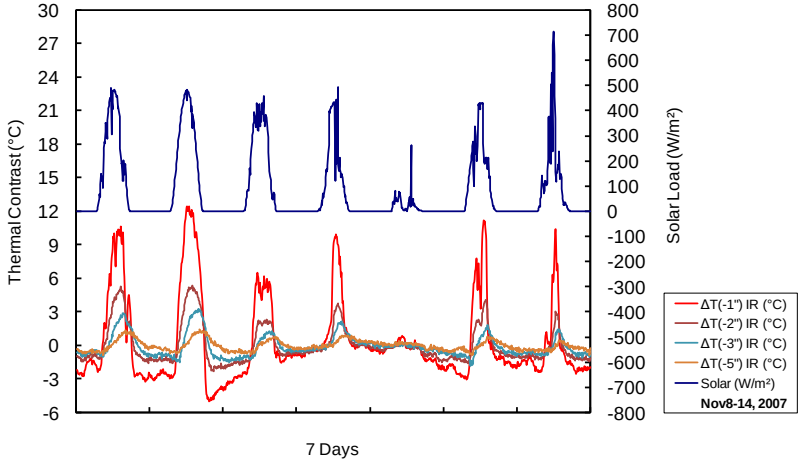
Thermal Contrast (°C)
Solar Load (W/m²)
7 Days
ΔT(-1") IR (°C)
ΔT(-2") IR (°C)
ΔT(-3") IR (°C)
ΔT(-5") IR (°C)
Solar (W/m²)
Nov8-14, 2007

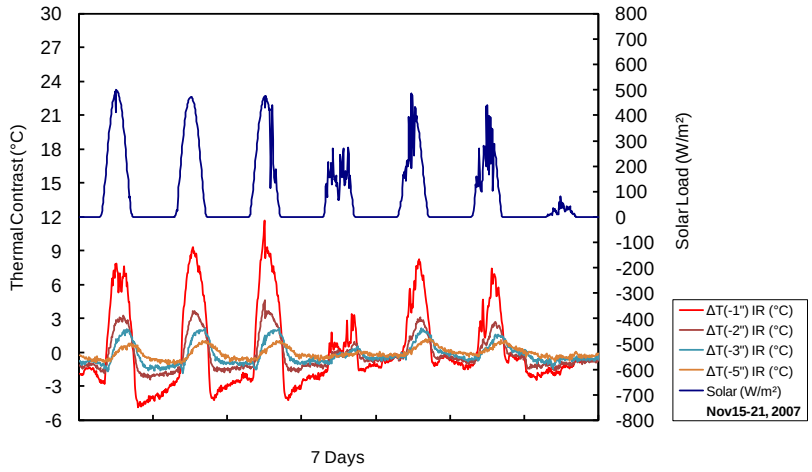
Thermal Contrast (°C)
Solar Load (W/m²)
7 Days
ΔT(-1") IR (°C)
ΔT(-2") IR (°C)
ΔT(-3") IR (°C)
ΔT(-5") IR (°C)
Solar (W/m²)
Nov15-21, 2007

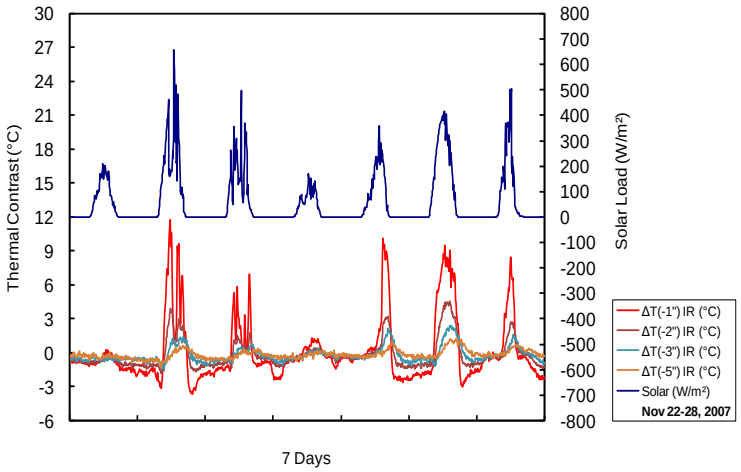
Thermal Contrast (°C)
Solar Load (W/m²)
7 Days
ΔT(-1") IR (°C)
ΔT(-2") IR (°C)
ΔT(-3") IR (°C)
ΔT(-5") IR (°C)
Solar (W/m²)
Nov 22-28, 2007

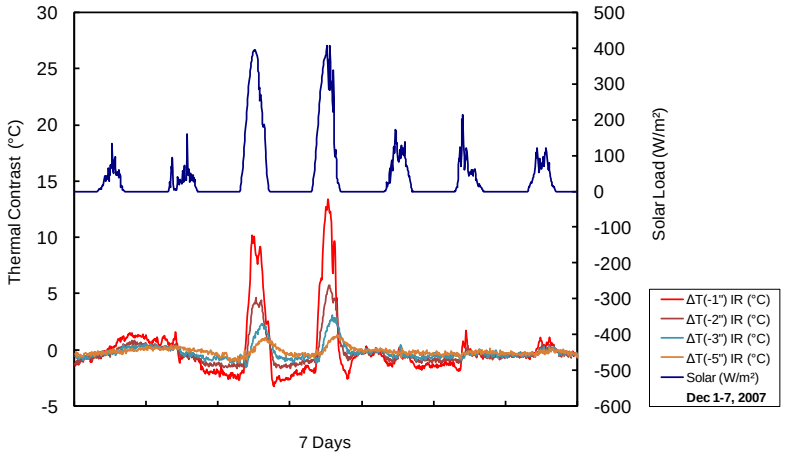
Thermal Contrast (°C)
Solar Load (W/m²)
7 Days
ΔT(-1") IR (°C)
ΔT(-2") IR (°C)
ΔT(-3") IR (°C)
ΔT(-5") IR (°C)
Solar (W/m²)
Dec 1-7, 2007

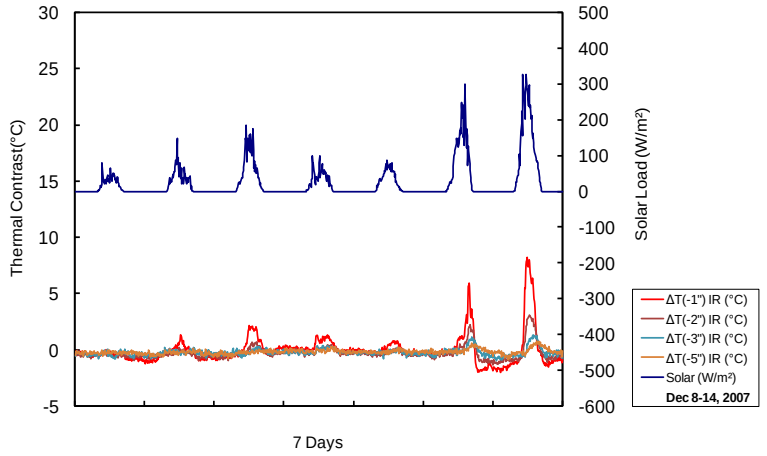
Thermal Contrast(°C)
Solar Load (W/m²)
7 Days
ΔT(-1") IR (°C)
ΔT(-2") IR (°C)
ΔT(-3") IR (°C)
ΔT(-5") IR (°C)
Solar (W/m²)
Dec 8-14, 2007

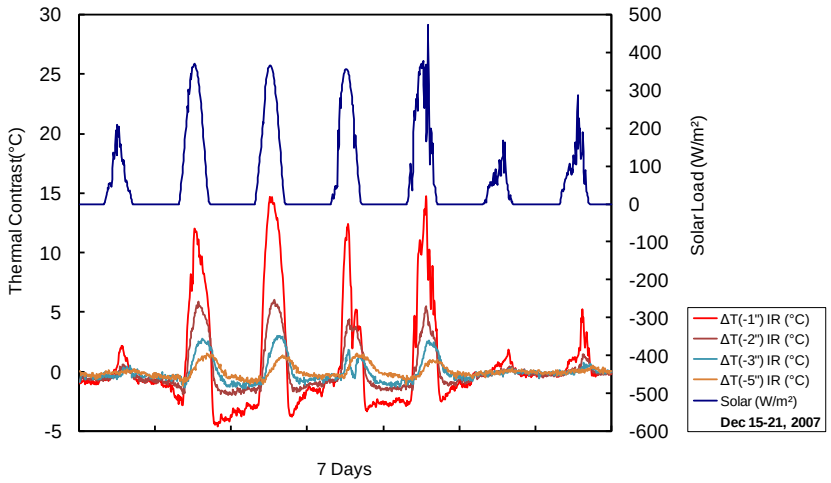
Thermal Contrast(°C)
Solar Load (W/m²)
7 Days
ΔT(-1") IR (°C)
ΔT(-2") IR (°C)
ΔT(-3") IR (°C)
ΔT(-5") IR (°C)
Solar (W/m²)
Dec 15-21, 2007

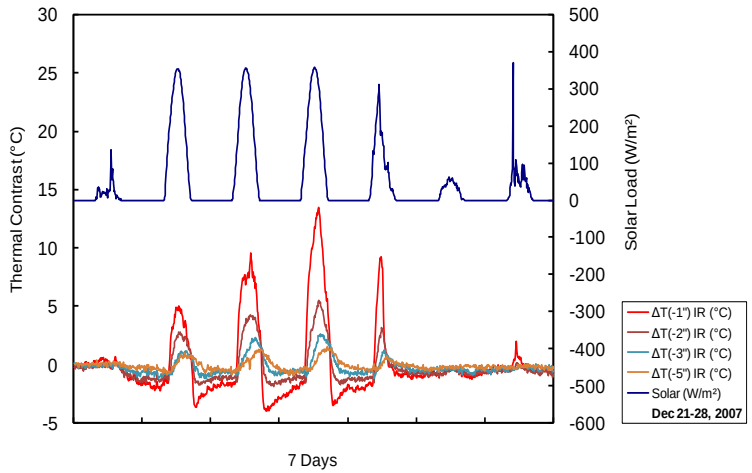
Thermal Contrast (°C)
Solar Load (W/m²)
7 Days
ΔT(-1") IR (°C)
ΔT(-2") IR (°C)
ΔT(-3") IR (°C)
ΔT(-5") IR (°C)
Solar (W/m²)
Dec 21-28, 2007

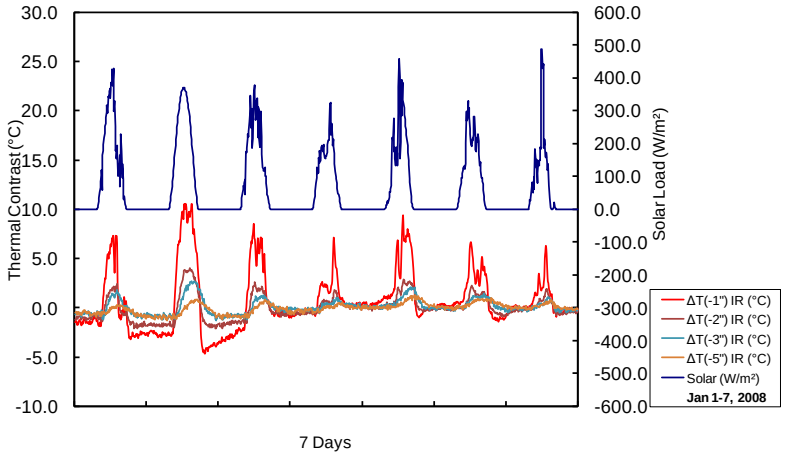
Thermal Contrast (°C)
Solar Load (W/m²)
7 Days
ΔT(-1") IR (°C)
ΔT(-2") IR (°C)
ΔT(-3") IR (°C)
ΔT(-5") IR (°C)
Solar (W/m²)
Jan 1-7, 2008

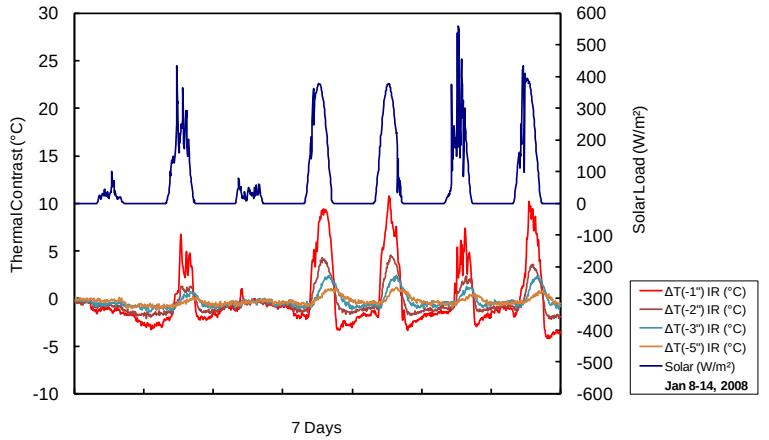
Thermal Contrast (°C)
Solar Load (W/m²)
7 Days
ΔT(-1") IR (°C)
ΔT(-2") IR (°C)
ΔT(-3") IR (°C)
ΔT(-5") IR (°C)
Solar (W/m²)
Jan 8-14, 2008

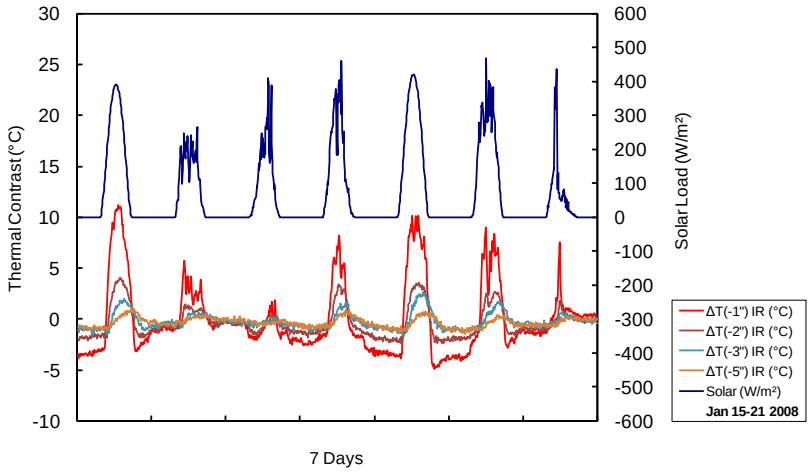
Thermal Contrast (°C)
Solar Load (W/m²)
7 Days
ΔT(-1") IR (°C)
ΔT(-2") IR (°C)
ΔT(-3") IR (°C)
ΔT(-5") IR (°C)
Solar (W/m²)
Jan 15-21 2008

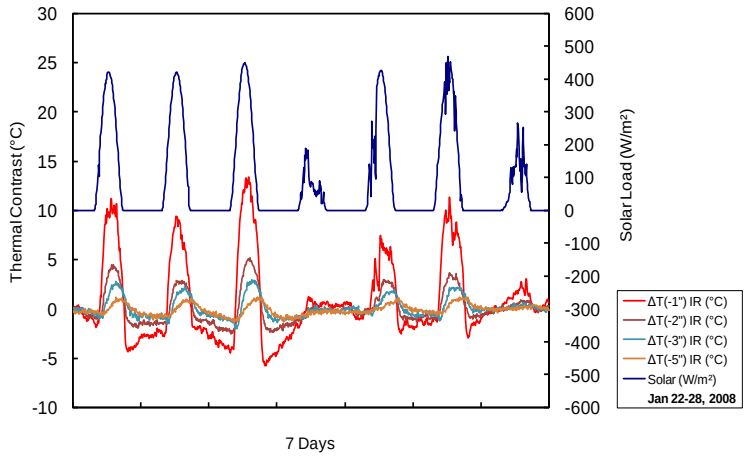
Thermal Contrast (°C)
Solar Load (W/m²)
7 Days
ΔT(-1") IR (°C)
ΔT(-2") IR (°C)
ΔT(-3") IR (°C)
ΔT(-5") IR (°C)
Solar (W/m²)
Jan 22-28, 2008

APPENDIX D

In this appendix all the graphs with the Wind Speed against the thermal contrast for different target depths on a weekly basis for the three months are shown periodically. The first four weeks of each month are shown in chronological order.

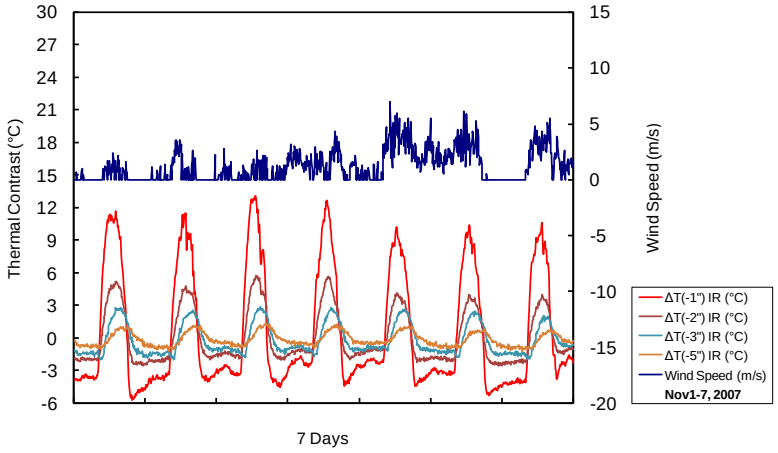
Thermal Contrast (°C)
Wind Speed (m/s)
7 Days
ΔT(-1") IR (°C)
ΔT(-2") IR (°C)
ΔT(-3") IR (°C)
ΔT(-5") IR (°C)
Wind Speed (m/s)
Nov1-7, 2007

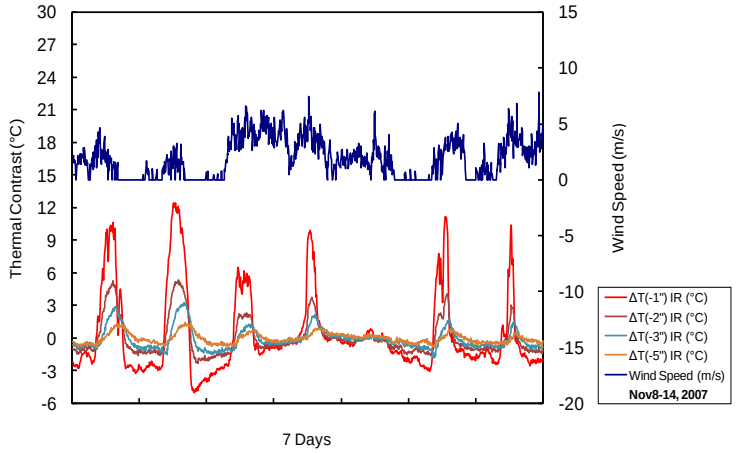
Thermal Contrast (°C)
Wind Speed (m/s)
7 Days
ΔT(-1") IR (°C)
ΔT(-2") IR (°C)
ΔT(-3") IR (°C)
ΔT(-5") IR (°C)
Wind Speed (m/s)
Nov8-14, 2007

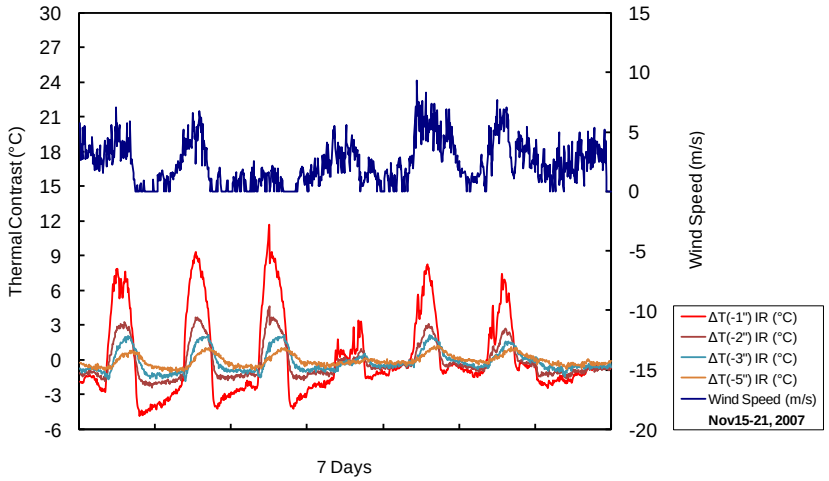
Thermal Contrast (°C)
Wind Speed (m/s)
7 Days
ΔT(-1") IR (°C)
ΔT(-2") IR (°C)
ΔT(-3") IR (°C)
ΔT(-5") IR (°C)
Wind Speed (m/s)
Nov15-21, 2007

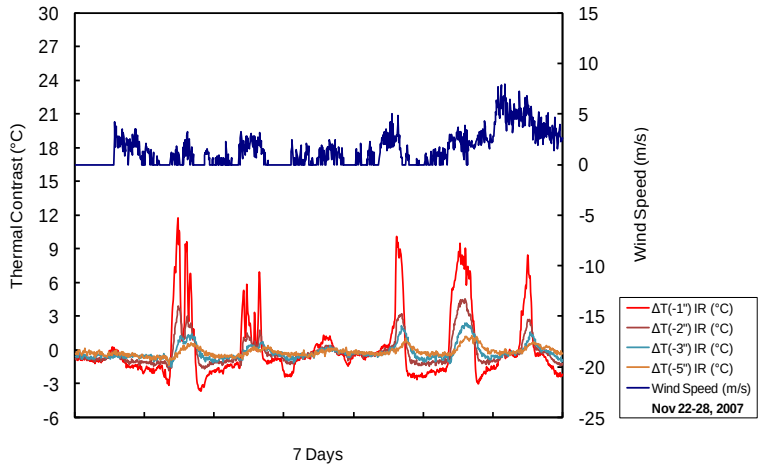
Thermal Contrast (°C)
Wind Speed (m/s)
7 Days
ΔT(-1") IR (°C)
ΔT(-2") IR (°C)
ΔT(-3") IR (°C)
ΔT(-5") IR (°C)
Wind Speed (m/s)
Nov 22-28, 2007

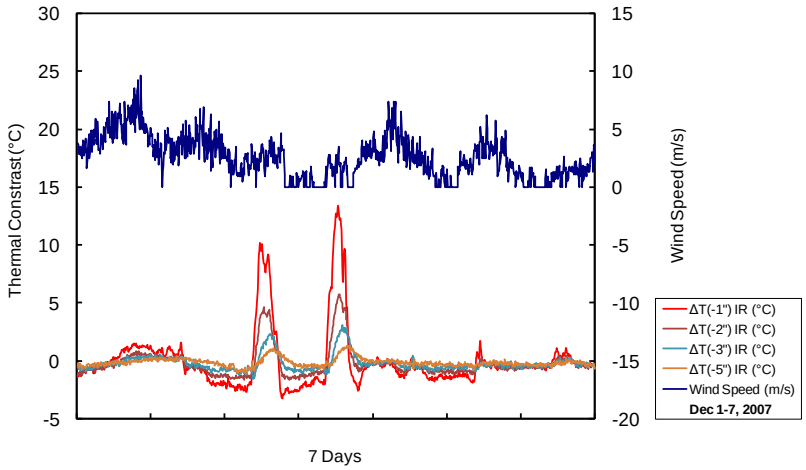
Thermal Constrast (°C)
Wind Speed (m/s)
7 Days
ΔT(-1") IR (°C)
ΔT(-2") IR (°C)
ΔT(-3") IR (°C)
ΔT(-5") IR (°C)
Wind Speed (m/s)
Dec 1-7, 2007

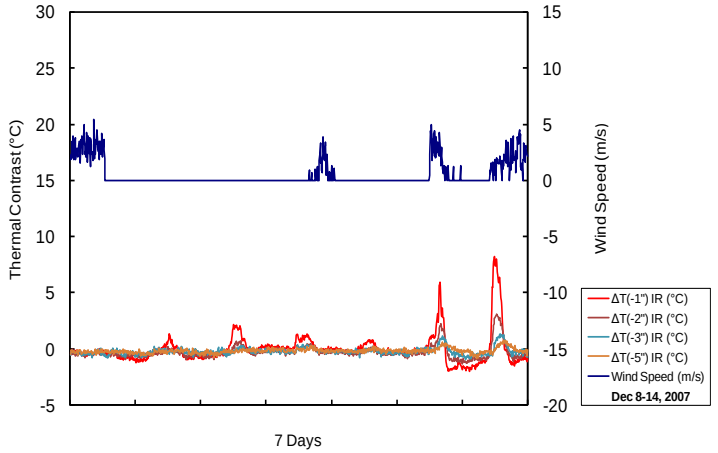
Thermal Contrast (°C)
Wind Speed (m/s)
7 Days
ΔT(-1") IR (°C)
ΔT(-2") IR (°C)
ΔT(-3") IR (°C)
ΔT(-5") IR (°C)
Wind Speed (m/s)
Dec 8-14, 2007

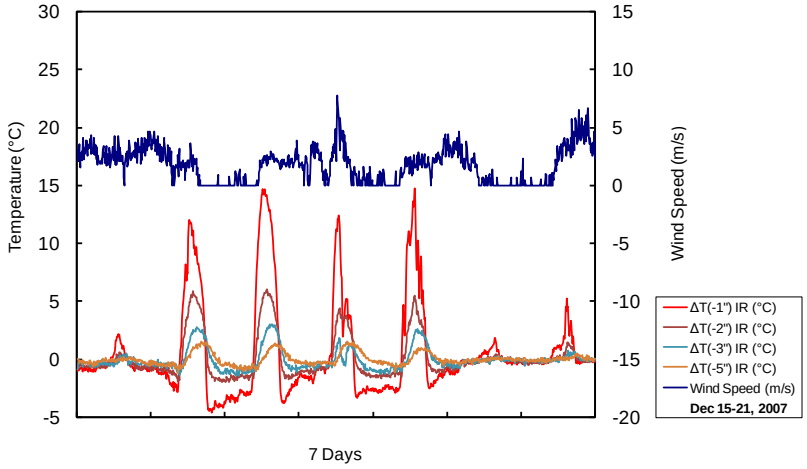
Temperature (°C)
Wind Speed (m/s)
7 Days
ΔT(-1") IR (°C)
ΔT(-2") IR (°C)
ΔT(-3") IR (°C)
ΔT(-5") IR (°C)
Wind Speed (m/s)
Dec 15-21, 2007

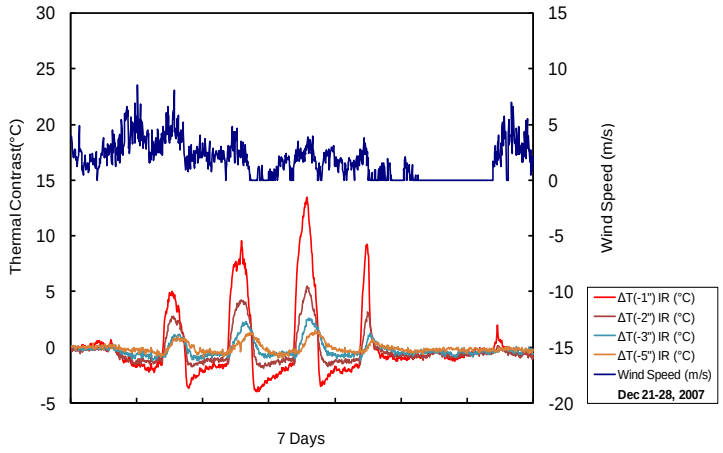
Thermal Contrast(°C)
Wind Speed (m/s)
7 Days
ΔT(-1") IR (°C)
ΔT(-2") IR (°C)
ΔT(-3") IR (°C)
ΔT(-5") IR (°C)
Wind Speed (m/s)
Dec 21-28, 2007

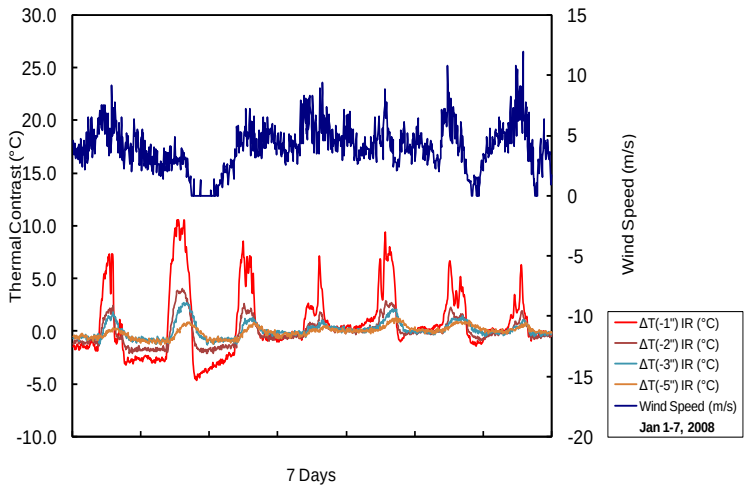
Thermal Contrast (°C)
Wind Speed (m/s)
7 Days
ΔT(-1") IR (°C)
ΔT(-2") IR (°C)
ΔT(-3") IR (°C)
ΔT(-5") IR (°C)
Wind Speed (m/s)
Jan 1-7, 2008

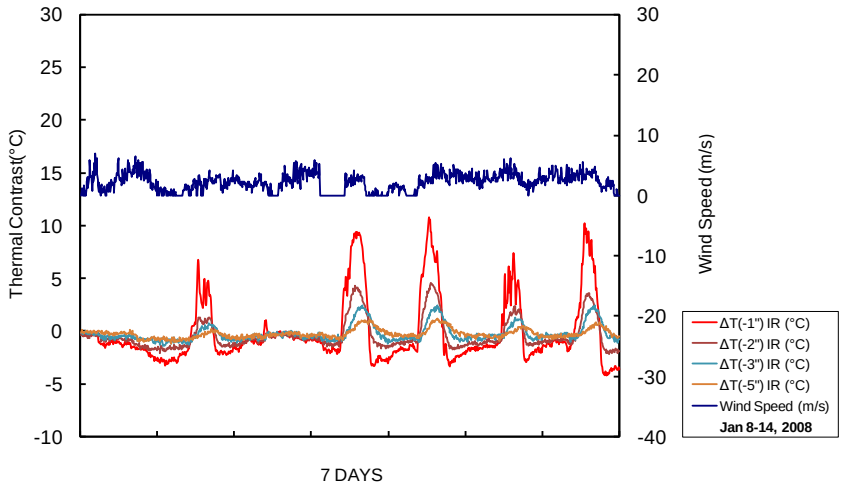
Thermal Contrast(°C)
Wind Speed (m/s)
7 DAYS
ΔT(-1") IR (°C)
ΔT(-2") IR (°C)
ΔT(-3") IR (°C)
ΔT(-5") IR (°C)
Wind Speed (m/s)
Jan 8-14, 2008

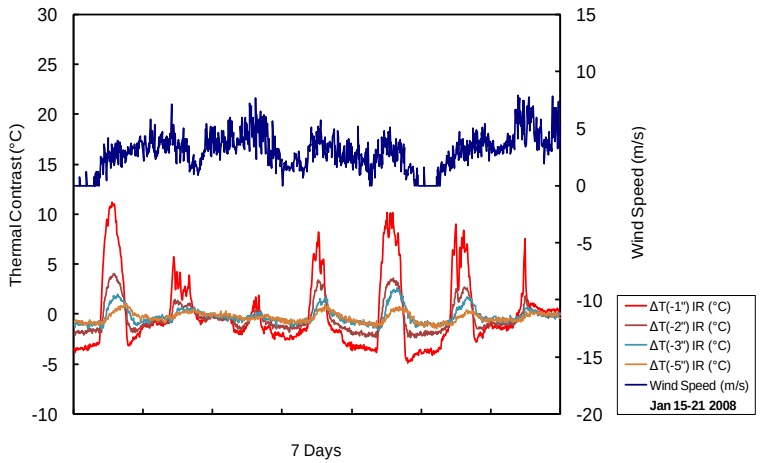
Thermal Contrast (°C)
Wind Speed (m/s)
7 Days
ΔT(-1") IR (°C)
ΔT(-2") IR (°C)
ΔT(-3") IR (°C)
ΔT(-5") IR (°C)
Wind Speed (m/s)
Jan 15-21 2008

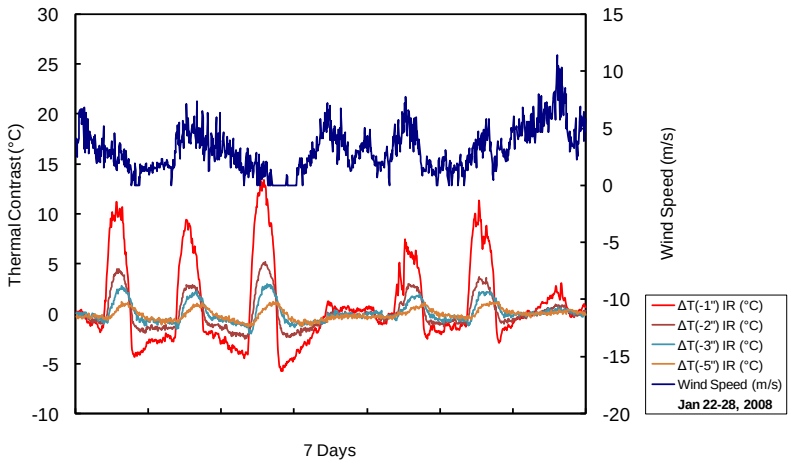
Thermal Contrast (°C)
Wind Speed (m/s)
7 Days
ΔT(-1") IR (°C)
ΔT(-2") IR (°C)
ΔT(-3") IR (°C)
ΔT(-5") IR (°C)
Wind Speed (m/s)
Jan 22-28, 2008

APPENDIX E

In this appendix all the graphs with the Relative Humidity against the thermal contrast for different target depths on a weekly basis for the three months are shown periodically. The first four weeks of each month are shown in chronological order.

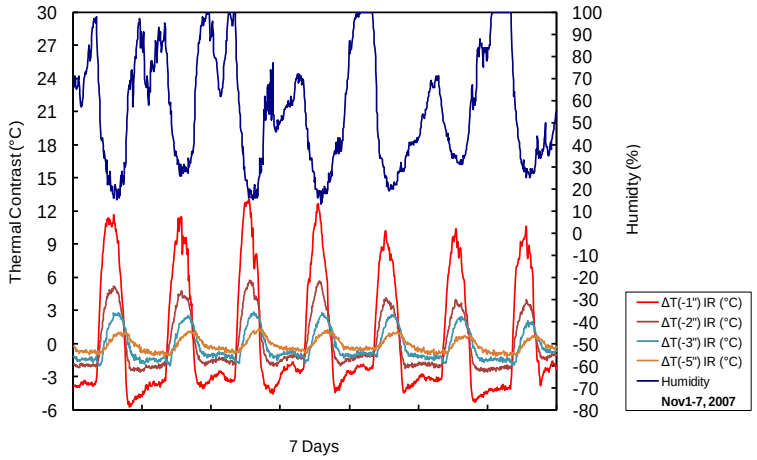
Thermal Contrast (°C)
Humidty (%)
7 Days
ΔT(-1") IR (°C)
ΔT(-2") IR (°C)
ΔT(-3") IR (°C)
ΔT(-5") IR (°C)
Humidity
Nov1-7, 2007

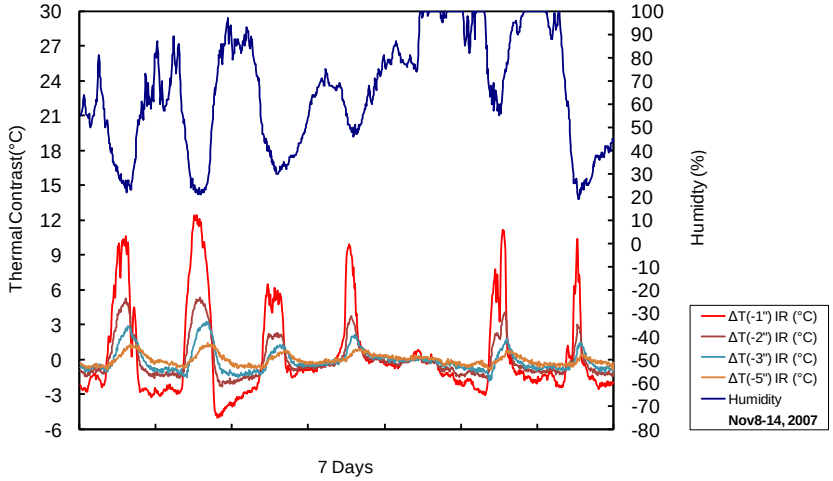
Thermal Contrast(°C)
Humidty (%)
7 Days
ΔT(-1") IR (°C)
ΔT(-2") IR (°C)
ΔT(-3") IR (°C)
ΔT(-5") IR (°C)
Humidity
Nov8-14, 2007

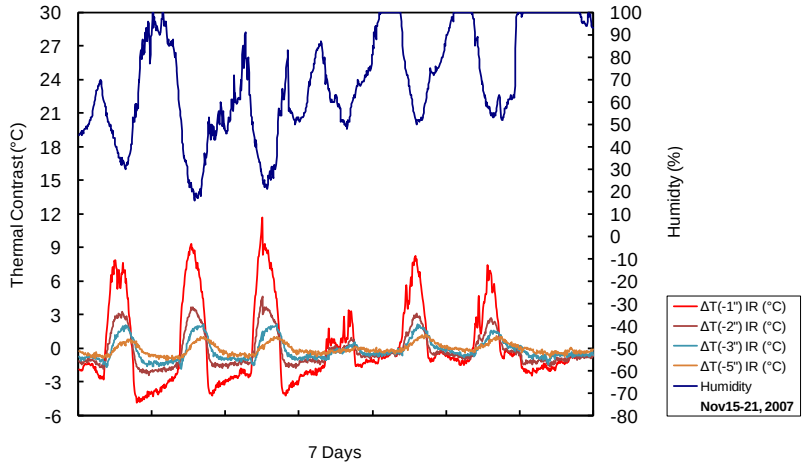
Thermal Contrast (°C)
Humidty (%)
7 Days
ΔT(-1") IR (°C)
ΔT(-2") IR (°C)
ΔT(-3") IR (°C)
ΔT(-5") IR (°C)
Humidity
Nov15-21, 2007

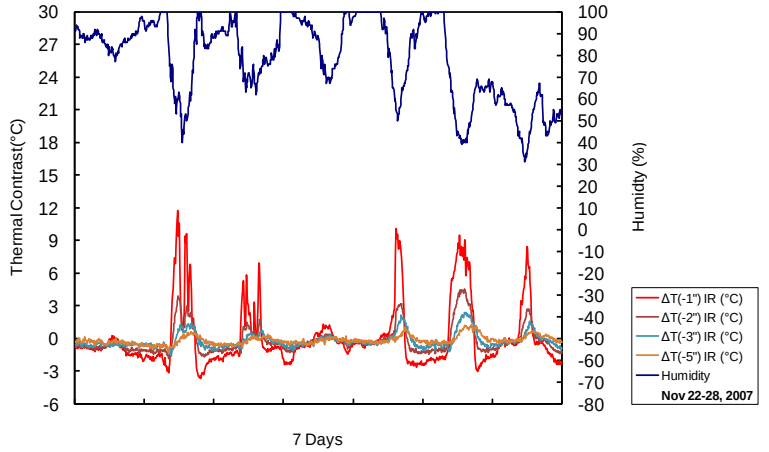
Thermal Contrast(°C)
Humidty (%)
7 Days
ΔT(-1") IR (°C)
ΔT(-2") IR (°C)
ΔT(-3") IR (°C)
ΔT(-5") IR (°C)
Humidity
Nov 22-28, 2007

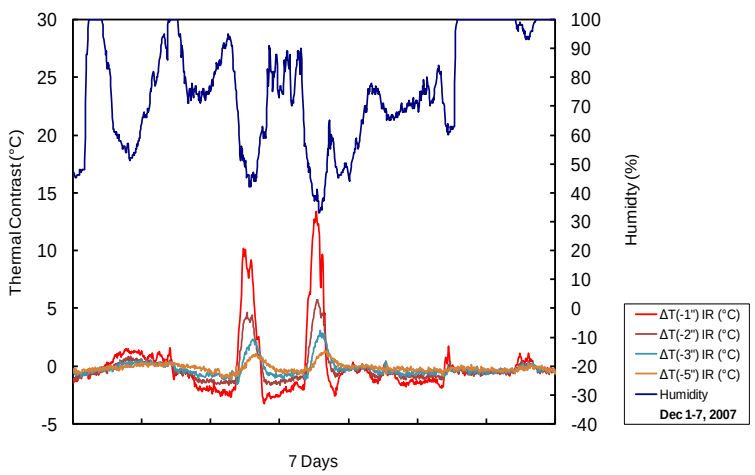
Thermal Contrast (°C)
Humidity (%)
7 Days
ΔT(-1") IR (°C)
ΔT(-2") IR (°C)
ΔT(-3") IR (°C)
ΔT(-5") IR (°C)
Humidity
Dec 1-7, 2007

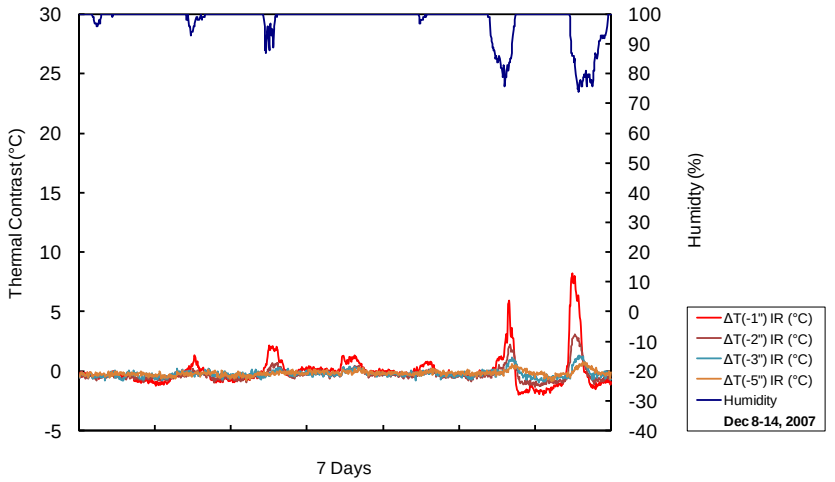
Thermal Contrast (°C)
Humidity (%)
7 Days
ΔT(-1") IR (°C)
ΔT(-2") IR (°C)
ΔT(-3") IR (°C)
ΔT(-5") IR (°C)
Humidity
Dec 8-14, 2007

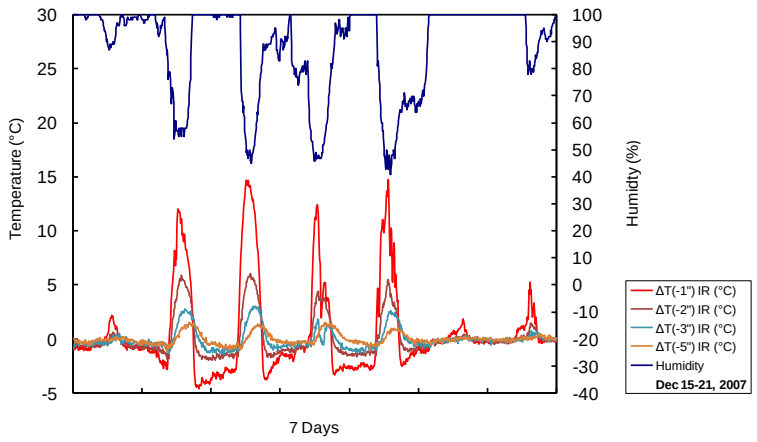
Temperature (°C)
Humidity (%)
7 Days
ΔT(-1") IR (°C)
ΔT(-2") IR (°C)
ΔT(-3") IR (°C)
ΔT(-5") IR (°C)
Humidity
Dec 15-21, 2007

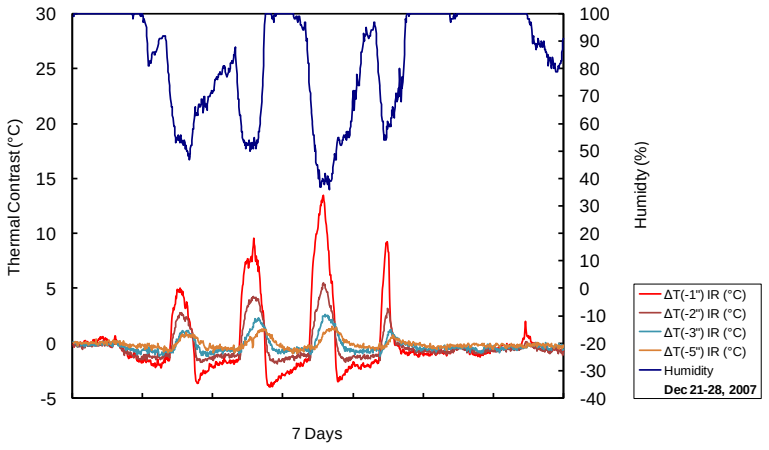
Thermal Contrast (°C)
Humidity (%)
7 Days
ΔT(-1") IR (°C)
ΔT(-2") IR (°C)
ΔT(-3") IR (°C)
ΔT(-5") IR (°C)
Humidity
Dec 21-28, 2007

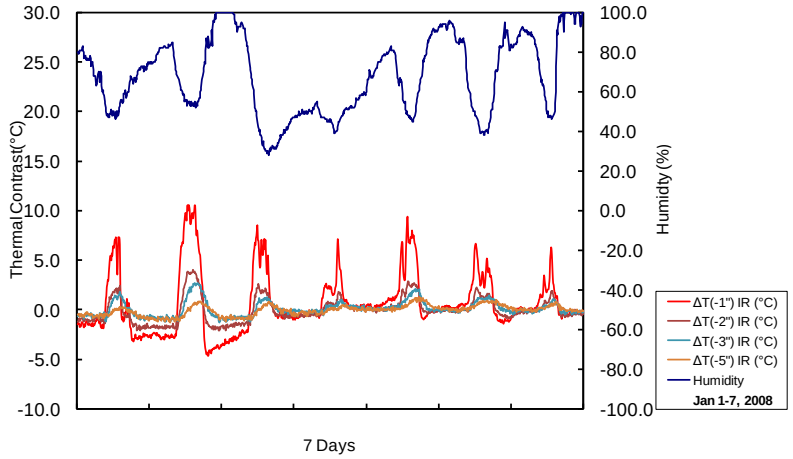
Thermal Contrast(°C)
Humidty (%)
7 Days
ΔT(-1") IR (°C)
ΔT(-2") IR (°C)
ΔT(-3") IR (°C)
ΔT(-5") IR (°C)
Humidity
Jan 1-7, 2008

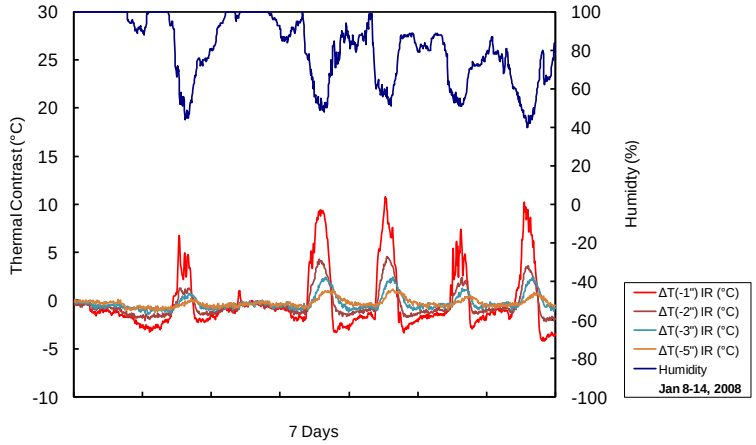
Thermal Contrast (°C)
Humidty (%)
7 Days
ΔT(-1") IR (°C)
ΔT(-2") IR (°C)
ΔT(-3") IR (°C)
ΔT(-5") IR (°C)
Humidity
Jan 8-14, 2008

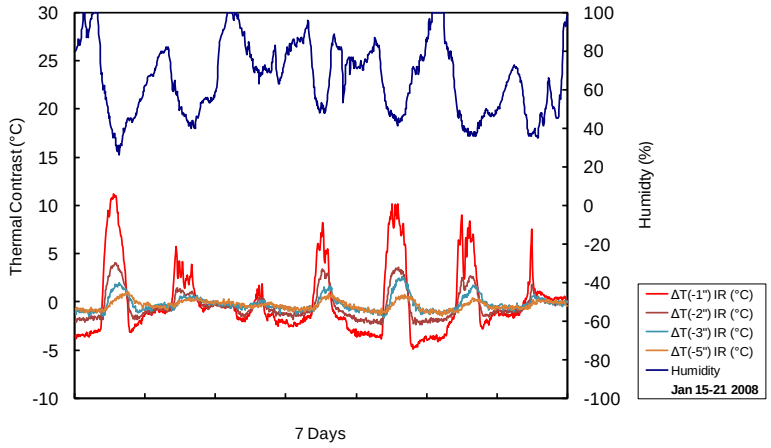
Thermal Contrast (°C)
Humidty (%)
7 Days
ΔT(-1") IR (°C)
ΔT(-2") IR (°C)
ΔT(-3") IR (°C)
ΔT(-5") IR (°C)
Humidity
Jan 15-21 2008

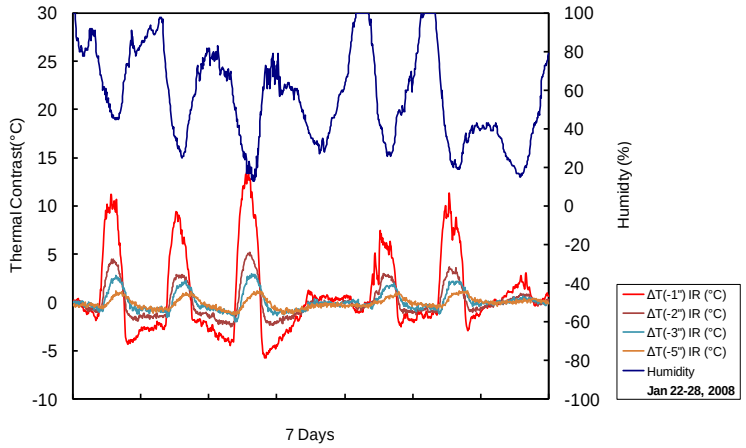
Thermal Contrast(°C)
Humidty (%)
7 Days
ΔT(-1") IR (°C)
ΔT(-2") IR (°C)
ΔT(-3") IR (°C)
ΔT(-5") IR (°C)
Humidity
Jan 22-28, 2008